Frontispiece, Chapter A. Autumn view of the dunes and Sangre de Cristo Mountains from Zapata Falls Recreation Area. National Park Service photograph by Patrick Myers.

Chapter A — Field Trip Day 1 Quaternary Geology of Great Sand Dunes National Park and Preserve, Southern Colorado

By Andrew Valdez, Steve Forman, Richard Madole, James McCalpin, Michael Machette, Randy Schumann, Mike Rupert, Shannon Mahan, and Fred Bunch

CHAPTER A

Orientation for Day 1 — Friday, Sept. 7, 2006

Speakers: Michael Machette and Fred Bunch
Location: Dunes parking lot, Great Sand Dunes National Park and Preserve
1.1 road mi (1.8 km) southwest of Pinyon Flats Campground
0.9 road mi (1.4 km) northwest of the Park's Visitor Center
Zapata Ranch 7.5' quadrangle
GPS: NAD27, Zone 13, 454450 m E., 4176800 m N.
Elevation: 8,060 ft

Welcome to the 2007 Rocky Mountain Section Friends of the Pleistocene (FOP) field trip to the San Luis Basin. An introduction to this year's FOP trip will be presented by field trip organizer Michael Machette (USGS) and we'll discuss some basic aspects of field trip logistics and our general route through the San Luis Basin for the next three days (see fig. A1). A brief discussion of the Quaternary geology of local area will be presented using posters. Finally, Fred Bunch of the National Park Service (NPS), Chief of Resource Management at Great Sand Dunes National Park and Preserve (GSD-NPP), will welcome our group and provide an overview of the Park (http://www.nps.gov/grsa).

Overview

Day 1 will focus on surficial deposits of the eastern Alamosa Basin, a subbasin of the Rio Grande rift (fig A–1). The dominant feature is an eolian system that appears to be fed by a playa lake system. Most of the research conducted in this area has focused on modern (Holocene) geological and hydrological processes as well as on archeology of the same time period. Few details are known about the geologic history of the eolian deposits. It was once assumed that the dunes were a product of glacial outwash and dated to around 12,000 yr B.P. Drilling during groundwater exploration has revealed that the eolian sand extends hundreds of feet into the subsurface, so potentially they could be much older than 12,000 years as the creation of accommodation space in a rift valley is a slow process. Where penetrated, the eolian sands start within about 10 feet of a lacustrine deposit known locally as the blue clay layer. If this clay is from Lake Alamosa (discussed on day 2), then the eolian system may have been initiated by the lake retreat (see cover photo) and been a continuous feature since.

The trip begins at the terminal end of the eolian system, the main dune field of Great Sand Dunes (fig A–2), proceeds up the wind gradient into an extensive playa system, and then heads south where eolian sand thins and stream erosion has exposed some peat deposits. NPS geologist Andrew Valdez will present an overview of the eolian system and the geologic processes that influence its development. Figure A–3, which is a genetic classification of eolian sand dunes based on processes, vegetation, and topography, provides a basis for much of the discussion of dunes and dune forms. Steve Foreman, University of Illinois, Chicago, has used optically stimulated luminescence (OSL) dating on samples collected near the main dune field and on the sand sheet. He will be talking about the depositional history of the dunes and how parabolic dunes respond to climatic variations. Rifting creates the depositional setting of the basin. To understand that setting, Jim McCalpin, GeoHaz Consultants, conducted a paleoseismology study on exposed fault scarps, and he present his results. The irregular surface of the sand sheet must have been a productive hunting ground for Paleoindians, as Pegi Jodry of the Smithsonian Institution will explain. Rich Madole, U.S. Geological Survey (USGS), has developed a Quaternary stratigraphy for the upper eolian deposits and mapped the deposits based upon his stratigraphic identifications. Rich will explain his logic and keys to identifying these units. Next up, Mike Rupert, USGS, will present his findings

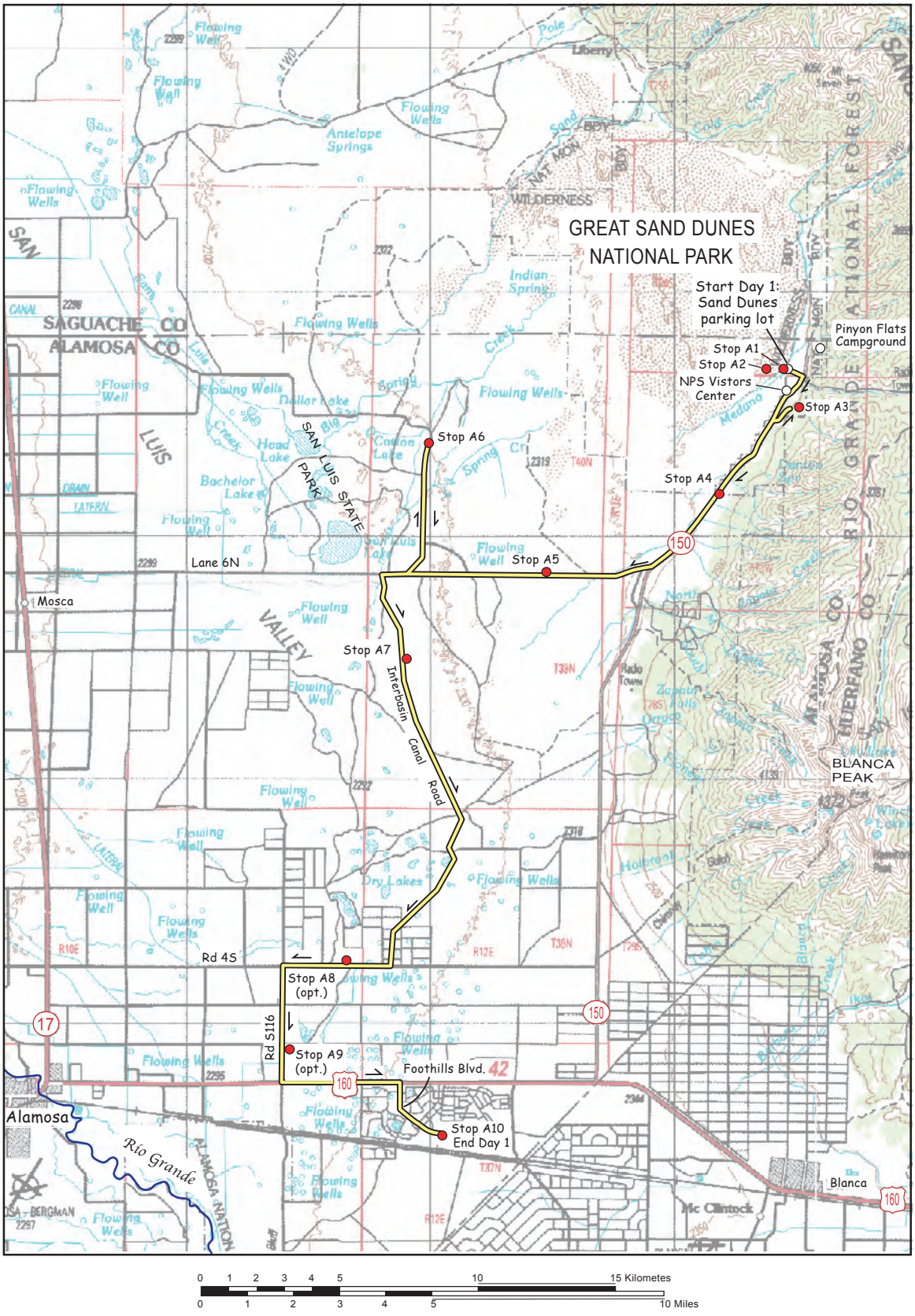

Figure A-1. Route and stops of field trip day 2.

on dating groundwater. The several aquifers in the Alamosa Basin each contain water with a distinct residence time. The trip will then proceed along the edge of the playa lake area for a closer examination of the features of the sabkha; quick stops will be led by Andrew Valdez, Michael Machette, and Randy Schumann. The field trip ends at a paleostream valley east of Alamosa where peat and tufa deposits indicate a vastly different environment than that of the present.

The day ends with a catered dinner at the Bachus pit (stop B1), which serves as our official FOP campground in Alamosa. It's a few miles southwest of Alamosa and the starting point for day 2. However, Alamosa has numerous other restaurants, motels, and camping options.

Acknowledgments

We would not be able to visit any of the stops on this or other days of the field trip without the permission of the landowners. Therefore, we would like to thank the following for allowing access to their properties during day 1 of the field trip:

Stops A1–A3: National Park Service, Mosca, Colo.
Stop A4: Patty Vittoria, owner, Great Sand Dunes Oasis (general store)
Stop A5: National Park Service, Mosca, Colo., and Medano Ranch (The Nature Conservancy)
Stop A6: National Park Service, Mosca, Colo., and Zapata Ranch (The Nature Conservancy)
Stop A7: U.S. Bureau of Reclamation, Closed Basin Division, Alamosa, Colo.
Stop A8: U.S. Bureau of Reclamation, Closed Basin Division, Alamosa, Colo.
Stop A9: The Cisneros family, Alamosa, Colo. (no trespassing please)
Stop A10: Adrian Absmeier, Absmeier Landscaping (previously RMMP), Alamosa, Colo.

In addition, we appreciate the constructive and helpful comments of Margaret Berry (USGS) and Daniel Muhs (USGS), who reviewed a preliminary version of this manuscript. However, any errors that may remain are the responsibility of the authors.

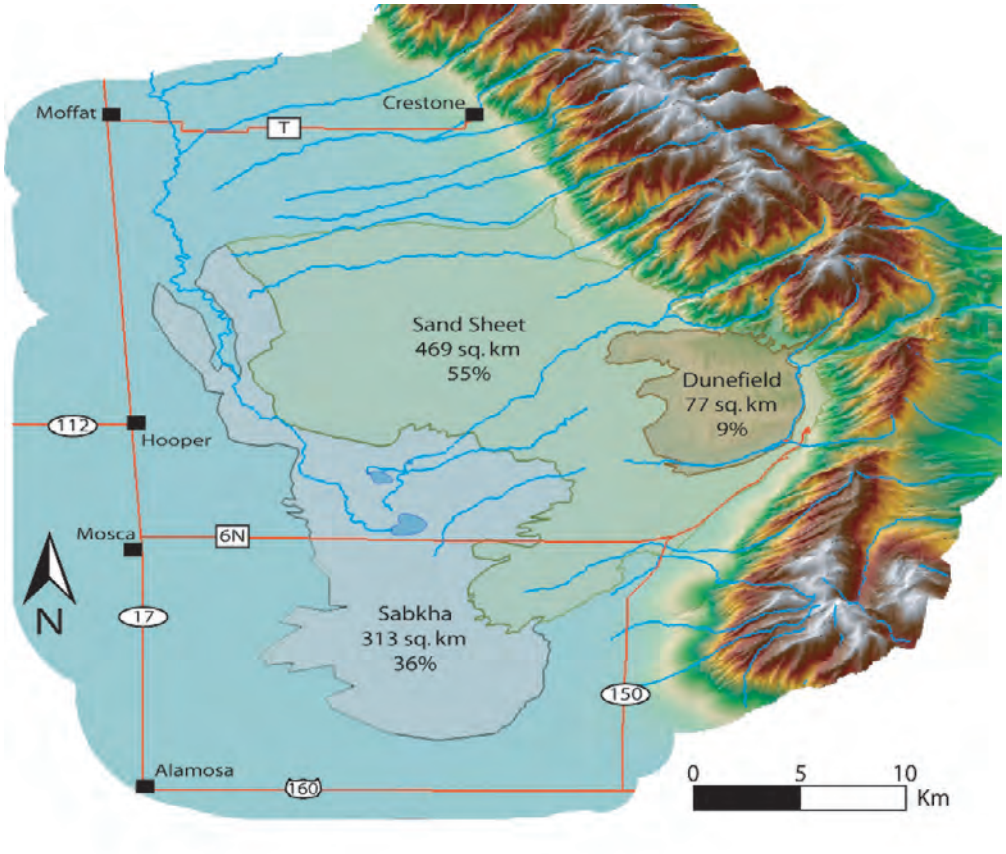

Figure A–2. Aerial view of the Great Sand Dunes and adjacent parts of the San Luis Valley and Sangre de Cristo Mountains. The dune field, sand sheet, and sabkha are subjects of the field trip. A digital elevation model is draped over topography to create a three-dimensional image of the area.

Toward a Genetic Classification of Aeolian Sand Dunes

Kevin R. Mulligan, Department of Economics and Geography, Texas Tech University Lubbock, Texas
Vatche P. Tchakerian, Department of Geography and Geology & Geophysics, Texas A&M University, College Station, Texas

Aeolian sand dunes occur in a wide variety of forms in many different environmental settings. Although several notable attempts have been made to classify dune forms (e.g. Hack, 1941; McKee, 1979; Pye and Tsoar, 1990; Cooke *et. al.*, 1993, Lancaster, 1995; Livingstone and Warren, 1996; Thomas, 1997), the problem of dune classification is complicated by the diverse terminology used in the literature and a lack of consensus among geomorphologists. More importantly, most dune classification systems fail to emphasize the genetic linkage between different dune types. In many situations dune morphologies can be represented as part of a continuum from one dune type to another.

The purpose of this paper is to outline a simple dune classification system that stresses the genetic linkage between the different types of dunes controlled by autogenic processes, vegetation and topography.

Dunes Related to Autogenic Processes
In the first case, dunes controlled by autogenic processes reflect bedform self-organization and the nature of dune morphology is largely a function of the wind regime, sand supply and time. Over very long time scales these dunes can become part of larger draas or ergs in depositional basins or sinks.

Dunes Related to Vegetation
In the second case, vegetation is considered to be an important controlling variable and dunes are classified as part of a continuum reflecting the degree of sand accumulation or deflation. In the absence of vegetation (either natural or human induced), these dunes can take on the form of autogenic dunes.

Dunes Related to Topography
Lastly, dunes are classified in relation to topography, expressed as either sloped terrain or cliffed terrain. In this case, dune forms are controlled by their relative position with respect to the dominant wind direction and slope.

REFERENCES

Cooke, R., Warren, A., and Goudie, A., 1993, *Desert Geomorphology*, UCL Press, London, p. 526.

Hack, J.T., 1941, Dunes of the western Navaho county, *Geographical Review*, v. 31, p. 240-263.

Lancaster, N., 1995, *Geomorphology of Desert Dunes*, Routledge Press, London, 290 p.

Livingstone, I., and Warren, A., 1996, *Aeolian Geomorphology*, Longman, Essex, 211 p.

McKee, E.D., 1979, Introduction to a study of global sand seas, in E.D. McKee (ed) *A Study of Global Sand Seas*, U.S.G.S. Professional Paper 1052, p. 1-19.

Pye, K., and Tsoar, H., 1990, *Aeolian Sand and Sand Dunes*, Unwin Hyman, London, 396 p.

Thomas, D.S.G., 1997, *Arid Zone Geomorphology*, John Wiley and Sons, London, 713 p.

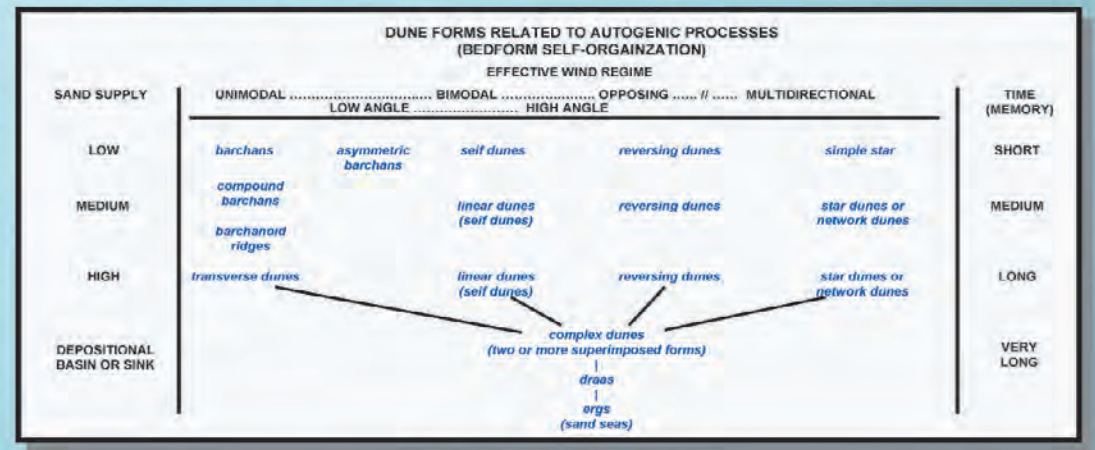

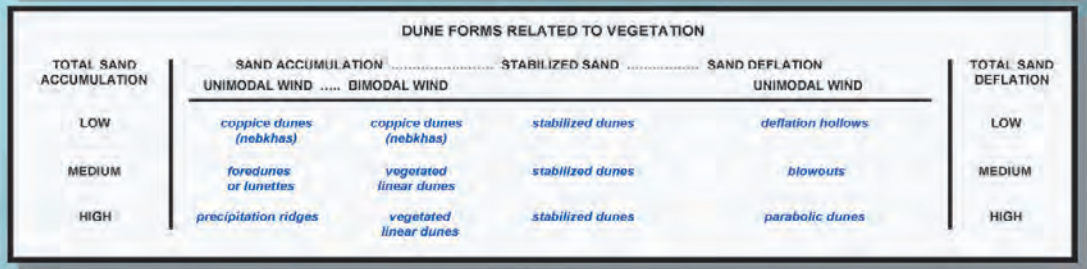

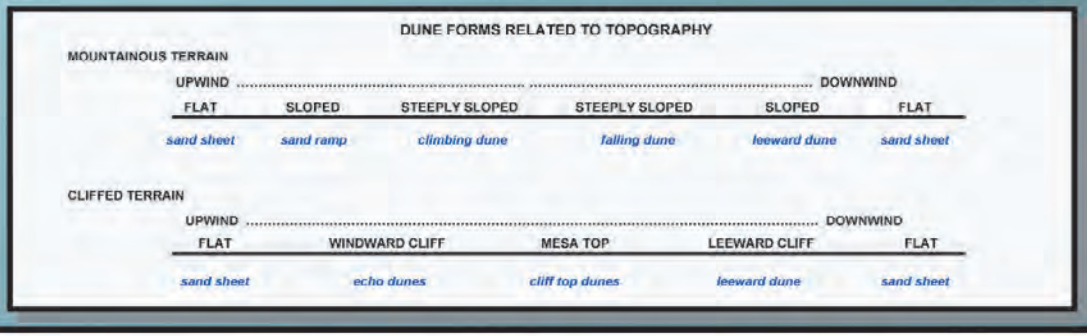

Figure A–3. A genetic classification of eolian sand dunes (Mulligan and Tchakerian, written commun. to Andrew Valdez, 2006).

Stop A1 — Development and Eolian Geomorphology of Great Sand Dunes

Speaker: Andrew Valdez
Location: Medano Creek, 200 m west of Dunes Picnic Area, Great Sand Dunes National Park and Preserve
Zapata Ranch 7.5' quadrangle
GPS: NAD27, Zone 13, 454300 m E., 4176740 m N.
Elevation: 8,060 ft

Synopsis

The Alamosa Basin contains several eolian sand deposits that extend from the axis of the basin (its topographic low points) eastward to the Sangre de Cristo Mountains. With increasing elevation these sand deposits transition from a sabkha to a sand sheet, then to a dune field, and finally into sand ramps. The setting for the eolian deposits is created by the sediment-filled San Luis Basin (upper Rio Grande rift), and dunes are modified by variations in wind regime, transport of sand by streams, the presence of vegetation, and near-surface groundwater. The interaction of these processes results in multiple sand deposits and also causes variations in dune configuration and dune types.

Discussion

The Great Sand Dunes eolian system is located in south-central Colorado, U.S.A., in a physiographic area known as the San Luis Valley (fig. A1–1). The San Luis Valley occupies the San Luis Basin, which is part of the Rio Grande rift, an eastern portion of the Basin and Range Province. It is bound by the San Juan Mountains on the west and the Sangre de Cristo Mountains on the east. Eolian deposits are well developed in the Alamosa subbasin, which is the northern part of the San Luis Basin.

The eolian system changes along a topographic gradient from sabkha to sheet sand to dune field and terminates as a sand ramp (fig. A1–2). In a simple view, this system can be described as a process whereby (1) streams deposit sand in sabkha areas; (2) wind transports the sand across the sand sheet; and (3) sand is ultimately deposited in the dune field and up onto a sand ramp (Fryberger, 1990a). The extent of the Great Sand Dunes eolian system can be traced upwind to the playa area, suggesting that the sand had its sources in a playa system (Madole and Romig, 2002).

Dune types also differ along this topographic gradient (fig. A1–3). Vegetation-related dune forms develop on the lower gradient where sand movement is inhibited. As the gradient and amount of sand exposure increases, autogenic (self-organizing) dunes are formed. Along the mountain front, topography controls the development of dunes. Coppice dunes and lunettes (crescent- or tongue-shaped dunes) are common near the sabkha, whereas blowouts, parabolic dunes, and transverse dunes develop downwind of the sabkha. Reversing and star dunes are the primary dune types of the dune field.

The variation in sand deposits and dune types results from the interaction of five geologic processes that are fundamental to the development of the eolian system. At Great Sand Dunes these processes are (1) crustal rifting, extension, uplift, and basin formation, all leading to topography favorable for sediment deposition; (2) sand transport by stream flow; (3) sand transport related to wind regime; (4) sand stabilization by vegetation growth; and (5) sand cementation by evaporite minerals. Rifting creates a closed basin allowing sand to accumulate. It also is responsible for the development of a playa-lake system and the configuration of the Sangre de Cristo Mountains, which provide topographic controls on wind flow. Wind regime controls dune type and behavior; streams modify the perimeter of the dune field, and vegetation stabilizes surfaces.

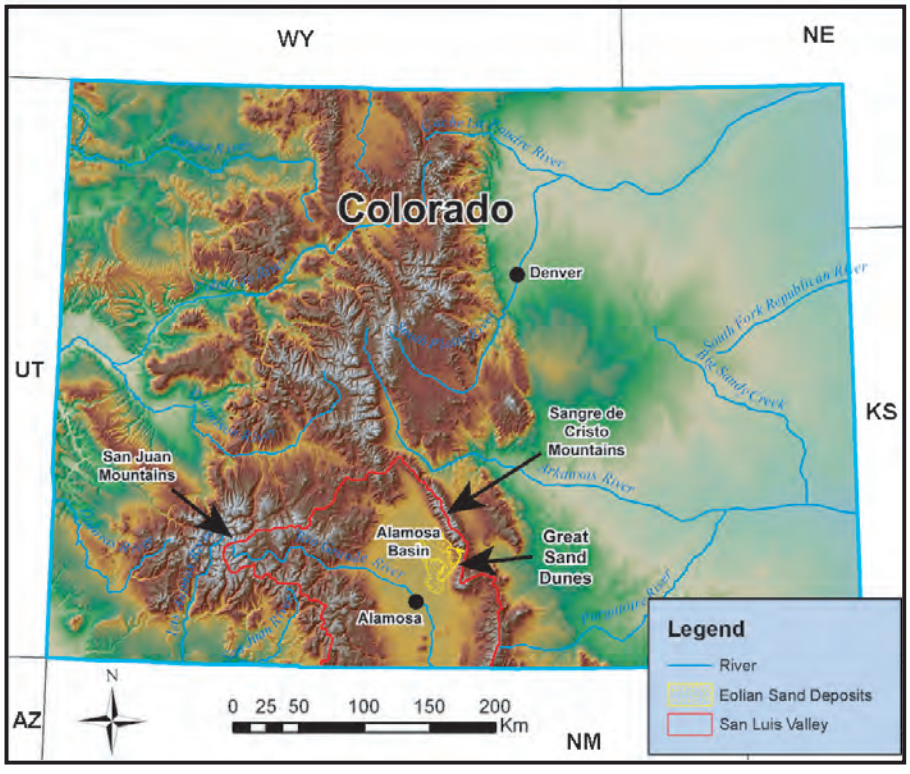

Figure A1–1. Location of San Luis Valley and Great Sand Dunes in southern Colorado.

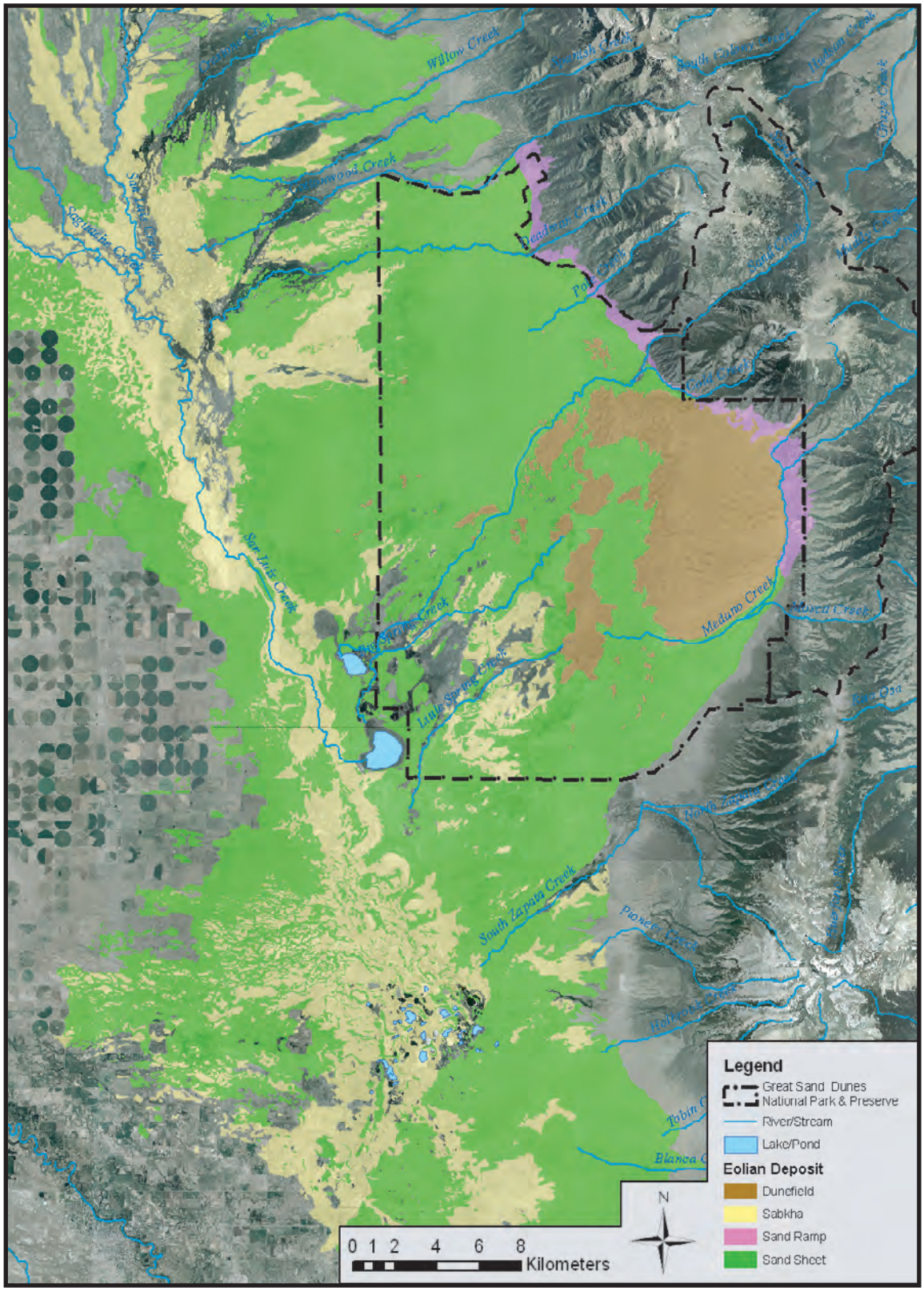

Figure A1–2. Eolian sand deposits near Great Sand Dunes, southern Colorado. Dashed line shows boundary of Great Sand Dunes National Park and Preserve; larger lakes are part of San Luis Lakes State Park.

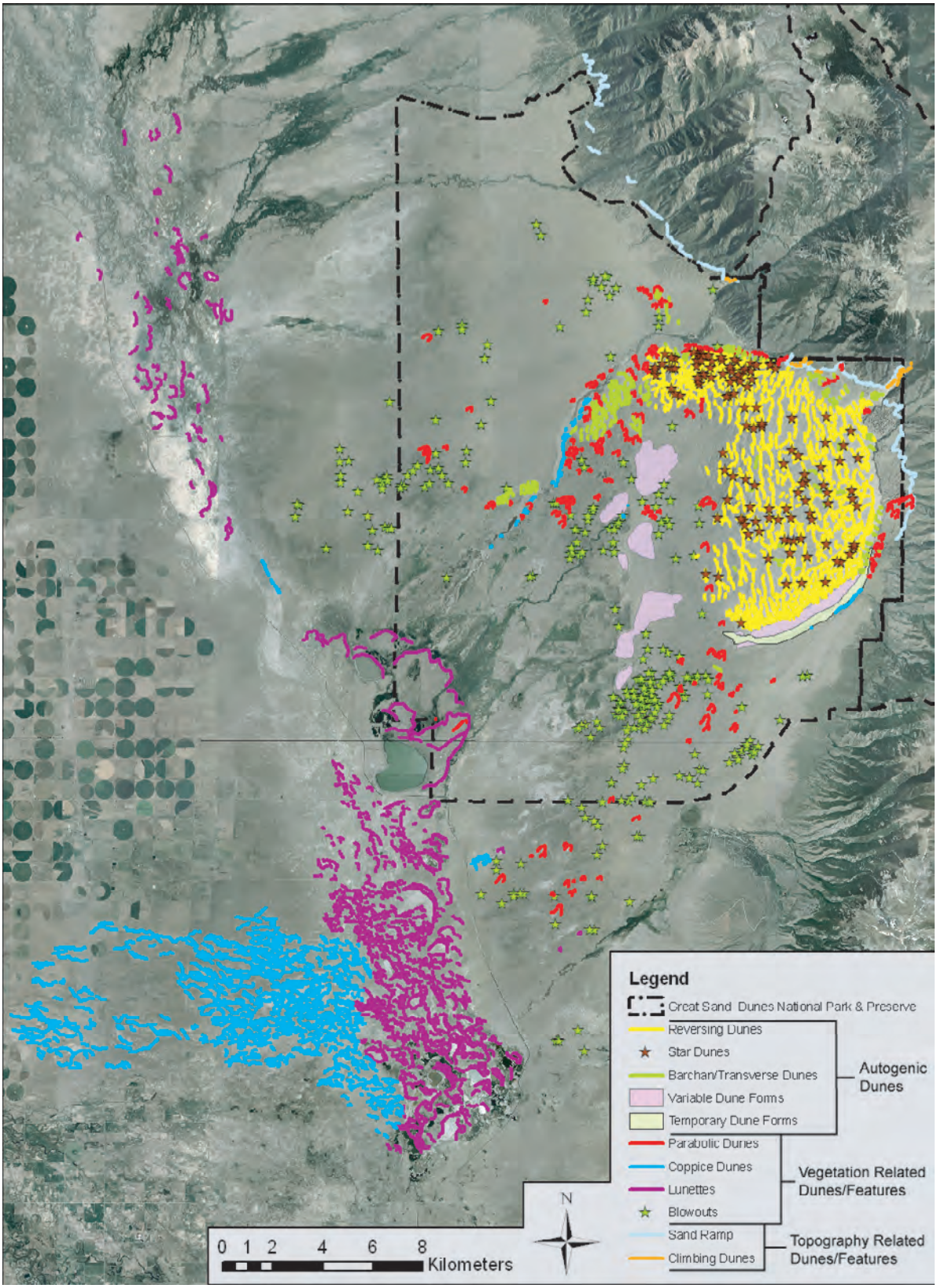

Figure A1–3. Dune types near Great Sand Dunes, Colorado.

Areas that have near-surface groundwater have sediments that are commonly cemented by evaporite minerals.

The Great Sand Dunes sabkha has formed where basin subsidence is greatest and a depression, known locally as the "closed basin," has developed. Playa lakes are common here and because the water-table gradient is flat, the primary means of water outflow is through evaporation, resulting in saline groundwater. Sabkhas can also form when deflation lowers the ground surface to the groundwater's capillary fringe. Sodium carbonate, calcite, and other evaporite minerals precipitate, cementing the sand to form a sabkha (Krystinik, 1990). The primary features of the sabkha are mineralized salt flats, fine-grained lake deposits, coppice dunes, and lunettes.

As the topographic gradient increases toward the east, the ground surface rises above the capillary fringe zone and sand sheets accumulate on the piedmont, which is mostly covered by vegetation dominated by shrubs and grasses. The north and south ends of the sand sheet have a planar surface marked by parabolic dunes developed around their margin. The average rate of parabolic dune migration has been measured at about 10 m/yr (Marin and others, 2005), but the rate increases during intervals of drought (Forman and others, 2006), such as the one we have had this decade. Conversely, the central sand sheet is currently less vegetated and has parabolic and transverse dune forms superimposed on it. The unvegetated areas have dunes that transition with time between dome, transverse, and reversing dunes. Sand ramps with climbing dunes form where the sand sheet laps onto the mountain front.

The Great Sand Dunes (dune field) covers 78 km^2. The dune field is a classic draa—a large sand dune tens of kilometers long and hundreds of meters high, often with smaller dunes on the leeward and windward faces. It has five depositional centers of greater sand thickness. Each deposition center can also be considered a draa (fig. A1–4). The primary dune types are reversing and star dunes. The tallest dune reaches a height of 229 m above the plain of the valley floor. The dune field is crescent-shaped and has three areas of distinct dune development: the (1) Sand Creek star dune complex, (2) central dune field, and (3) Medano Creek dune ridge (fig. A1–4). The Sand Creek star dune complex has reversing dune ridges radiating out from central high points that form the star dunes. The central dune field is composed of large north-south trending reversing dunes separated by large troughs. The Medano Creek dune ridge has more closely spaced, north-south-trending dune ridges and a secondary dune ridge that trends northeast, filling the troughs of the north-south-trending dunes. Along the dune field margins and adjacent to the creeks are smaller dunes that transition between dome, barchan, barchanoid ridge, transverse, and reversing dunes depending on wind conditions and sand supply.

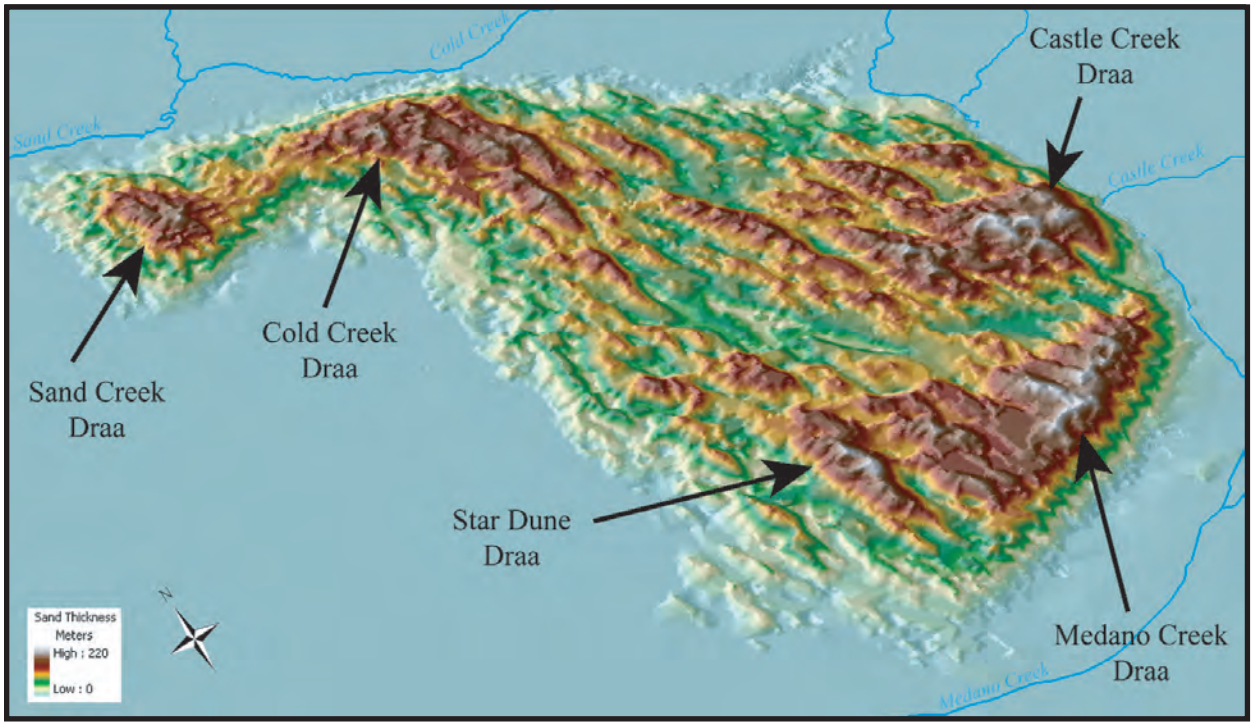

Figure A1–4. Sand thickness within the main dune field of Great Sand Dunes, southern Colorado. The main dune field is about 10 km (north-south) by 6 km (east-west).

Stop A2 — Optical Dating of Episodic Dune Movement at Great Sand Dunes National Park and Preserve

Speaker: Steve Forman
Location: Base of main dune field, 600 m west of Dunes Picnic Area, Great Sand Dunes National Park and Preserve
Zapata Ranch 7.5' quadrangle
GPS: NAD27, Zone 13, 453850 m E., 4177020 m N.
Elevation: 8,060 ft

Synopsis

The Great Sand Dunes National Park and Preserve in the San Luis Valley, Colo., contains a variety of eolian landforms that reflect Holocene drought variability. The most spectacular is a dune field banked against the Sangre de Cristo Mountains, which is fronted by an extensive sand sheet with stabilized parabolic dunes. Stratigraphic exposures of parabolic dunes on the sand sheet and associated luminescence dating of quartz grains by single aliquot regeneration (SAR) protocols indicate eolian deposition of unknown magnitude occurred about 1290–940, 715±80, 320±30, and 200–120 years ago and in the 20th Century. Preliminary SAR ages from the dune field near Medano Creek indicate sand movement about 300 years ago. Eleven drought intervals are inferred from the tree-ring record of the past 1,300 years at Great Sand Dunes and are potentially associated with dune movement, although only 5 eolian depositional events are currently recognized in the stratigraphic record. There is evidence for eolian transport associated with dune movement in the 13th Century, which may coincide with the "Great Drought," a 26-year-long dry interval identified in the tree ring record and associated with migration of Anasazi people from the Four Corners areas to wetter areas in southern New Mexico. This nascent chronology indicates that the transport of eolian sand across San Luis Valley was episodic in the late Holocene; appreciable dune migration in the 8th, 10–13th, and 19th Centuries ultimately nourished the dune field against the Sangre de Cristo Mountains.

Discussion

Many intermountain basins in the western United States are mantled by complex sequences of eolian deposits, a testament to the significant drought variability in the Holocene (Gaylord, 1989; Morrison, 1991; Stokes and Gaylord, 1993; Forman and Pierson, 2003; Lancaster and Tchakerian, 2003). Numerous studies in the past two decades document compelling evidence for large-scale and repeated reactivation of dune systems in the Great Basin and adjacent western Great Plains during the Holocene and as recently as <2,000 years ago (for example, Wells and others, 1990; Forman and others, 1992, 1995, 2001; Madole, 1994, 1995; Muhs and others, 1996, 1997; Stokes and Swinehart, 1997; Wolfe and others, 2001; 2002; Goble and others, 2004; Mason and others, 2004). Tree-ring time series from across North America show severe multidecadal droughts during the 13th and 16th Centuries (Woodhouse and Overpeck, 1998; Stahle and others, 2000) and in the middle 18th Century for the Rocky Mountains. These droughts surpassed conditions during the driest years of the 20th Century (Woodhouse and others, 2002; Fye and others, 2003). A late 13th Century dry period in the southwestern United States, referred to as the "Great Drought" (Larson and others, 1996), is associated with large-scale environmental degradation and was one of many factors for depopulation of Anasazi centers (Fish and Fish, 1994; Lekson, 2001, 2002; Nelson and Schachner, 2002). This stop examines the record of eolian sand deposition in the Park (fig. A2–1). Questions remain as to whether or not dunes in intermountain, semiarid landscapes have been reactivated with droughts in the past 2000 years (Woodhouse and Overpeck, 1998). To address this question, we have employed recent advances in optically stimulated luminescence dating, specifically single-aliquot regeneration (Murray and Wintle, 2000, 2003) protocols, to provide the first quantitative dosimetric-based ages on formation of parabolic dunes in the sand-sheet area, upwind of the main dune field (fig. A2–1).

Geomorphic Setting

The Great Sand Dunes National Park and Preserve, with an area of 104 km^2, is located in the San Luis Valley, southern Colorado, in a small reentrant of the Sangre de Cristo Mountains (fig. A2–1*A*). The sand for these dunes is derived mainly from alluvium of the Rio Grande River, blown by prevailing southwesterly winds across the San Luis Valley (Johnson, 1967). The original sources of this sand are the volcanic rocks that form the San Juan Mountains on the western side of the valley and smaller amounts of crystalline and sedimentary rocks from the Sangre de Cristo Mountains on the valley's eastern side (Johnson, 1967; Wiegand, 1977).

The most prominent feature in the Park is a massive active dune field that is banked against the Sangre de Cristo Mountains (fig. A2–1*B*). This dune field is a complex of active and sinuous transverse to barchanoid ridges, generally oriented north-northwest–south-southeast and north-south. On top of the transverse dunes, toward the north and southwest, star dunes have formed in response to locally complex wind directions. Reversing dunes also formed at the crest of the primary ridges in response to short-term winds blowing from the northeast (Wiegand, 1977). The main dune field is confined between two perennial sandy-bed streams that flow westward from the Sangre de Cristo Mountains—Sand Creek to the north and west and Medano Creek to the east and south (fig. A2–1*C*). Although the flow of these streams rarely extends more than 3.5 km from the mountain front, it may reach 8 km

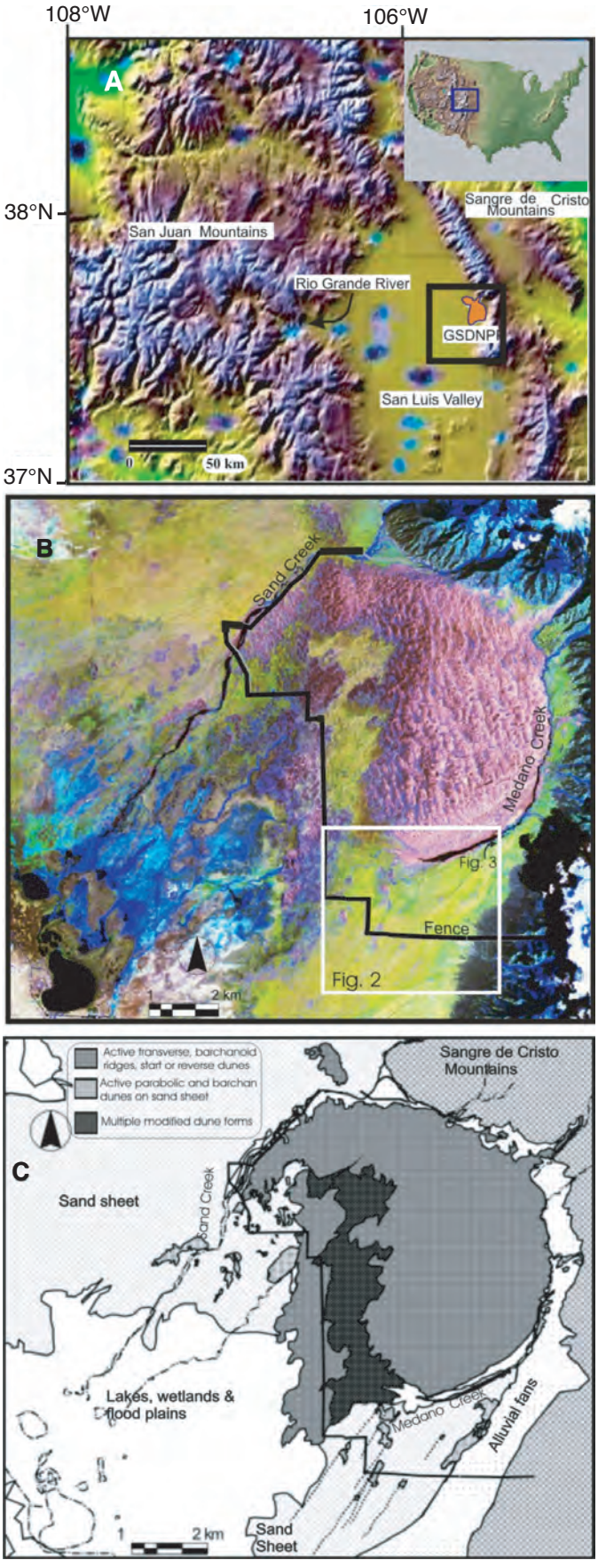

Figure A2–1. Index maps for the Great San Dunes National Park and Preserve in Colorado. *A*, Digital terrain model of the Park. San Luis Valley is bounded by San Juan and Sangre de Cristo Mountains to the west and east, respectively. *B*, False color composition (bands 5 in red, 4 in green and 7 in blue) of the Landsat 7 enhanced thematic mapper image acquired on July 26, 1999. The active dunes are shown in red tones, the sand sheet in magenta and blue, mountainous vegetation in dark green and brown, and the water in dark blue and black. *C*, Surficial geologic map of the Park. The southeast sand-sheet area is the focus of this study (from Forman and others, 2006).

during peak flow from May to July (Johnson, 1967; Wiegand, 1977). During floods, sand is eroded from the dunes by the creeks and is carried back toward the sand sheet (Fryberger, 1999); when the creeks dry, eolian sand is blown across the creeks' beds back into the main dune field (Johnson, 1967; Wiegand, 1977; Fryberger, 1999).

A vegetated low-relief sand sheet bounds the dune field for hundreds of kilometers to the north, west, and south. Scattered active parabolic dunes are distinctive on the south and southwestern areas of the sand sheet. These parabolic dunes have arms (McKee, 1979, p. 9) anchored by a variety of grasses and shrubs. The arms are as long as 3.5 km and are oriented 35°–40° NE., in response to predominant winds from the west-southwest (figs. A2–1 and A2–2). The arms, observed in aerial photographs as long parallel ridges, were originally interpreted by Johnson (1967) as longitudinal dunes, but Wiegand (1977) later recognized them as arms of parabolic dunes. Active barchan and reversing dunes oriented 40º–50° NE. are also superimposed on the sand sheet, near the western margin of the main dune field. Some of these barchan dunes are scattered, but the dunes next to Sand and Indian Creeks often coalesce to form compound barchanoid ridges with reverse tops. Alternatively, these dunes may be a hybrid dune type (for example, Carson and MacLean, 1986).

The climate of the San Luis Valley is arid with a mean annual precipitation of 15±8 cm/yr (1948–2002); however, orographic controls in the Park generate a locally wetter climate, with a mean annual precipitation 24±11 cm/yr (National Climatic Data Center, 1950–2002). More than 67 percent of the yearly precipitation occurs as scattered showers in spring and thunderstorms in summer. August is the wettest month with 50 percent of the total summer precipitation. The mean annual temperature at GSDNPP is approximately 6.7°C (Wiegand, 1977); summers and autumns are usually temperate, and they have average temperatures of 21.6°C and 19°C, respectively, and a maximum monthly temperature of 26.5°C in August (1950–2002) (National Climatic Data Center, 1950–2002).

Opposing wind regimens prevail at Great Sand Dunes (Wiegand, 1977). The southwest winds blow throughout the year, whereas winds from the northeast are both seasonal (July, August, and September) and diurnal (cold air flowing from the mountains at night) (Johnson, 1967; Wiegand, 1977). The synoptic-scale circulation of the Rocky Mountain region and the topographic configuration of the San Luis Valley are reflected in the wind pattern. Upper-level cyclonic storm centers move eastward across central North America along a track that passes north of Colorado during most of the year. Storm tracks during winter lie south of Colorado, also producing surface winds from the southwest (Wiegand, 1977). Northeast winds reflect a local orographically influenced circulation pattern caused by the presence of tall peaks coupled with low

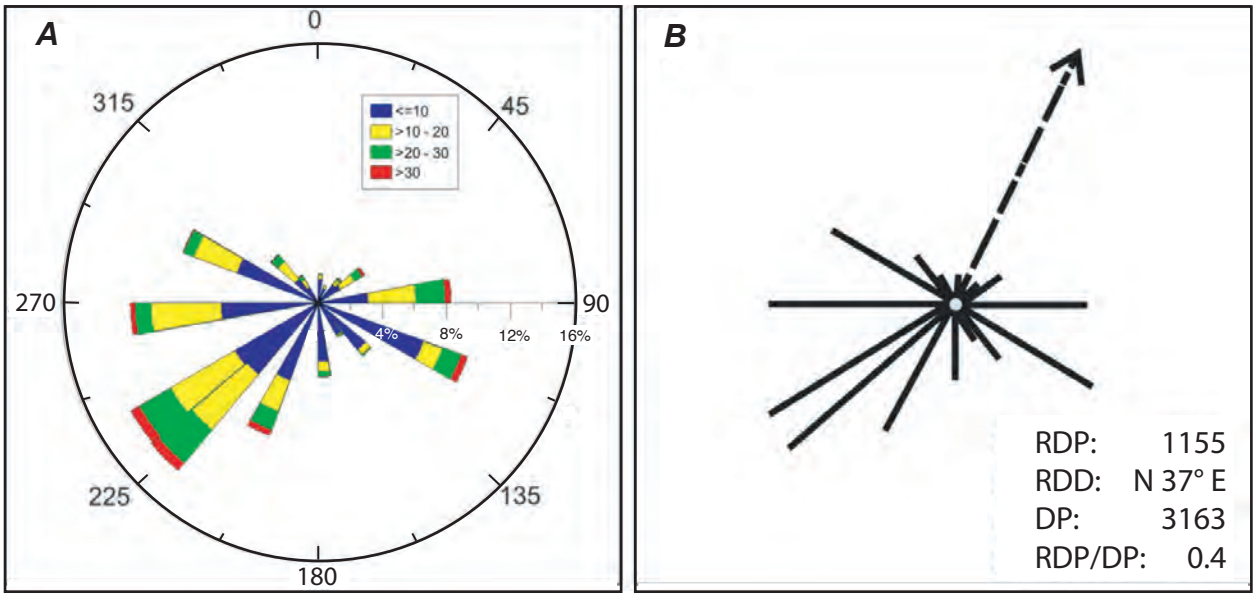

Figure A2–2. Wind roses and sand drift potential for Great Sand Dunes National Park and Preserve. *A*, Wind roses generated from data from July 2002 to April 2003. Wind velocity represented by color: blue, velocities ≤10 m/s; yellow, velocities >10 m/s. *B*, Sand drift potential from vectorial analyses of the wind data from part *A*, following Fryberger and Dean (1979, p. 147). The data are based on calculations of over 10,000 wind measurements every 10 minutes during an interval of 3 years, which form a unique data set that yields relative high values of resultant drift potential and drift potential. Abbreviations: RDP, resultant drift potential; RDD, resultant drift direction; DP, drift potential; RDP/DP, ratio of resultant drift potential to resultant drift direction.

mountain passes that funnel winds through them. These winds may also reflect a thermal convection cell produced by differential heating and cooling between the mountains and the valley (Wiegand, 1977; Alexander, 1979). Wind data collected at Great Sand Dunes show a strong southwestern component, with wind directions of similar magnitude originating from the southeast and northwest. The drift potential for sand movement has a resultant drift direction of N. 37° E., coinciding with parabolic dune orientation (fig. A2–2).

Optical Dating

Optically stimulated luminescence (OSL) geochronology is based on the time-dependent dosimetric properties of silicate minerals, predominately quartz (Aitken, 1998). The single-aliquot regenerative (SAR) (Murray and Wintle, 2000, 2003) method was used to estimate the equivalent dose of the 150–250 μm quartz fractions from dune sands. Eolian sands at Great Sand Dunes are mineralogically immature, consisting of well-sorted medium sand, with median grain sizes ranging from 290 to 350 μm, composed of 51.7 percent volcanic rock fragments, 27.8 percent quartz, and the remaining grains of mixed lithology (Wiegand, 1977). The quartz fraction was isolated by density separations using the heavy liquid Na–polytungstate, and a 40-minute immersion in hydrofluoric acid (HF) was applied to etch the outer 10+ microns of grains, which are affected by alpha radiation (Mejdahl and Christiansen, 1994). The purity of the quartz separate was evaluated by petrographic inspection and point counting of a representative aliquot. Samples that show >1 percent of nonquartz minerals are retreated with HF and again checked petrographically. Duplicate or triplicate reaction with HF is often needed to obtain a pure quartz separate. The purity of quartz separates from selected samples is tested by exposing small aliquots to infrared excitation (880 μm), which preferentially excites feldspar minerals. Samples measured showed only weak emissions (<300 counts) with infrared excitation, indicating a spectrally pure quartz extract.

An automated Risø TL/OSL–DA–15 system (Bøtter-Jensen and others, 2000) was used for SAR analyses. Blue light excitation (470±20 nm) was produced by an array of 30 light-emitting diodes that delivers about 15 mW/cm^2 to the sample position at 90 percent power. A Thorn EMI 9235 QA photomultiplier tube coupled with three 3-mm-thick Hoya U-340 detection filters, transmitting between 290 and 370 nm, measured photon emissions. Laboratory irradiations used a calibrated ^{90}Sr/^{90}Y beta source coupled with the Risø reader. All SAR emissions were integrated over the first 0.8 s of stimulation out of 500 s of measurement, with background based on emissions for the last 90- to 100-s interval.

Before the application of SAR protocols, a series of experiments evaluated the effect of preheating at 180°, 200°, 220°, and 240°C on the regenerative signal (Murray and Wintle, 2000). These experiments show that preheat temperatures of 200°C yielded the highest and most consistent equivalent doses; therefore aliquots were preheated at this temperature for 10 s for the SAR protocols. Tests for dose recovery were also performed and for samples the last dose coincides well with the initial dose (at 1-sigma errors).

A critical analysis for luminescence dating is the dose rate, which is an estimate of the amount of ionizing radiation acting upon the sediment during the burial period. The contents of U and Th (each assumed to be in secular equilibrium in their decay series) and ^{40}K were determined by inductively coupled plasma–mass spectrometry (ICP-MS) analysis by Activation Laboratory LTD, of Ontario, Canada. The beta and gamma doses were adjusted according to grain diameter to compensate for mass attenuation (Fain and others, 1999). A small cosmic ray component between 0.31 and 0.22±0.01 mGy/yr, depending on depth of sediment, was included in the estimated dose rate (Prescott and Hutton, 1994). A moisture content of 5±2 percent was assumed, which is between field capacity and hydroscopic limit for sandy soils in semiarid environments (Brady, 1974, p. 191–193). The dose rate for these samples is relatively high at about 5 mGy/yr, reflecting the abundances of mica and associated minerals in mafic and granite rock fragments.

At many study localities, near-surface eolian sand has yielded SAR ages between 50 and 20 years. To verify that such young SAR ages are truly finite estimates, sample UIC1077, which yielded an age of 20±2 yr, was subsequently reset with 2 h of solar exposure. This “zero-age” sample yielded no SAR age (that is, 0 yr). However, the associated error is large (80 yr) because of the low signal-to-noise ratio (<5). Similar young but apparently accurate ages have been previously reported for other eolian systems (for example, Bailey and others, 2001; Ballarini and others, 2003; Stokes and others, 2004; Forman and others, 2005).

Backhoe Trenches A and B Across Parabolic Dune Arms

Two backhoe trenches (A and B) were excavated across stabilized limbs of parabolic dunes in the sand sheet area to reveal their stratigraphy (fig. A2–3). These trenches were difficult to excavate because of the inherent instability of the sand; therefore, the depth of excavation was limited to about 2 m. There was a noticeable lack of paleosols exposed in the trenches, compared to what has been found in other eolian sand depositional sequences in the western United States (for example, see Forman and others, 2001).

The basal unit (A–1) exposed in trench A is a moderately well sorted, medium- to coarse-grained sand having common, scattered angular to subrounded (pea-gravel size) clasts, 2–5 mm in diameter (fig. A2–4). The median particle size for this unit is 370 to 310 μm (n=5). Grain lithology includes fragments of gneiss and mafic rock and feldspar and quartz minerals. Numerous burrow fills indicate considerable bioturbation, but in places millimeter-scale, low-angle, cross-stratification is preserved, with beds dipping to west. The upper 40 cm of unit A–1 contains the most abundant coarse sand

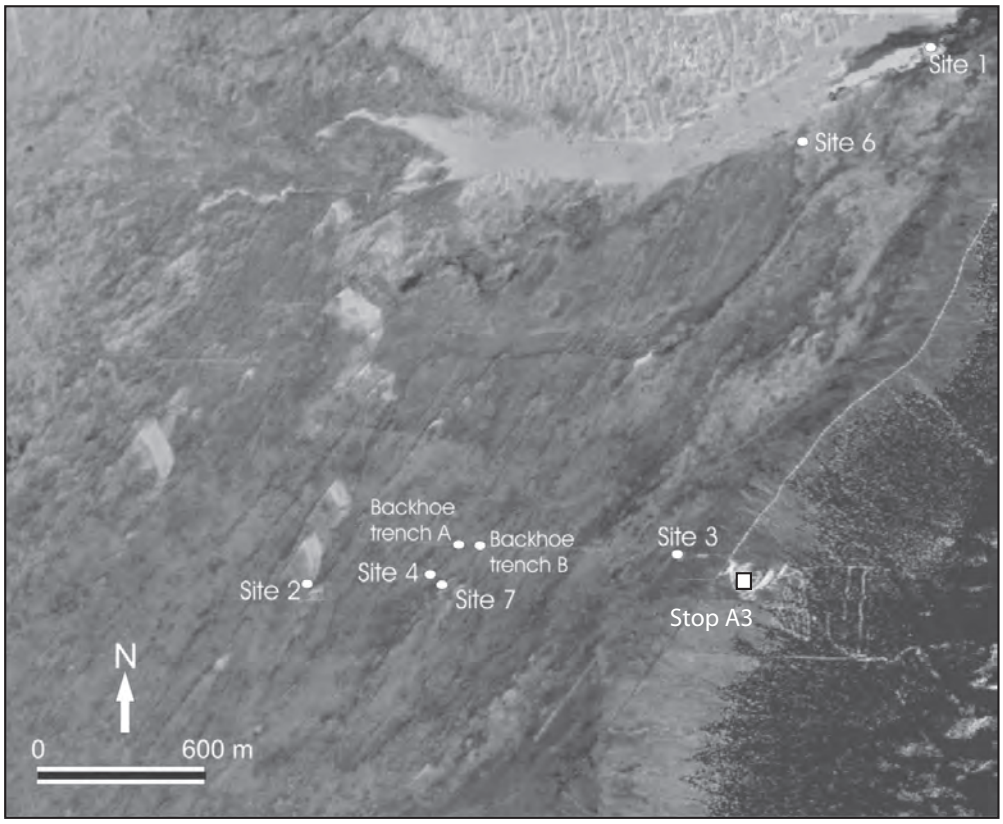

Figure A2–3. Sand dunes at and west of stop A3. Sites and trenches are those mentioned in the text.

and gravel, reflecting lag deposition prior to the emplacement of the overlying unit A–2. Unit A–2 is a well-sorted medium sand having grain and clast lithologies similar to those of unit A–1. The median particle size for unit A–2 is 310 to 270 μm (n=7) and is somewhat finer than underlying unit A–1. The sediment in unit A–2 often appears massive, but in places millimeter- to centimeter-scale bed fragments are preserved, particularly in the lower 30 cm. The surface soil is weakly developed as marked by a weak 20- to 25-cm-thick cambic horizon. SAR dating of quartz grains from units A–1 and A–2 indicate an unconformity, with the basal unit (A–1) yielding ages of 940±80 yr (UIC1086) and 700±75 (UIC1137) yr and the overlying unit A–2 giving ages of 210±30 yr (UIC1238), 230±30 yr (UIC1138), and 170±30 yr (UIC1235).

Backhoe trench B through an adjacent parabolic arm ~200 m east of backhoe trench A has similar lithostratigraphy (Fig. A2–4), but the boundary between upper and lower units is less clear. The lower unit (B–1) is a well-sorted medium sand that exhibits 2- to 30-cm-long bed fragments in the upper 40 cm with horizontal and subhorizontal bedding dipping to the east in the basal 40 cm. Upper unit (B–2) is a massive, well-sorted, medium sand, with common 2–5 mm diameter gravel in the upper 20 cm. This unit has been extensively burrowed. A lag of coarse sand and pebbles marks the boundary between units B–1 and B–2. Quartz grains from unit B–1 yielded SAR ages of 710±70 yr (UIC1260) and 735±90 yr (UIC1260), similar to the ages of basal sediments in backhoe-trench A. Sediments from unit B–2 yielded an SAR age of 120±20 yr (UIC1259), confirming the presence of a lacuna between units B–1 and B–2.

Sedimentary Structure and Age of the Dune Field Adjacent to Medano Creek

A striking and defining landform at Great Sand Dunes National Park and Preserve is the massive dune field that lies adjacent to the western margin of the Sangre de Cristo Mountains. Questions remain on the age and origin of this dune field. One that we address herein is, “Did the dune field expand during periods of eolian transport in the past 1,500 years on the adjacent sand sheet?” Recently we have initiated research that couples OSL dating with detailed sedimentologic assessments to determine the age or ages of the dune field.

The dune field is demarcated by star dunes that reflect multiple wind directions. The flanks of the dune field, near Medano Creek, host 10- to 30-m-high reversing dunes with noticeable interdunal scour. Exposures in the dunes show water-bearing, cohesive sand that has high- and low-angle dune cross bedding. These sediments often contain 5–20 percent water that reflects local perched water tables within the dune field; the wet sediment provides grain cohesion and resistance against eolian erosion and transport (Chen and others, 2004). Water-bearing eolian sediment has been observed in many exposures adjacent to Medano Creek and in boreholes into the dune field. Thus, the upper 20–50 m of sand is mobile;

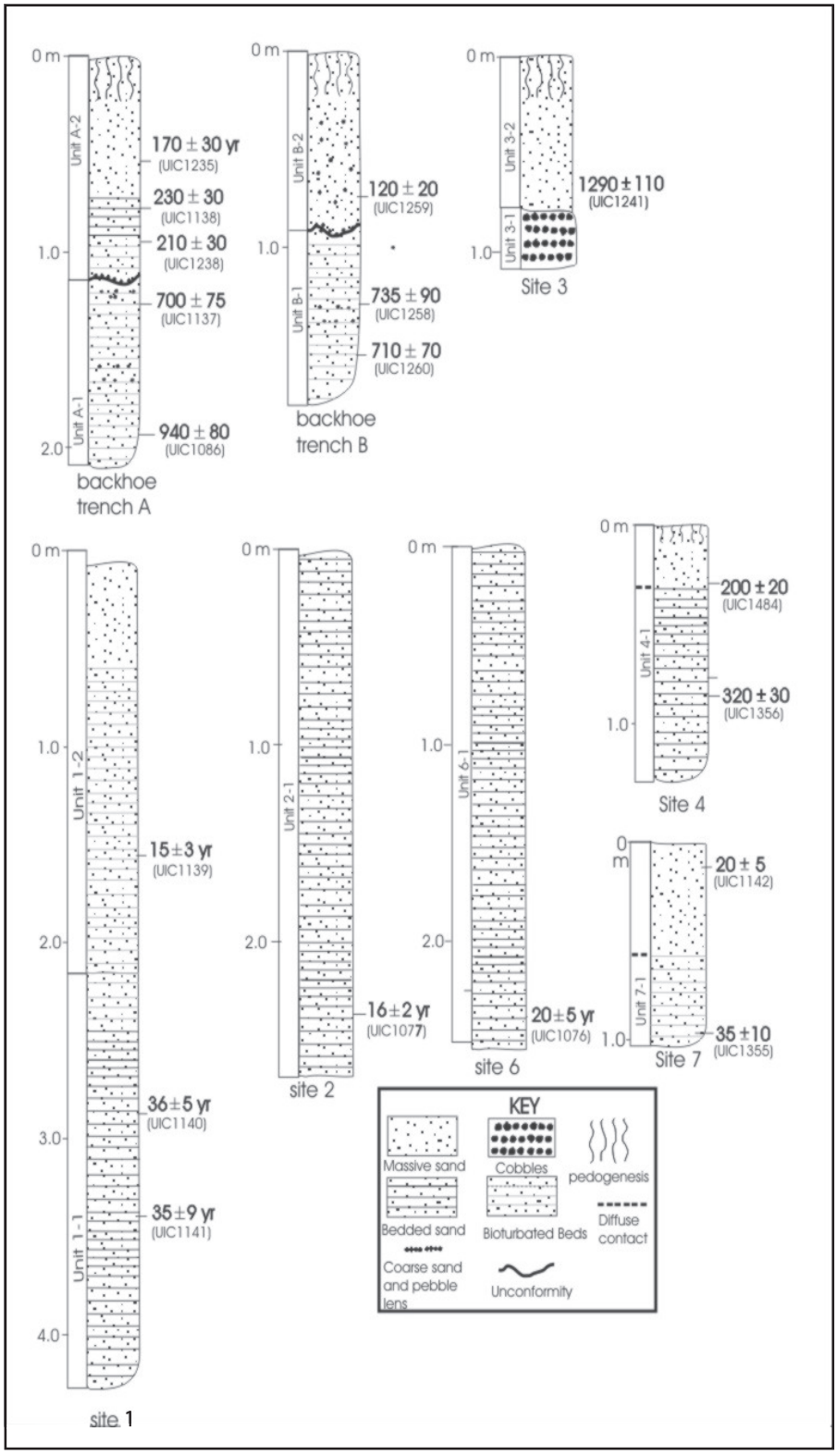

Figure A2–4. Stratigraphic sections of eolian sand deposits at sites and trenches west of stop A3, as shown in figure A2–3.

it forms star, barchan, transverse, and reversing dunes, whereas the subjacent moisture-bearing sand is cohesive and forms a boundary for eolian transport.

Preliminary OSL dating of eolian sand from these water-bearing sands indicates that the lower sand is about 270 years old, whereas the uppermost sand was deposited in the past 60 years (fig. A2–5). These early results indicate that part of the dune field adjacent to Medano Creek was accreted in the past 300 years.

Eolian Sand Depositional History

In the past 1,300 years there have been at least 13 droughts of sufficient magnitude to result in dune remobilization to varying extent at GSDNPP. These droughts are inferred from the tree-ring-derived Palmer Drought Severity Index (PDSI) and annual precipitation records (fig. A2–6). The severest droughts, lasting decades and with broad impact across North America, occurred during the 8th, 11th, 13th and 16th Centuries (Woodhouse and Overpeck, 1998; Stahle and others, 2000). These droughts were equal to or more severe than the driest conditions in the 20th Century for which we have documented changes in dune migration and vegetation coverage at in the Park (Marin and others, 2005). Our field- and laboratory-based study provides a conservative assessment of dune reactivation or formation with at least seven potential events at about 1280±100, 715±80, 310±30, 200±20, 130±10 years ago, and in the 20th Century. However, some of the severest droughts are not represented in the stratigraphic record; thus, this incomplete assessment reflects the paucity of well-dated stratigraphic localities and the vagaries of erosion and deposition in parabolic dune systems. The nascent chronology does indicate that the transport of eolian sand across San Luis Valley, ultimately nourishing the dune field against the Sangre de Cristo Mountains, was an episodic process during the late Holocene, with appreciable dune migration in the 8th, 10–13th, and 19th Centuries.

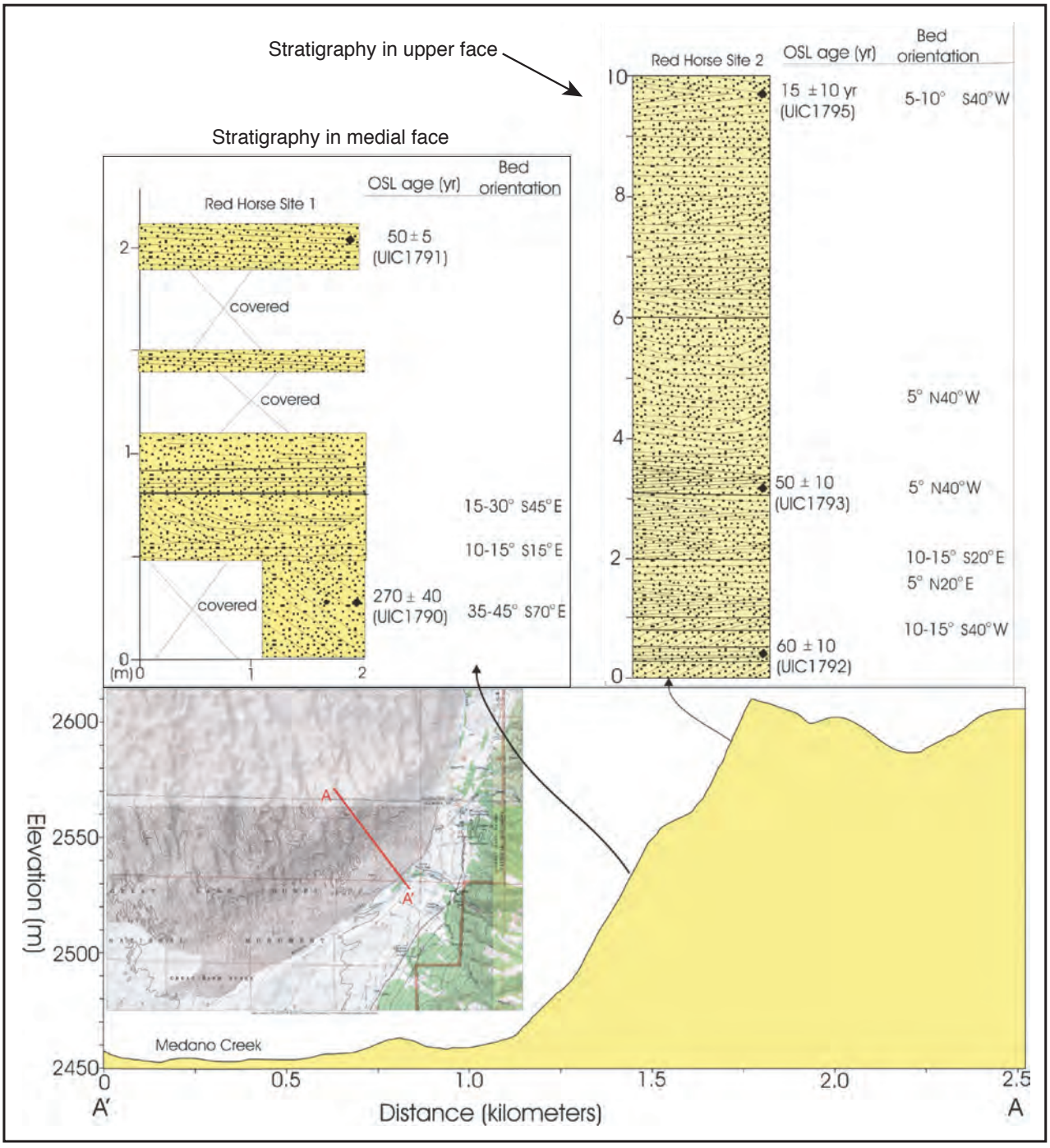

Figure A2–5. Optically stimulated luminescence ages of eolian sand deposits on the accreting face of the large dune west of stop A1.

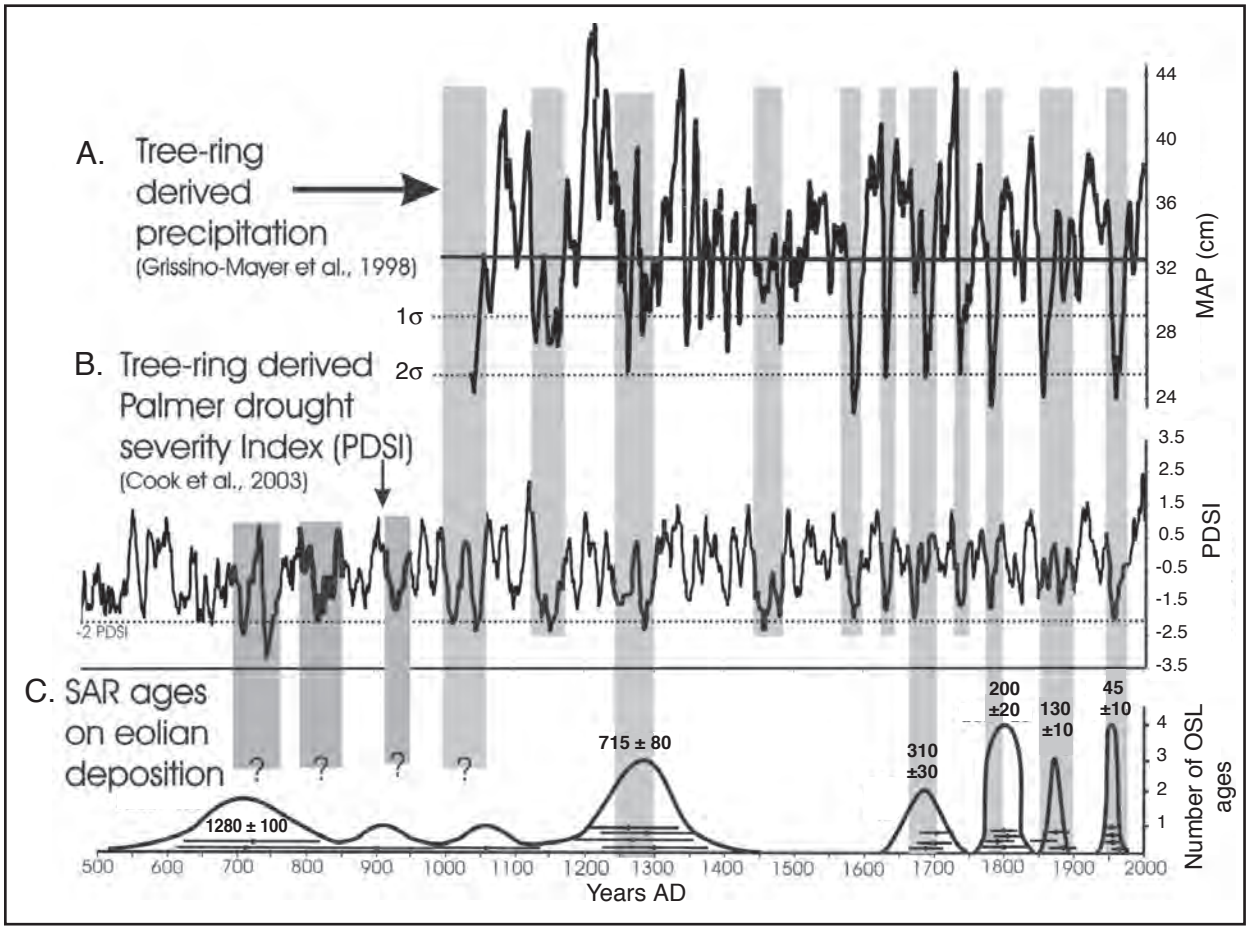

Figure A2–6. Climatic data and times of eolian sand deposition. *A*, Inferred mean annual precipitation (MAP) since AD 1000 near lower treeline at Great Sand Dunes National Park and Preserve (GSDNPP) from tree-ring time series (Grissino-Mayer and others, 1998). *B*, Inferred summer Palmer Drought Severity Index (PDSI) for upper treeline since AD 500 from tree-ring time series (point #132: 37.5° N., 105.0° W.; Cook and others, 2003). *C*, Frequency distribution showing 2-sigma range of single-aliquot regeneration (SAR) ages on eolian sand depositional events at GSDNPP. Horizontal black bars indicate individual SAR ages. Vertical grey bars indicate possible correspondence between eolian depositional events and droughts in the tree-ring record. There is greater uncertainty in associating drought where there is just a single SAR age constraining eolian depositional events as is shown by shorter grey bands ending in a question mark.

Stop A3 — Paleoseismology of Range-Front Fault Scarps at Great Sand Dunes

Speaker: James McCalpin
Location: Great Sand Dunes National Park and Preserve, near NPS residential water tank
Zapata Ranch 7.5' quadrangle
GPS: NAD27, Zone 13, 455170 m E., 4175333 m N.
Elevation: 8,320 ft

Synopsis

At this stop we will examine fault scarps on Quaternary deposits along the range-front traces of the northern Sangre de Cristo normal fault zone. In 2002 and 2003, a research team from the Crestone Science Center mapped fault scarps and excavated four trenches for paleoseismology in the Morris Gulch and Visitor Center areas (fig. A3–1). The trenches across the Morris Gulch scarps exposed evidence for two post-Pinedale (post-15 ka to 35 ka) surface-rupturing earthquakes, each with vertical displacements of about 1.7–2.3 m. Those displacements alone imply that the earthquakes had moment magnitudes of about 6.9–7.0. The most recent event occurred about 5.3–5.5 ka, whereas the prior event occurred sometime in the early Holocene or latest Pleistocene (10–15 ka?). Thus, the recurrence interval could range from 4.5 to 9.7 k.y. The most-recent-event elapsed time of 5.3–5.5 k.y. composes 55–122 percent of the most recent recurrence interval. In contrast, a trench across the scarp directly below the GSDNPP Visitor Center failed to expose a tectonic fault but instead exposed an old landslide(?) failure plane. The scarp is probably caused by stream erosion, which unweighted the toe of the failed material. Therefore, we interpret the Visitor Center scarp as a probable fluvial scarp eroded by ancestral Medano Creek that poses no direct threat to the Visitor Center. The only infrastructure at the Park directly threatened by future fault surface rupture is the water tank, which stores potable water for the park headquarters and employee housing area. However, all structures in the Park would be subjected to strong ground shaking in the event of an **M** 7 earthquake. This ground shaking could reach horizontal and vertical accelerations of as much as 0.5–1 g and last for 30–40 s. However, with a return time of about 5,000 to 10,000 years for such earthquakes, the annual probability of such strong ground shaking is on the order of 1/5,000 to 1/10,000. A more complete discussion of these subjects is included in a comprehensive contract report to the National Park Service (McCalpin, 2006).

Tectonic Setting

The Park lies astride the northern Sangre de Cristo fault zone, which is the eastern-margin fault of the San Luis Valley. This fault zone is a west-dipping, normal, and the master fault of the San Luis Valley, which is in turn two east-tilted half-grabens and an intervening horst. Geophysical data suggest that the total Neogene throw on the northern Sangre de Cristo fault zone is at least 4 km (Brister and Gries, 1994). The Mapco State geothermal test well drilled in the graben 5 km west of Great Sand Dunes reached Precambrian basement at a depth of 2.9 km, but it was not located in the deepest gravity low (see also fig. A7–1, stop A7). Thus, the depth of basin-filling sediment probably exceeds 3 km in depth.

The fault zone has remained active into the Holocene, as evidenced by single-event fault scarps that displace Holocene deposits about 1.5–2.5 m (McCalpin, 1982). Mapping of older deposits such as Pinedale, Bull Lake, and pre-Bull Lake alluvial fans is based on topographic location, geomorphic expression, and soils. These three groups of glacial-age deposits have range-front fault scarps 3–8 m high, 5–13 m high, and as much as 85 m high, respectively. Given its length (about 120 km), its average vertical slip rate (0.1–0.3 mm/yr), and its recent movement (mid-Holocene), the northern Sangre de Cristo fault zone is considered Colorado's most active and hazardous fault.

The fault zone was divided into three sections by Widmann and others (1998). Stop A3 is on the Zapata section, a linear, 23- to 27-km-long section of the fault zone that trends N. 10° E. from the western foot of Blanca Peak to Medano Creek, north of which the northern Sangre de Cristo Range changes strike by 45°, suggesting that it may be a section boundary (see discussion in chapter J, this volume).

Quaternary Faulting on the Zapata Section

Fault scarps are more or less continuous across the heads of range-front alluvial fans in the Zapata section, all of which were assigned to the Pinedale glaciation by McCalpin (1982) (fig. A3–1). Where the fault zone is expressed as a single fault scarp, its vertical surface offset (vertical separation) ranges from 2.8 to 6.0 m. In several places south of the Park there are two closely spaced, parallel, down-to-the-west fault scarps at the fanhead, and these double scarps have combined vertical surface offsets of 5.9–7.2 m. In general, surface offsets increase southward from the Pinon Flats Campground in GSDNPP (3.4 m) to South Arrastre Creek (7.2 m), a distance of 6 km, in deposits of presumably identical age. The fault zone is expressed at the range front by a single trace, and pre-Pinedale-age deposits on the hanging wall are everywhere buried by Pinedale fans. Generally along the northern Sangre de Cristo fault zone, pre-Pinedale deposits are exposed only if multiple parallel traces exist with sufficient late Quaternary throw to bring up pre-Pinedale deposits in a fault-bounded sliver. [NOTE: the published 1:24,000-scale USGS geologic maps (Johnson and others, 1989; Bruce and Johnson, 1991) do not map the range-front Quaternary fault scarps, but instead generalize the fault zone as a dotted line placed arbitrarily across the upper to middle parts of the alluvial fans.]

The southern end of the Zapata section is difficult to identify because scarps south of South Arrastre Creek are no

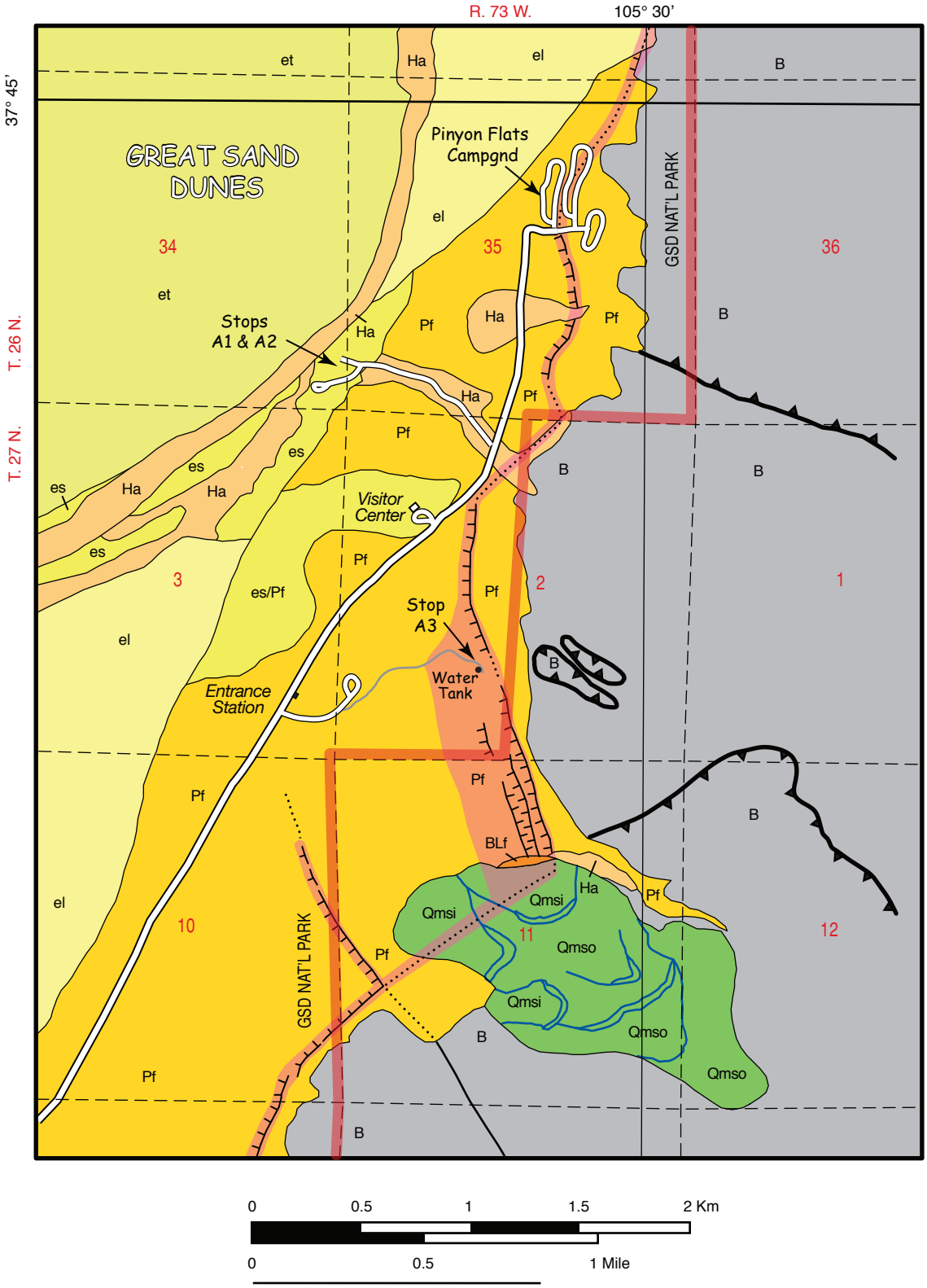

Figure A3–1. Geology of Great Sand Dunes National Park in the vicinity of the Visitors Center. Geologic units and mapping modified slightly from McCalpin (2006). Eolian sand units: et, transverse dunes; el, longitudinal dunes; es, undivided sand. Alluvial units: Ha, Holocene; Pf, Pinedale (late Pleistocene); BLf, Bull Lake (late middle Pleistocene). Landslide deposit units: Qmsi, younger; Qmso, older. Other units: B, bedrock (undivided Pennsylvanian Minturn Formation and Precambrian granitic gneiss). Shaded zone along faults indicates high hazard from surface fault rupture. Morris Gulch and trenches shown on figure A3–2.

longer continuous along the base of the range front. Instead, the southernmost Quaternary fault scarp is an anomalous 2.6 km-long scarp that crosses Urraca Creek, 14.7 km south of this stop. The anomalous scarp trends N. 10° W. and lies 1.7 km west of the range front, at the toe (rather than the head) of the alluvial fan. It is also 5 km south of the nearest range-front scarp. On this short scarp, early Holocene deposits are displaced 2.0–2.1 m vertically, Bull Lake deposits 6.1–7.1 m, and pre-Bull Lake deposits 8.4–10.6 m vertically (McCalpin, 1982). The paleoearthquake responsible for faulting the early Holocene deposit occurred about 5 ka.

What We See at Stop A3 (Water Tank)

Stop A–3 shows several fault scarps on the Pinedale-age (inferred) alluvial fan of Morris Gulch (fig. A3–2). Compared to fault scarps elsewhere in the section, this fault scarp is anomalous in several ways: (1) there are four parallel fault scarps (A, B, C, D) of subequal height in a zone 300 m wide; (2) the scarps trend north-northwest, but the range front trends north-northeast; and (3) owing to their north-northwest trend, the scarps obliquely cross contours and some stream flow has followed along their bases.

Paleoseismology of the Morris Gulch Scarps

The Morris Gulch scarps (A–D) represent two surface-faulting events that displace the surface of a Pinedale-age alluvial fan in a wide zone of parallel scarps. The cumulative vertical displacement across the scarps is on the order of 8 m, which is slightly greater than the 5.2–7.2 m of throw calculated for scarps south of Morris Gulch (McCalpin, 2006). Trenches B, C, and D indicate that the per-event displacement on each scarp during these events ranges from about 1.5 m (the 3 m net displacement on scarp B, divided by 2), to 1.7 m (single-event displacement from trench C; see fig. A3–3), to 1.65 m (net displacement of 3.3 m in trench D, divided by two). The average cumulative displacement per event on all three scarps would thus range from 3.15 m (without the single scarp C event) to 4.85 m (with the scarp C displacement), if we neglect any component of back-rotation between the scarps. These displacements of 3.15–4.85 m are roughly similar to those measured south of Morris Gulch, where the average per-event displacement was 3.15 m.

Those per-event displacements imply earthquakes of moment magnitude (**M**) 6.96–7.10 if the displacements are assumed to be the maximum that occurred in the event, or **M** 7.10–7.22 if they are assumed to represent an average displacement (Wells and Coppersmith, 1994). The larger magnitude is probably a better estimate, considering the fact that each surface rupture was associated with meter-scale displacement on at least 3, and perhaps 4, parallel fault strands.

The radiocarbon ages from this study indicate that the most recent event occurred about 4.8–5.3 ka, at least on scarp D. Simultaneous rupture on scarps B and C is supported by the overall stratigraphy in their respective trenches. This age is similar to the age of surface rupture deduced by McCalpin (1982) at the Urraca Creek trench south of the Monument, which had a closely limiting maximum of about 5.5 ka. The timing of the paleoevent (PE) is not constrained by numerical ages but must be post-Pinedale. The degree of soil development in trench B suggests that the interevent time between the most recent event (PE1) and PE2 is on the same order as the

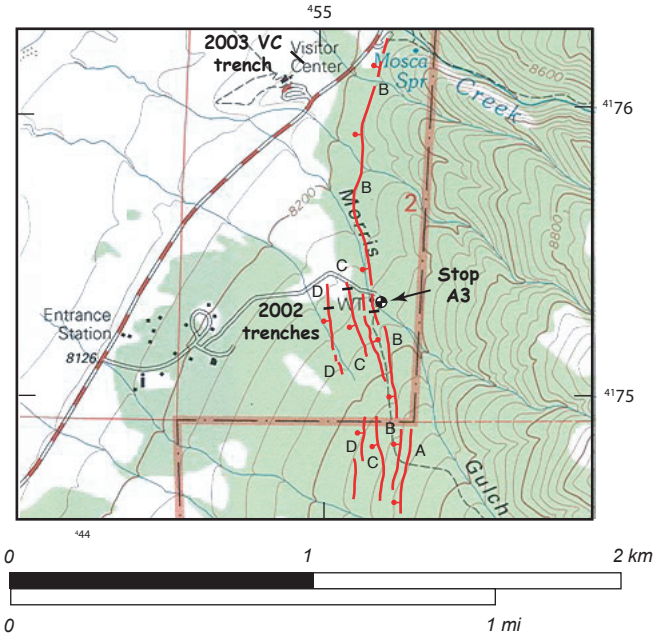

Figure A3–2. Faults on the alluvial fan of Morris Gulch and location of stop A3, Water Tank trench site. Red lines A–D, fault strands with ball on downthrown side; black bars, trenches. Map scanned from Zapata Ranch, Colorado, 7.5-minute topographic map.

Figure A3–3. Trenching operations during 2002 at scarp C. View to the northwest from the top of the fault scarp. Dunes visible in background.

time between the most recent event and present, or roughly 5,000 years. However, McCalpin (1982) estimated that the long-term (post-Bull Lake) recurrence on the Zapata section of the northern Sangre de Cristo fault zone was on the order of 10–20 k.y.

Large Bedrock Landslide South of Morris Gulch

South of Morris Gulch, fault scarps end at the flank of a west-protruding bedrock ridge but then reappear at the range front south of the ridge (red lines in fig. A3–4). The surface morphology of this ridge does not resemble that of any other ridge along the range front of the Sangre de Cristo Mountains. Rather than being a narrow-crested, steep, erosional ridge as is typical of faceted-spur range fronts, this ridge has a broad, low-gradient crest composed of alternating benches and scarps (yellow lines in fig. A3–4). In addition, there are several closed or nearly closed depressions on the ridge crest. Overall, the ridge looks like a giant landslide, yet the entire ridge is mapped as Precambrian gneiss by Bruce and Johnson (1991).

Field reconnaissance reveals that outcrops of Precambrian gneiss do exist throughout the ridge crest, but the foliation directions are random. Gullies cut into the flanks of the ridge expose outcrops of red sandstones and siltstones of the late Paleozoic Minturn Formation about 10–15 m below the ridge crest. As shown by Bruce and Johnson (1991), this part of the Sangre de Cristo range is composed of thrust sheets of Precambrian gneiss thrust eastward over Paleozoic sedimentary rocks; the thrust strikes N. 5° E. to N. 10° E. and dips 19° W.

It appears that the landslide ridge is underlain by a thin sheet of highly fractured Precambrian gneiss no more than 10–15 m thick, lying on a Laramide thrust fault that dips west at about 19°. The moderately steep dip of this thrust fault toward the valley and its weak (?) material properties have combined to induce incipient westward landsliding and dismemberment of the Precambrian slab. Westward slippage was probably also induced by the strong earthquake shaking that accompanies **M**>7 earthquakes on the northern Sangre de Cristo fault zone here roughly every 10,000 years (see discussion in McCalpin, 2006). As the range has been uplifted above the valley floor, this west-dipping Laramide thrust fault has been progressively "daylighted" on the range-front slopes. The daylighting removes the lateral support from the downslope end of the west-tilted slab of gneiss, allowing it to begin to stretch and extend valleyward.

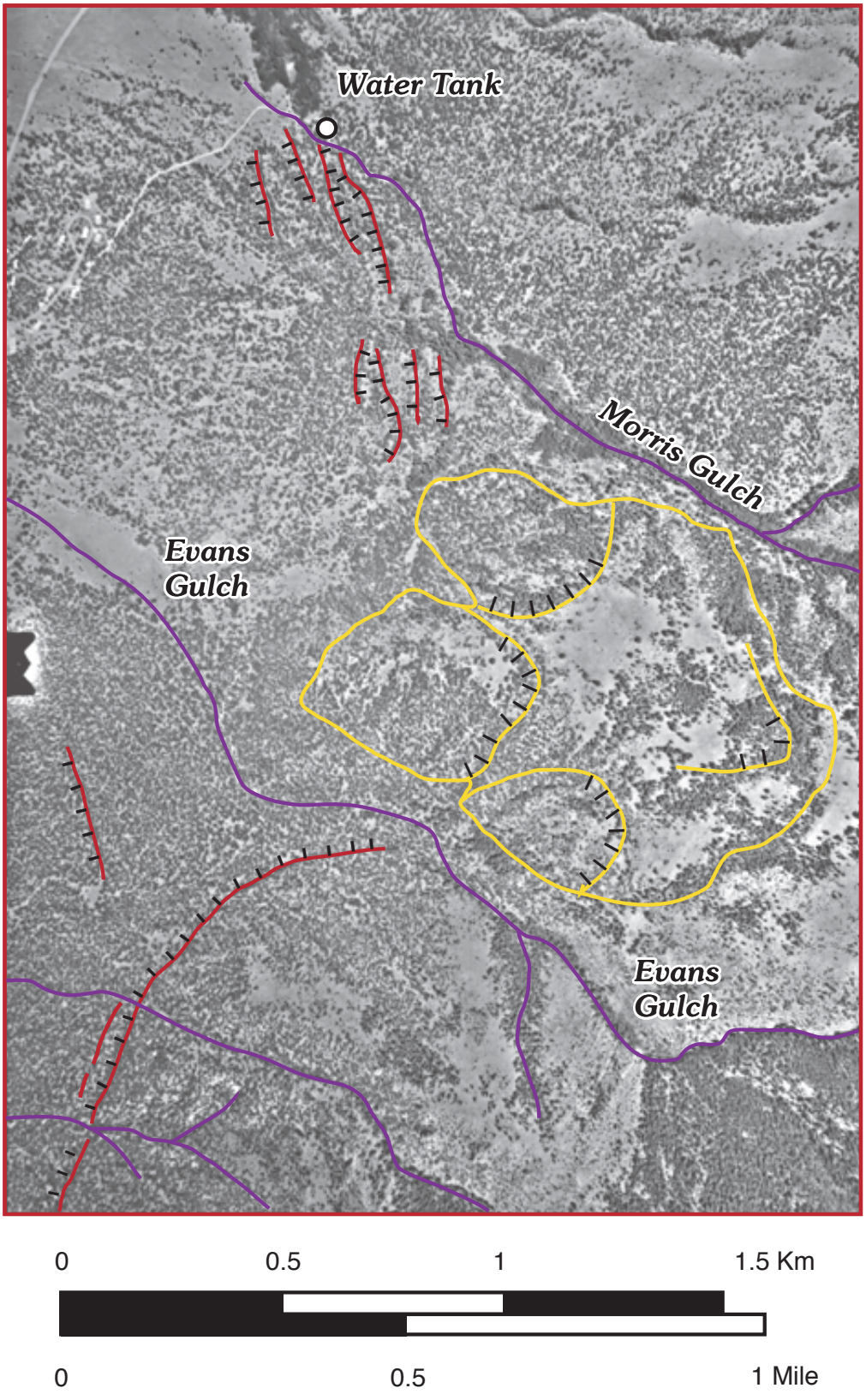

Figure A3–4. Fault scarps (red lines), landslides (yellow lines), and stream drainages (blue lines) along and adjacent to Morris Gulch. Location of Water Tank shown on figures A3–1 and A3–2.

Stop A4 — Parabolic Dune Migration Across the Southern Sand Sheet

Speaker: Steve Forman
Location: Great Sand Dunes Oasis (general store) parking lot
Zapata Ranch 7.5' quadrangle
GPS: NAD27, Zone 13, 451720 m E., 4171630 m N.
Elevation: 7,970 ft

Synopsis

The Great Sand Dunes National Park and Preserve in Colorado contains one of the largest and tallest intermountain dune systems in North America (fig. A2–1). This active dune field rises to heights of 250 m above the San Luis Valley, is banked against the Sangre de Cristo Mountains, and contains a rich variety of dune types. The response of the Park's dune system to well-documented droughts that affected large parts of western North America in the past 70 years (1930s, 1950s, 1960–64, 1971–74, 1977–81, 1989–90, and 2000–04) is the focus of both recent and other ongoing research (Marin and others, 2005).

The focus of this study is the sand sheet area, which fronts the dune field to the north, south, and west. The sand sheet harbors mostly vegetated and stabilized kilometer-long parabolic and barchanoid dunes that indicate dominant winds from the west-southwest. The distinct morphology of these dunes, well-defined wind formational processes, and readily identifiable forms in remotely sensed images provide straightforward targets to assess changes in dune position. To evaluate the response of these active parabolic and barchanoid dunes, a time series of aerial photographs and remotely sensed images from 1936 to 1999 was studied by image analysis and geographic information system (GIS) techniques and complemented with field assessment. The extent of dune migration was evaluated with respect to climate parameters, such as precipitation and the Palmer Drought Severity Index (PDSI), to understand better the landscape's response to varying levels of drought in the 20th Century. This stop provides insight into how semiarid landscapes respond to drought and quantifies thresholds and rates for dune migration at Great Sand Dunes National Park.

Discussion

Understanding dune dynamics in the western United States is critical to assessing semiarid landscape response to past climate variability (Overpeck, 1996; Woodhouse and Overpeck, 1998; Forman and others, 2001). The stratigraphic and geomorphic records of eolian deposition in the Basin and Range Province and Great Plains serve as proxies for the timing and magnitude of large-scale droughts in the past 10,000 years of sufficient severity for the widespread movement and accumulation of eolian sand (for example, Wells and others, 1990; Forman and others, 2001, 2006; Forman and Pierson, 2003; Mason and others, 2004). A variety of paleoclimatic studies in central North America show possible relationships between episodes of past eolian activity and drought intervals for the past 2,000 years (for example, Muhs and others, 1997; Woodhouse and Overpeck, 1998 and references within; Forman and others, 2001, 2006; Wolfe and others, 2001; Forman and Pierson, 2003). Periods of aridity in the western United States directly affects growing season moisture and vegetation; this lack of moisture is associated with reduction in rainfall and increases in evapotranspiration (Schlesinger and others, 1990; Lancaster, 1997). However, sustained drought in semiarid areas is associated with complex surficial processes that promote the heterogeneous distribution of soil nutrients leading to degradation of grasslands and subsequent invasion by desert shrubs (Shulka and Mintz, 1982; Schlesinger and others, 1990; Huenneke and others, 2002). Other surface disturbances such as grazers and off-road vehicles increase soil heterogeneity and erosion, enhancing the availability of sediments for eolian entrainment (Schlesinger and others, 1990). Questions remain on the sensitivity of dune systems in semiarid landscapes, such as that at Great Sand Dunes, to drought variability in the 20th and beginning of the 21st Centuries.

Remote Sensing of Eolian Landforms

Remote sensing and GIS techniques are powerful tools for registering land surface changes and for quantifying dune migration at Great Sand Dunes. This stop will highlight a digital database of 15 remotely sensed images that are used to understand changing surficial processes with evolving drought conditions at Great Sand Dunes. Fourteen sets of aerial photographs that cover all or a portion of the area were obtained from Great Sand Dunes and scanned into digital format with an original resolution of 0.8 m/pixel. This database contains aerial photography from 1936, 1937, 1938, 1941, 1953, 1955, 1957, 1966, 1975, 1979, 1981, 1983, 1988, 1995, and 1998 (table A4–1). A Landsat Enhanced Thematic Mapper Plus (ETM+) image from 26 July 1999 (Path 33, Row 34) processed with radiometric, geometric, and precise correction of parallax error was added to the database (fig. A4–1, table A4–1). This image served as a reference to assess dune position and land cover changes. False color composition images from the Landsat ETM+ using visible (1, 2, and 3) and infrared (4, 5, and 7) bands (25-m resolution) and panchromatic (10-m resolution) are superb for identifying large-scale dune forms and to separate active eolian sand from areas covered by vegetation or water (Marin and others, 2005). To facilitate georeferencing and later comparison among images, the 1998 digital orthoquadrangle from the U.S. Geological Survey (Terraserver, 2004) at 2-m resolution and the ETM+ image were coregistered using image-to-image methods having first-order polynomial model universal transverse Mercator (UTM) coordinates (Zone 13, Clarke 1866 spheroid, and NAD

27 datum). Aerial photographs were coregistered with a 1998 orthoquadrangle using the same georeferenced model. Digital mosaics for each set of data were produced from the respective georeferenced aerial photographs. These mosaics have a spatial resolution of 2 m and errors ranging from 5 to 45 m, depending on the number and location of control points (that is, roads, buildings, and fence lines) in the image-to-image coregistration (table A4–1). The largest errors (42–45 m) were generated in the registration process of digital mosaics (1953, 1966, and 1979) provided for GRSDNPP by Hammond (1998). However, despite these spatial resolution and georeferencing errors, the images are appropriate for tracking decadal positional changes of individual and compound parabolic and barchan dunes, with total dune migrations between 150 and 650 m in the past 63 years. Additional geographic and topographic information for geomorphic assessments is from a digital terrain model (30 m resolution) from the U.S. Geological Survey (Mapmart, 2004). ENVI 3.4 and ERDAS Imagine 8.2 programs are used for imagery preparation, georeferencing, combination, and enhancement. GIS-ARC/View 3.2 is used for visual and quantitative analyses of landscape elements and to document changes in dune coverage, extent and form, vegetation cover, and water resources.

Quantitative Analysis of Parabolic Dune Migration From 1936 to 1999

The position of well-formed parabolic dunes (PD) on the sand sheet (figs. A4–1 and A4–2) is tracked using 16 sets of remote sensing data from 1936 to 1999 (table A4–1). The parabolic dunes are conspicuous on the images as elongated, "hairpin" forms that often occur in an en echelon configuration, forming compound parabolic dunes (fig. A4–2). The arms of the parabolic dunes are mostly vegetated by grasses and shrubs and can be traced for up to about 3.5 km. Individual dunes are conspicuous in images from the 1930s, whereas compound parabolic dunes are common in the late 20th Century (figs. A4–2 and A4–3). Today, these dunes are as much as 4 m high and are oriented N. 35° E. to N. 40° E., reflecting predominantly southwesterly winds (fig. A4–2). Dune migration is associated with blowout of the parabolic dune rim and downwind migration of the slip face (Greeley and Iversen, 1987, p.172–173).

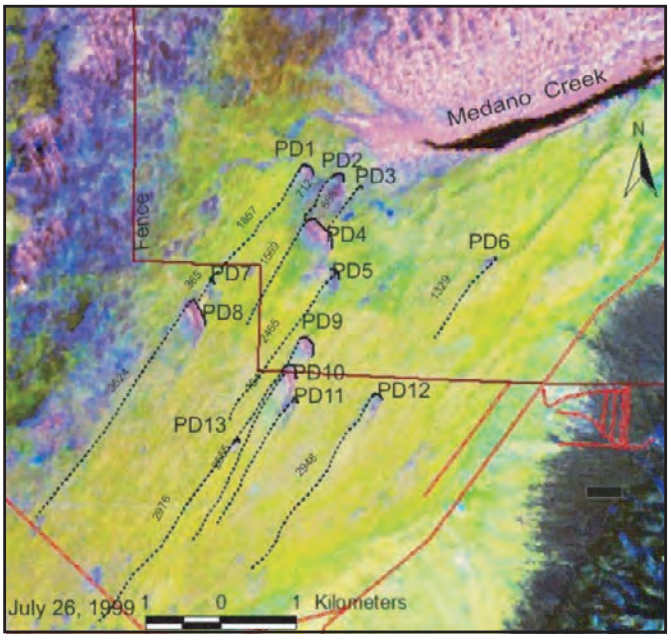

Figure A4–1. Digital terrain model of the southwest part of Great Sand Dunes National Park and Preserve. The southeast sand-sheet area (with site numbers, such as PD12) is the focus of this study (modified from Forman and others, 2006).

Changes in position of 13 parabolic dunes (PD1–PD13) were tracked on the remote sensing imagery time series (table A4–2, fig. A4–3). This analysis provides estimates for net, total, and rate of dune migration and associated errors (table A4–2). The extent of dune migration was assessed relative to a mosaic of the oldest aerial photographs that were taken on 12 August 1936 (table A4–1). The dunes on these photos range in length from about 0.7–3.5 km and are readily identified on images from all years (figs. A4–2 and A4–3, table A4–2). The longest parabolic dunes (about 3.5–2.5 km) are present to the south of the Park fence where the arms are minimally disturbed by a road that goes to San Luis Lake (parabolic dunes 5, 8, 10, 12, and 13 in fig. A4–3, table A4–2). North of the Park fence, the arms of parabolic dunes are truncated, merging into compound forms and often reworking sand from previously stabilized arms.

Evaluating dune migration at GSDNPP is constrained by the temporal spacing of aerial photographic coverage. Assessment of completeness in the geologic record stresses that the estimated rate of change increases with number of dated observations and that calculated rates often are underestimates (Sadler and Strauss, 1990; Sadler, 2004). Thus, estimates of the rate of dune migration in the Park may be minima, reflecting the variable time interval (1 to 13 years) between images. However, dune migration rates for successive years and for decadal intervals with more than three mosaics may provide close to finite estimates, specifically when longer time steps do not result in a reduction in rate compared with shorter intervals.

The 13 parabolic dunes monitored between 1936 and 1938 yield an apparent range of velocities between 2 and 70 m/yr, with an average velocity of 16 m/yr (table A4–2, fig. A4–4). Between 1938 and 1941, 12 of the 13 dunes (all except PD3) accelerated to one of the highest velocities measured (16 to 46 m/yr); the highest average migration rate was 32 m/yr (table A4–2). Dune migration rates decreased from 1941 to 1953, ranging from 0.3 to 10 m/yr and averaging 5 m/yr. Subsequently, between 1953 and 1955 drift rates increased for 7 (PD1, PD2, PD3, PD4, PD8, PD9, and PD11) of the 13 dunes; the rates ranged from 1 to 44 m/yr with an average 14 m/yr for all 13 dunes. The slowest rates of dune migration of (<10 m/yr) were registered between

Table A4–1. Remote-sensing imagery used to assess migration of parabolic and barchan dunes at Great Sand Dunes National Park and Preserve.

Georeferenced mosaics	Original scale	Pixel size (m)	RMS[c] (m)	UTM coordinates location[d]				Coverage GSDNPP (percent)	Source[e]
				ULX	ULY	LRX	LRY		
August 12, 1936	1:31,680	2	39	440838	4190169	456246	4162357	70	GSDNPP and SCS
September 26, 1937	1:20,000	2	35	442267	4188903	446869	4176191	30	GSDNPP and SCS
August 9, 1938	1:30,000	2	11	446927	4175580	451861	4170556	30	GSDNPP and SCS
November 15, 1941	1:20,000	2	15	438492	4185984	459420	4160848	80	National Archives
October, 1953	1:53,000	2	44	436028	4192183	458292	4167447	100	Hammond, 1998
August 22, 1955	1:20,000	2	42	442778	4179184	456050	4165752	50	GSDNPP and SCS
September 25, 1957	1:20,000	2	7	444438	4187469	450192	4181533	20	GSDNPP and SCS
July 2, 1966	1:20,157	2	45	440050	4190136	457322	4167314	50	Hammond, 1998
September 25, 1975	1:80,000	2	7	430687	4193302	448539	4169846	50	GSDNPP and SCS
September 5, 1979	1:78,000	2	45	433723	4193002	457619	4164562	100	Hammond, 1998
June 11, 1981	1:40.000	2	18	442549	4190336	456813	4154912	95	GSDNPP and SCS
September 16, 1983	1:58,000	2	18	444570	4190779	456576	4166533	90	GSDNPP and SCS
September 4, 1988	1:40,000	2	18	438702	4188794	457400	4169686	90	GSDNPP and SCS
July 26, 1995	1:24,000	2	21	443239	4175190	453843	4168622	30	GSDNPP and SCS
September 6, 1998	1:40,000		5	441653	4188608	457641	4164558	100	GSDNPP, SCS, USGS
PAN[a] July 26, 1999		10	10	422266	4194108	460791	4157533	100	EROS Data Center
IR/VISIBLE[b]		25	25	422266	4194108	460791	4157533	100	EROS Data Center

[a]Panchromatic band of the Landsat enhanced thematic mapper image.

[b]Infrared (bands 4, 5, and 7) and visible (bands 1, 2, and 3) of the Landsat enhanced thematic mapper image.

[c]Root mean squared error associated with the georeference process.

[d]ULX, ULY: Upper left X and Y coordinates. LRX, LRY: Lower right X and Y coordinates. Corresponds with UTM Zone 13, spheroid: Clarke 1866 and datum: NAD27.

[e]EROS, Earth Resources Observation System; GSDNPP, Great Sand Dunes National Park and Preserve; SCS, Soil Conservation Service; USGS, U.S. Geological Survey.

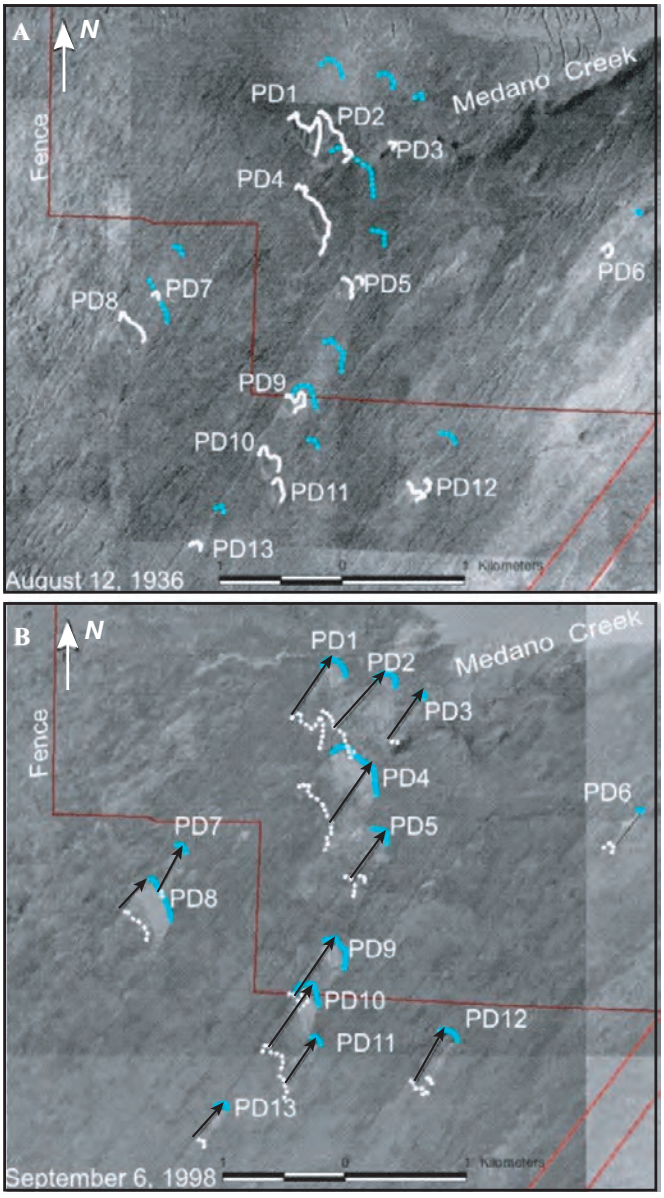

Figure A4–2. Aerial images of parabolic dunes in the Great Sand Dunes National Park and Preserve. Labels refer to studied dunes (that is, for instance, PD1). *A*, Aerial photograph from August 12, 1936. Solid white lines show the position of the parabolic dunes in 1936, and the dotted blue lines represent the position of the same dunes on a Landsat image from July 26, 1999. *B*, Aerial photograph from September 6, 1998. Solid blue lines show the position of the parabolic dunes on a Landsat image from July 26, 1999, and dotted white lines show the location of the dunes on August 12, 1936 (part *A*). Black arrows show the direction and magnitude of the dune advance in 63 years (modified from Forman and others, 2006).

1955 and 1979, followed by acceleration of 9 (PD4, PD5, PD6, PD7, PD8, PD9, PD10, PD11, and PD13) of the 13 dunes between 1979 and 1981 at velocities ranging from 2 to 37 m/yr and averaging 16 m/yr for all dunes (table A4–2). Dunes were relatively quiescent between 1981 and 1983; 8 of the 13 dunes yielded velocities of <8 m/yr. For the past 25 years (between 1983 and 1988, 1988 and 1995, and 1995 and 1998), dune migration rates remained low and velocities were <10 m/yr for at least 7 of the 13 dunes. The position of parabolic dunes between 1998 and 1999 changed dramatically, with 12 of the 13 dunes accelerating to 14 to 76 m/yr and 6 of the dunes (PD4, PD6, PD9, PD10, PD11, and PD13) showing the highest drift velocities yet measured (table A4–2). The average dune migration rate between 1998 and 1999 was 30 m/yr, which is similar to migration rates for the period 1938–1941, in which all dunes registered either the highest or next to highest recorded velocities (table A4–2, fig. A4–4).

Summary

In summary, the total parabolic dune migration from 1936 to 1999 for the 13 measured dunes ranges from 313–665 m toward the northeast; corresponding average rates for individual dunes range from 5–11 m/yr with an average rate of about 8±1.6 m/yr for all dunes (table A4–2, fig. A4–3). A significant observation is that between 1936 and 1999 the largest dunes with active areas of 0.04 km^2 to 0.23 km^2 (PD1, PD2, PD8, PD9, and PD10) show average migration rates (about 9 m/yr) that are 30 percent greater than rates (about 6 m/yr) observed for smaller dunes with areas of <0.004 km^2 (PD3, PD5, PD6, PD7, PD11, PD12, and PD13). Nearly half of the total dune migration between 1936 and 1999 occurred prior to 1955, mostly associated with drought intervals in the 1930s and 1950s. Approximately 30 percent of dune migration occurred between 1955 and 1981 and 15 percent from 1981 to 1995. As much as 10 percent of the total dune drift occurred since 1995 and 1998 for dunes 4, 7, 11, and 12 and dunes 6, 10, and 13 (respectively) reflecting drought conditions in the late 20 Century (table A4–2).

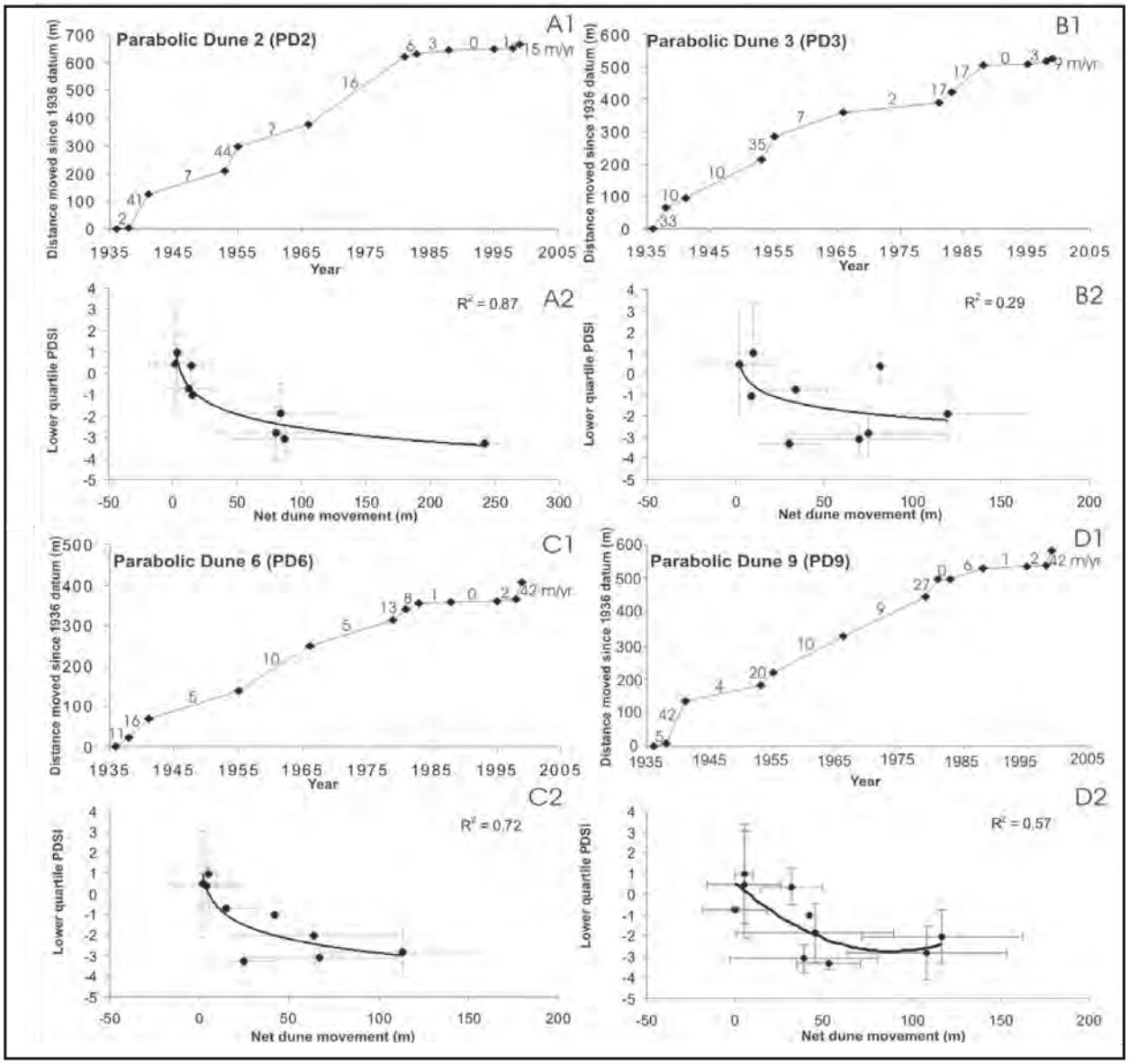

Figure A4–3. Quantitative analysis of parabolic dune migration rate from georeferenced mosaics of imagery from 1936 to 1999 (table A4–1, fig. A4–2). Graphs A1, B1, C1, and D1 show absolute migration (in meters) for parabolic dunes 2, 3, 6, and 9 relative to their position in 1936. The numbers adjacent to line segments are dune migration rates (meters/year). Graphs A2, B2, C2, and D2 show the logarithmic relation between net parabolic dune migration and the Palmer Drought Severity Index (PDSI) lower quartile. Shown are 1-sigma PDSI errors and net dune migration errors, reflecting the root mean squared errors from mosaicking and georeferencing images (table A4–2).

Table A4–2. Migration of parabolic dunes (PD) measured from 1936 to 1999 at the Great Sand Dunes National Park and Preserve (GRSA) and associated Palmer Drought Severity Index (PDSI).

Intervals	Net migration of parabolic dunes (m)														Migration rates for parabolic dunes (m/yr)													PDSI [b]
	PD1	PD2	PD3	PD4	PD5	PD6	PD7	PD8	PD9	PD10	PD11	PD12	PD13	Error (m)[a]	PD1	PD2	PD3	PD4	PD5	PD6	PD7	PD8	PD9	PD10	PD11	PD12	PD13	Ave. rate[c]	lowest 25%
1998-99	14	15	9	48	2	42	16	25	42	76	42	22	32	10	14	15	9	48	2	42	16	25	42	76	42	22	32	**30 ± 20**	-1.0
1995-98	0	3	10	44	3	5	3	26	5	21	30	17	31	5	0	1	3	15	1	2	1	9	2	7	10	6	10	5 ± 5	1.0 ± 2.4
1988-95	46	2	2	46	1	2	63	28	5	85	19	22	7	21	7	<1	0	7	0	0	9	4	1	12	3	3	1	4 ± 4	0.5 ± 2.6
1983-88	15	14	82	22	16	4	62	39	32	40	4	18	6	18	3	3	16	4	3	1	12	8	6	8	1	4	1	5 ± 5	0.4 ± 0.9
1981-83	53	12	34	0	0	15	2	5	0	12	43	0	27	18	27	6	17	0	0	8	1	3	0	6	22	0	14	8 ± 9	-0.7 ± 0.1
1979-81	na	na	na	37	74	25	40	43	53	13	25	9	3	18	na	na	na	19	37	13	20	22	27	6	13	5	2	**16 ± 11**	-3.0 ± 0.3
1966-79	na	na	na	18	65	64	3	72	117	121	8	5	41	45	na	na	na	1	5	5	0	6	9	9	1	<1	3	4 ± 3	-2.0 ± 1.3
1966-81	47	242	30	na	na	na	na	na	na	na	na	na	na	18	3	16	2	na	na	na	na	na	na	na	na	na	na	7 ± 8	-3.3 ± 0.3
1955-66	140	80	75	94	74	113	33	7	108	67	79	156	6	45	13	7	7	9	7	10	3	1	10	6	7	14	1	7 ± 4	-2.8 ± 1.3
1953-55	26	87	70	13	8	na	4	69	39	1	21	2	12	42	13	44	35	7	4	na	2	35	20	1	11	1	6	**15 ± 15**	-3.1 ± 0.7
1941-55	na	na	na	na	na	67	na	na	na	na	na	na	na	42	na	na	na	na	na	5	na	na	na	na	na	na	na	5	-3.1 ± 0.7
1941-53	79	84	120	92	117	na	18	4	45	100	33	39	50	44	7	7	10	8	10	na	2	<1	4	8	3	3	4	5 ± 3	-1.9 ± 1.4
1938-41	138	123	29	97	100	48	106	71	126	89	113	110	89	15	46	41	10	32	33	16	35	24	42	30	38	37	30	**32 ± 10**	
1936-38	5	3	65	20	23	22	25	139	10	15	62	6	9	11	3	2	33	10	12	11	13	70	5	8	31	3	5	**16 ± 19**	
Total dune movement (m)	563	665	526	531	483	407	375	528	582	640	479	406	313	Dune movement rate 1936-1999 (m/yr)	8.9	10.6	8.4	8.4	7.7	6.5	6.0	8.4	9.2	10.2	7.6	6.4	5.0	7.9 ± 1.6	
Arms length (m)	1857	712	688	1569	2465	1329	365	3524	1641	2555	1940	2948	2976	Minimum inferred age (yr)[d]	209	67	82	187	320	204	61	420	178	250	255	461	595		

[a] Root Mean Squared error associated to the georeference process.
[b] Palmer Drought Severity Index from 1950 to 2003, National Climatic Data Center, 2004 www.ncdc.noaa.gov/oa/ncdc.html.
[c] Bold figures indicate significant migration rates, above long-term average.
[d] Ages calculated by dividing parabolic arm length by dune migration rate for 1936-99.

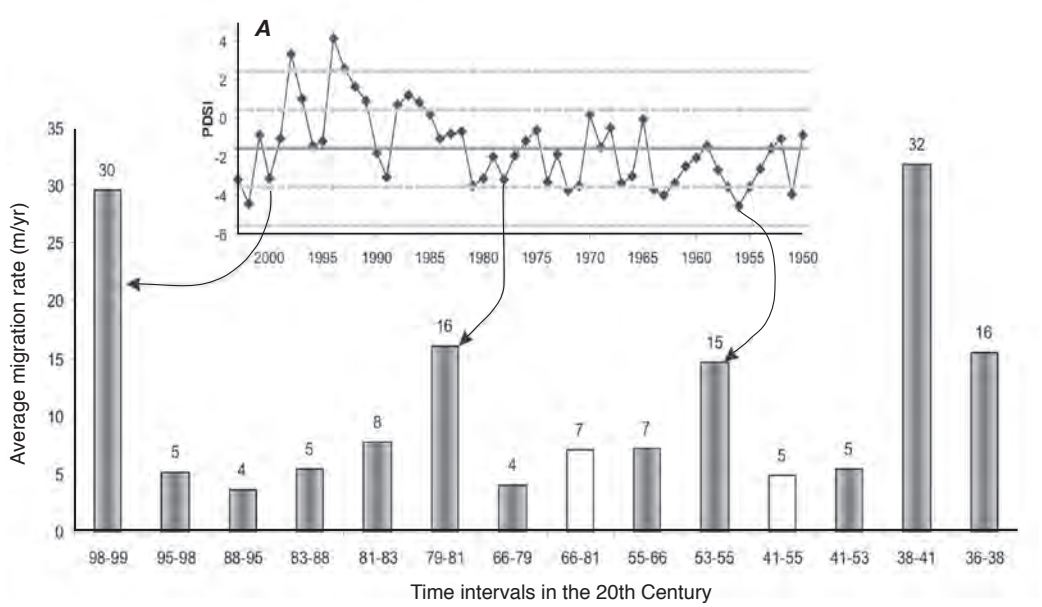

Fig A4–4. Migration rate for parabolic dunes over during measured time intervals in the 20th Century (from Marín and others, 2005). Shaded black bars indicate average drift rate for more than 3 parabolic dunes; white bar indicates average drift rate for fewer than 3 parabolic dunes. Inset graph (*A*) is the lower quartile time series of corresponding Palmer Drought Severity Index for the Great Sand Dunes National Park and Preserve.

Stop A5 — Cattle-Guard Paleoindian Site

Speaker: Fred Bunch and (or) Pedi Jodry
Location: Cattle Guard archeological site, Alamosa County Lane 6N.
Medano Ranch 7.5' quadrangle
GPS: NAD27, Zone 13, 444530 m E., 4168410 m N.
Elevation: 7,636 ft.

Discussion

Stewart's "Cattle-guard" site is an outstanding example of a Folsom bison kill site. Over 9,000 years ago, nomadic hunters killed 49 bison at this location (fig. A5–1). These bison (*Bison antiquus*) were a great deal larger than modern bison. Archaeologists from the Smithsonian Institution have been studying this site for two decades (see for example Jodry, 1987; Jodry and others, 1989; Jodry and Stanford, 1992), and the results of their research here have contributed greatly to the body of knowledge regarding Paleoindian tools and kill sites.

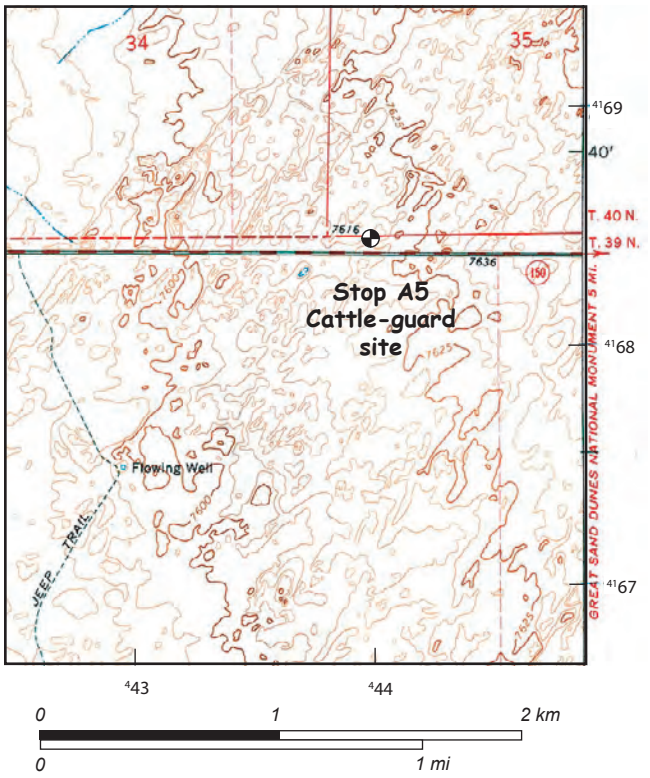

Figure A5–1. Topography around stop A5, Stewart's Cattle-guard site. Map scanned from Medano Ranch, Colorado, 7.5-minute topographic map.

Stop A6 — Medano Ranch Area

Speakers: Richard Madole, Shannon Mahan, and Michael Rupert
Location: Near former Medano Ranch headquarters
Medano Ranch 7.5' quadrangle
GPS: NAD27, Zone 13, 441650 m E., 4176460 m N.
Elevation: 7,650–7,665 ft

Medano Ranch

The Medano Ranch is one of the oldest continuously operated ranches in the San Luis Valley. The headquarters area of the ranch was established during the early years of the range cattle industry in Colorado when the Dickey brothers from Ohio brought large numbers of Texas cattle into the area. The Dickeys sold their beef to the booming mining camps of Leadville to the north. A post office was established at the ranch in 1877 with William Dickey as postmaster. In 1882, the Dickeys sold the ranch to Adee and Durkee (of the seasoning fame) who have been described as "cattle kings" with the largest beef production in the valley. The tenure of Adee and Durkee was impacted by severe weather, a steep drop in cattle prices, and the economic effects of the panic of 1890. In 1894, George Adams bought the ranch and sold it seven years later to Loren Sylvester of Monte Vista and Richard Holsford of Iowa, but cattle raising continued to be a depressed industry and in 1907 they sold the ranch back to the bank that had loaned them the money.

George W. Linger acquired the ranch in 1912 and ushered it into the modern era, changing it into fed-cattle business and introducing white-faced Herefords. Following George Linger's death in an airplane crash in 1921, his children continued the operation until 1947 when the ranch was sold to Malcolm Stewart, a Texas oilman. Stewart in turn sold the ranch in 1988 to Hisa Ota and others who started raising bison as well as cattle. Ota sold the ranch to the Nature Conservancy in late

summer of 1999. When the Nature Conservancy purchased the Zapata-Medano Ranch, they came into ownership of about 103,000 acres on the east side of the San Luis Valley bordering Great Sand Dunes on the north and the Rio Grande National Forest to the east. As a result, they became owners of one of the largest bison herds in Colorado.

The buildings at the Medano Ranch Headquarters were listed on the National Register of Historic Places in February 2004. The Nature Conservancy bison operation is centered on this portion of the Medano-Zapata. This portion of the property is also included within the newly authorized boundaries of the adjacent Great Sand Dunes National Park and Preserve located to the east. We'll discuss two intertwined topics at stop A6 on the Medano Ranch: the Quaternary stratigraphy in the Great Sand Dunes area (stop 6.1) and dating of ground water at Great Sand Dunes (stop 6.2)

Stop A6.1 — Overview of Quaternary Stratigraphy in the Great Sand Dunes Area

Speakers: Richard Madole and Shannon Mahan

Synopsis

At this stop, we will review eolian sand stratigraphy and also briefly discuss the noneolian deposits (fluvial, lacustrine, paludal, and sheetwash) in the area. Stop A6.1 is on eolian sand (unit Qes2; fig. A6.1–1) that ranges in age from middle Holocene (defined here as 8–4 ka) to the early part of late Holocene time. Sand from just below the thin, case-hardened $CaCO_3$-bonded ledge seen here has an estimated age of 3,640±260 OSL yr B.P. Eolian sand of unit Qes3 forms the "hills" 2 km to the southwest, which are less than 1,000 years old. Latest Pleistocene eolian sand (unit Qes1) is not visible at this stop. However, most of the area within view is underlain by upper Pleistocene sediment, chiefly alluvium, at shallow depths (1–6 m).

Discussion

A nearly continuous belt of windblown sand of variable width extends along the east side of the San Luis Valley between Rito Alto Creek on the north and the Dry Lakes area on the south, a distance of about 70 km. The Great Sand Dunes cover about 12 percent of this sand area. Although most of the eolian sand at the surface is Holocene, stratigraphic and geomorphic evidence indicate that eolian sand has been accumulating here since late-middle Pleistocene time. Within and adjacent to deposits of eolian sand are large areas of sediment that accumulated in lakes, ponds, marshes, and alluvial flats on the lower piedmont slope and basin floor. Stop A6.1 is in an area where noneolian sediment, mostly alluvium, is particularly widespread (fig. A6.1–1). Alluvium is the dominant noneolian surficial material present. Most alluvium consists of poorly sorted sand and fine- to coarse-pebble gravel. In addition, thin (1.0–1.5 m) deposits of calcareous silty fine sand and sandy silt are extensive in some places. These deposits are probably "river-end"

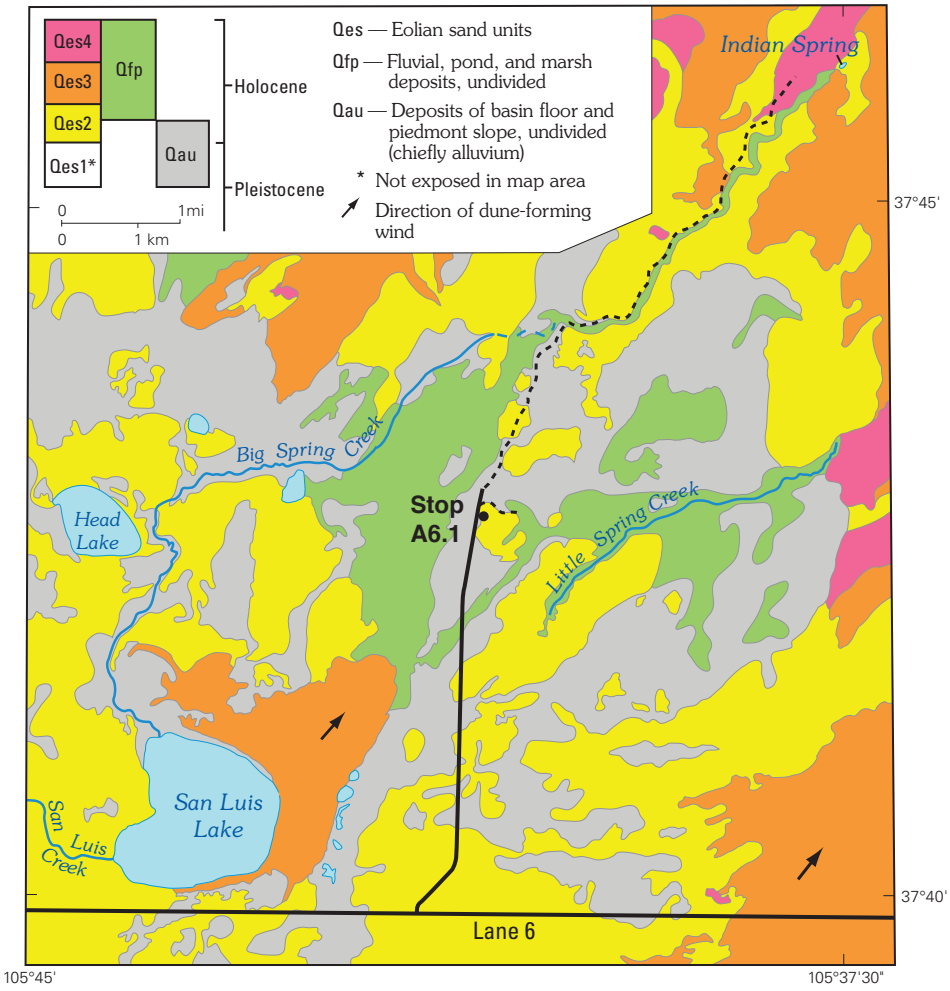

Figure A6.1–1. Eolian, fluvial and alluvial deposits in the vicinity of stop A6.1. (Derived from Richard Madole, unpub. data, 2007).

sediment that was delivered to the lower piedmont slope and basin floor primarily by sheetwash and ephemeral streams that originated higher on the piedmont slope. Differences in degree of soil development and a few radiocarbon ages indicate that some of the alluvium is late Pleistocene and some is Holocene. In several places, a veneer (0.5–1.5 m) of Holocene alluvium overlies Pleistocene alluvium.

Eolian sand can be divided into four mappable units on the basis of physical properties, topographic expression of dunes, differences in degree of soil development, and stratigraphic relations (fig. A6.1–2). The youngest unit (Qes4) consists of sand that has been active during historic time. It is at the surface in about 15 percent of the eolian sand area. Most of unit Qes4 blankets the Great Dunes, but smaller deposits also are present elsewhere. The next oldest unit (Qes3) was deposited episodically between about 1,300 and 300 years ago. This age range is based partly on radiocarbon ages from this area and partly on correlations with similar deposits on the plains of eastern Colorado for which there is more numerical age control. Unit Qes3 is at the surface in about 60 percent of the eolian sand area. It forms (1) fields of parabolic dunes north, northwest, and southwest of the Great Sand Dunes National Park and Preserve, (2) lunette dunes in southern part of the area, and (3) compound parabolic dunes that extend northeast from San Luis Lake, the leeward edge of which are visible (looking southwest) from this stop (fig. A6.1–1).

Unit Qes2 includes sand that was deposited at different times during the middle Holocene (8–4 cal yr ka) and early part of the late Holocene (4–0 cal yr ka). It is at the surface in about 25 percent of the area, primarily the west-central part (fig. A6.1–3) and in broad-crested lunette dunes in the southern part. Unlike unit Qes3, which is noncalcareous and has little or no soil development, unit Qes2 has a very weakly developed soil in most places and everywhere contains secondary $CaCO_3$ in the upper 1–1.5 m. We are on unit Qes2 at this stop. Eolian sand from just below the thin ledge formed here by case-hardened, $CaCO_3$-bonded sand has an estimated age of 3,640±260 OSL yr B.P. (fig. A6.1–4).

Unit Qes1 is of late Pleistocene age. Little is known about its lateral extent and material properties because younger deposits—eolian sand, alluvium, and lacustrine sediment—bury it in most places. Exposures of unit Qes1 are primarily in stream banks, blowouts, and excavations (fig. A6.1–5). Except for the Great Dunes, the area within view from stop A6.1 is underlain at shallow depths (1–6 m) by late Pleistocene sediment, chiefly alluvium.

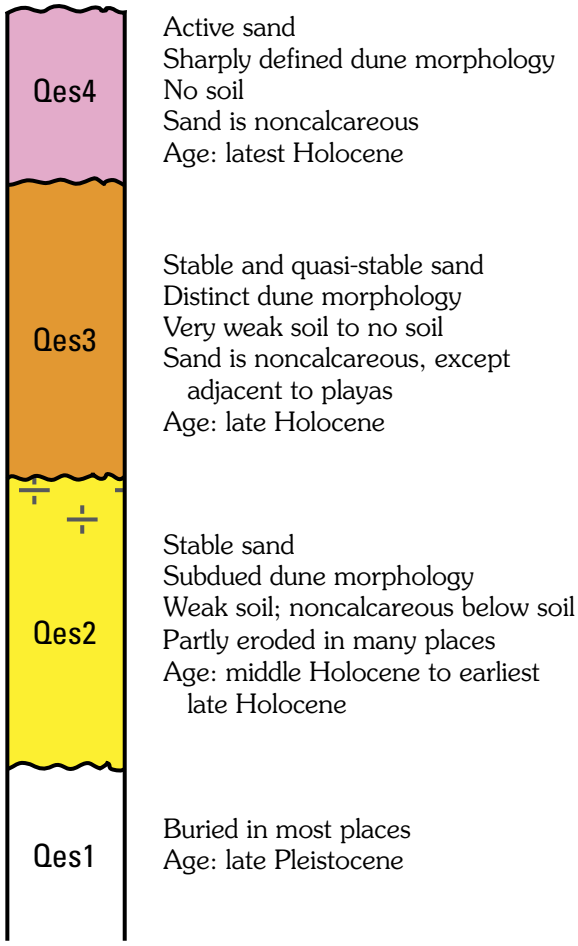

Figure A6.1–2. Composite section of eolian sands. Four mappable units defined on the basis of physical properties, topographic expression of dunes, differences in degree of soil development, and stratigraphic relations.

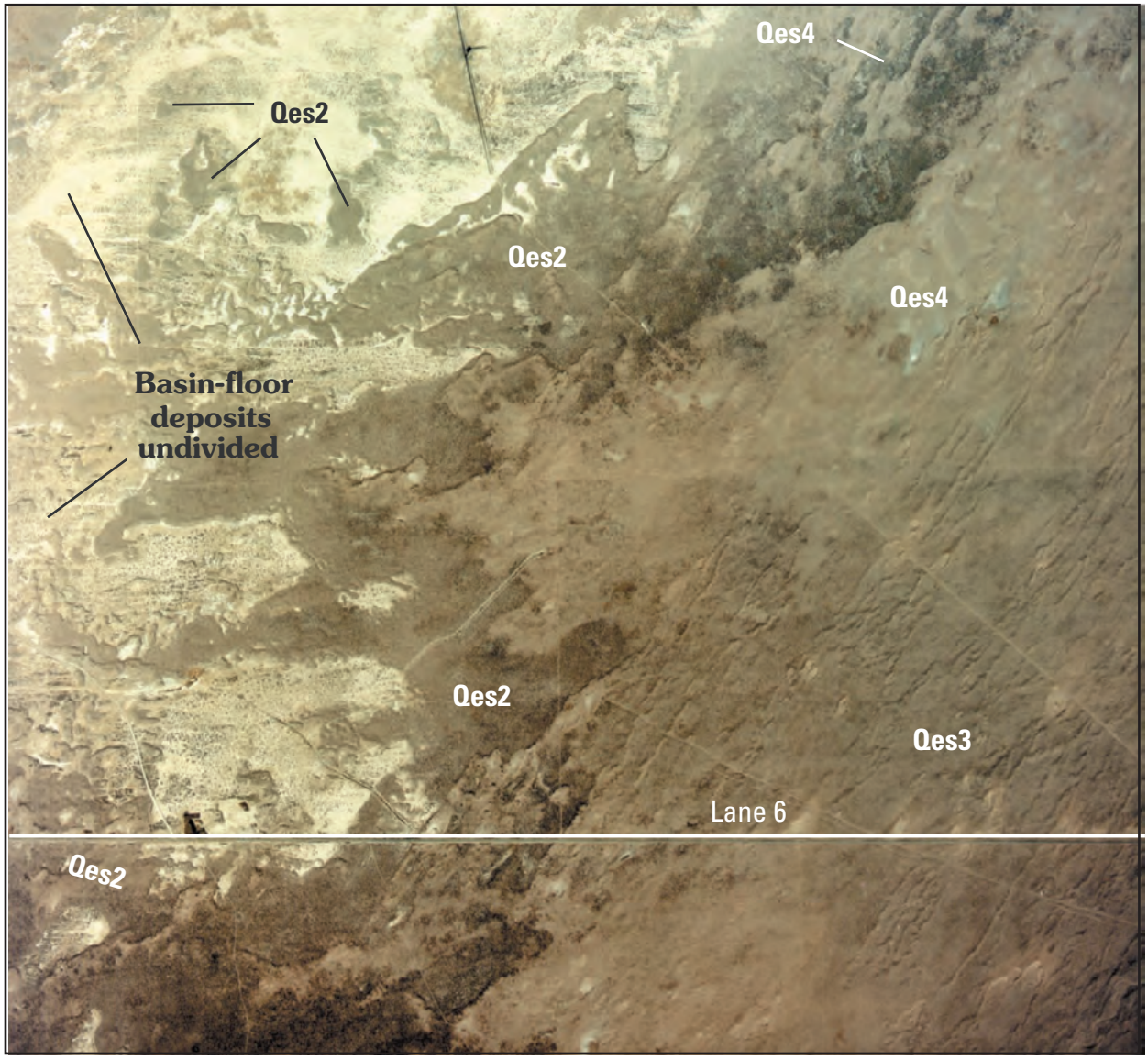

Figures A6.1–3. Typical distribution of three of the four eolian sand units shown in figure A6.1–2. We travel down Lane 6 on the way to stop A6.

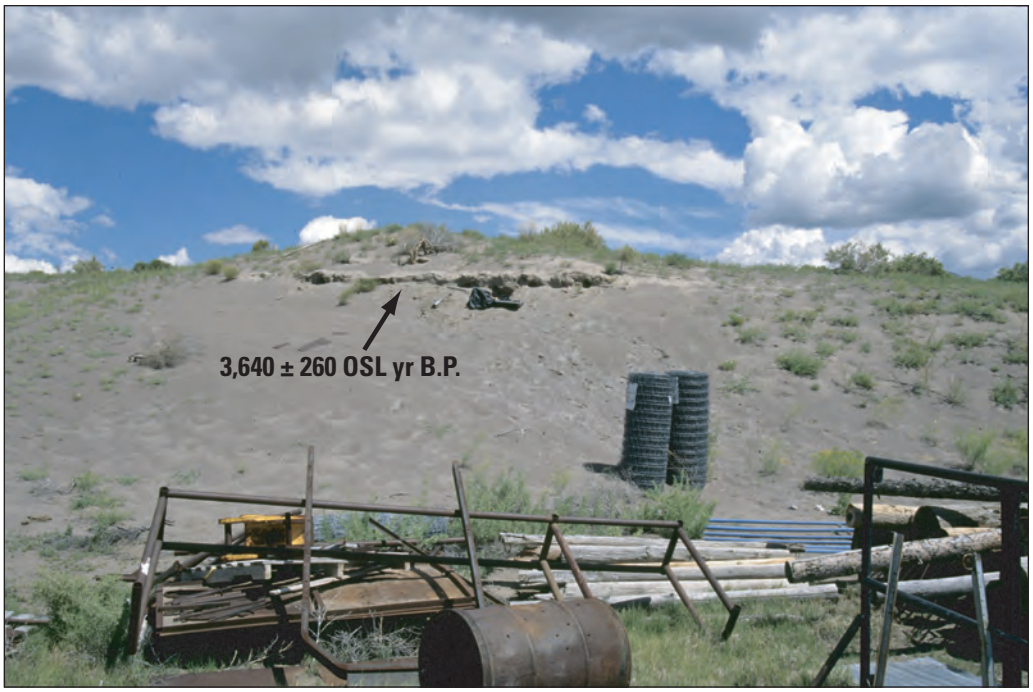

Figures A6.1–4. Age of eolian sand of unit Qes2 has an estimated age of 3640±260 OSL yr B.P. Sample is from below the thin ledge of case-hardened, $CaCO_3$-bonded sand.

Figure A6.1–5. Exposures of unit Qes1, the oldest of four sand units, are primarily in stream banks, excavations, and blowouts as shown in this photograph.

Stop A6.2 — Dating Groundwater at Great Sand Dunes National Park and Preserve

Speaker: Michael Rupert

Overview

There are the two principal aquifers at the Great Sand Dunes National Park and Preserve: a shallow unconfined aquifer and a deeper confined aquifer. Ground water in the unconfined aquifer is recharged by Medano and Sand Creeks near the Sangre de Cristo Mountain front, flows underneath the main dune field, and discharges to Big and Little Spring Creeks on the western margin of the dune field. It takes more than 60 years for the ground water to flow from Medano and Sand Creeks to Big and Little Spring Creeks (fig. A6.2–1), a distance of about 10 km (chapter D, this volume). During this time, ground water in the upper part of the unconfined aquifer is recharged by numerous precipitation events. This recharge from precipitation events causes the apparent ages determined using chlorofluorocarbons and tritium to become younger, because relatively young precipitation water is mixing with older waters derived from Medano and Sand Creeks. Radiocarbon dating of ground water in the confined aquifer (well Y) indicates it is about 30,000 years old (plus or minus 3,000 years). The peak of the last major ice advance (Pinedale glacial, OIS 2) occurred about 20,000 years ago; ground water from the confined aquifer is much older than that. A more complete discussion of these subjects is included in chapter D of this volume.

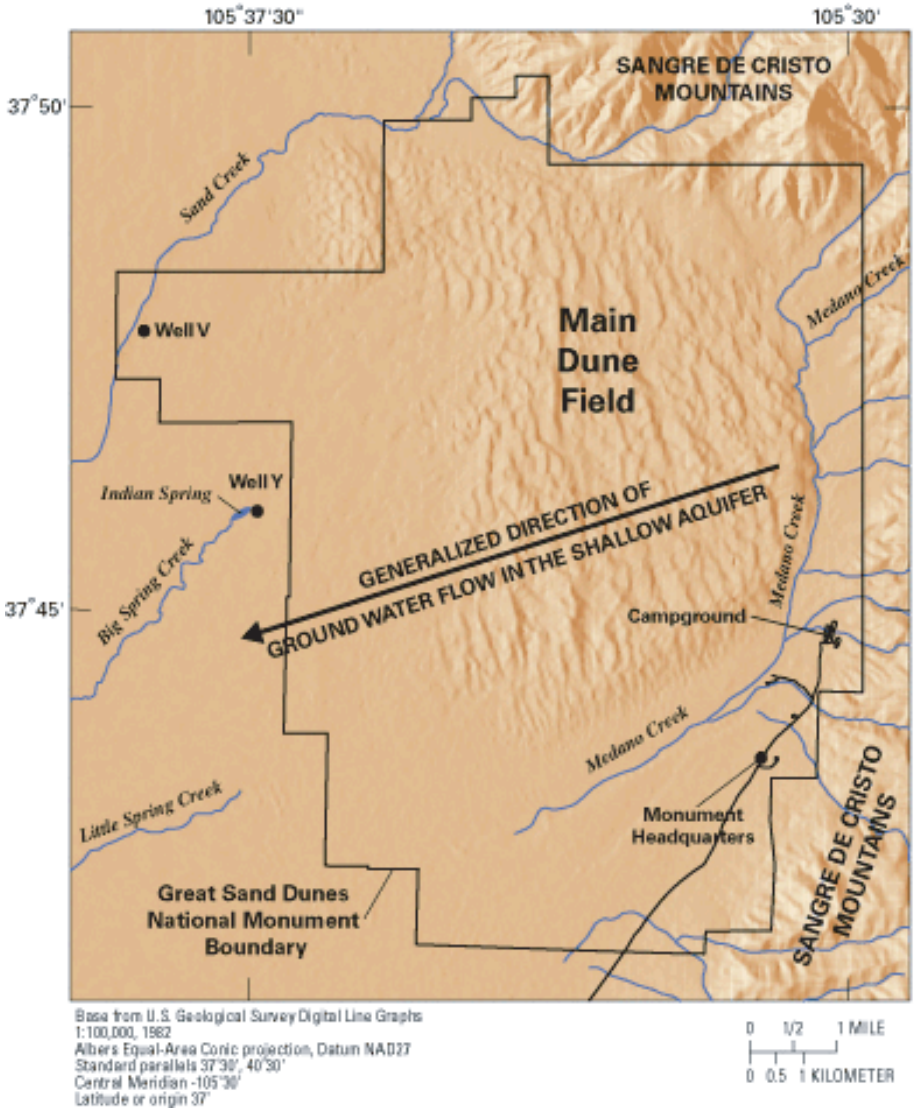

Figure A6.2–1. Generalized direction of ground-water flow beneath the Great Sand Dunes (main field).

Stop A7 — Sabkha overlook

Speaker: Andrew Valdez
Location: Closed Basin Canal, Zapata Ranch
Medano Ranch 7.5' quadrangle
GPS: NAD27, Zone 13, 438810 m E., 4164850 m N.
Elevation: 7,525 ft

Synopsis

This stop allows a close examination of a sabkha (salt-encrusted plain). Sabkhas form in areas of internal drainage where basin subsidence exceeds stream deposition, although wind deflation may also contribute to formation of local depressions. Playa formation is common and appears to be a critical factor in the accumulation of adjacent eolian sand deposits. Little is known about how Pleistocene climates would have affected the area and the input of sand. A group discussion on possible Pleistocene climatic effects will be sought.

Discussion

Sabkha is an Arabic term that refers to a salt-encrusted plain. The geologic definition refers to a coastal environment characterized by evaporites and eolian deposits. In the literature, it has been adapted to include similar environments away from coastlines, such as playas. At Great Sand Dunes, areas of sabkha are also found upgradient from the playas where deflation lowers the ground surface to the groundwater capillary fringe, and evaporation from that fringe produces evaporites.

The subsurface, rift structure of the Alamosa subbasin (of the San Luis Basin) exerts some control over the current basin surface in a manner that leads to the maintenance of the current eolian system. Drilling and geophysical-based petroleum exploration indicates that the basin is asymmetrical, dips to the east, and is subdivided into different crustal blocks (fig. A7–1). The western block is the moderately deep Monte Vista half graben. In the center, but in the subsurface, is the Alamosa horst. This elevated block may be spatially related to the San Luis Hills horst that is exposed south of the Alamosa subbasin (see chapter B). The eastern block is the relatively deeper and younger Baca graben. Here, basin-fill sediment of the Santa Fe Group (upper Cenozoic) is estimated to be as much as 5.6 km thick (Brister and Gries, 1994). Subsidence of the Baca graben and possibly wind deflation of the surface has created a subtle depression known locally as the “closed basin” since the area normally lacks external drainage. A playa or lake system has developed along the axis of the closed basin. During wet periods, the playas can fill to the point of overflowing the closed basin and thus become ephemeral tributaries to the Rio Grande. The last known occurrence of overflow was in the 1920s. Currently there is little opportunity for the basin to fill as most of the surface water is diverted for agricultural use upgradient from the playas.

The playa system commonly is associated with a poorly lithified, sandy deposit. The water-table gradient of the area is essentially flat, so the only known output of water is by evapotranspiration. This factor has resulted in saline water conditions and the precipitation of evaporite minerals and

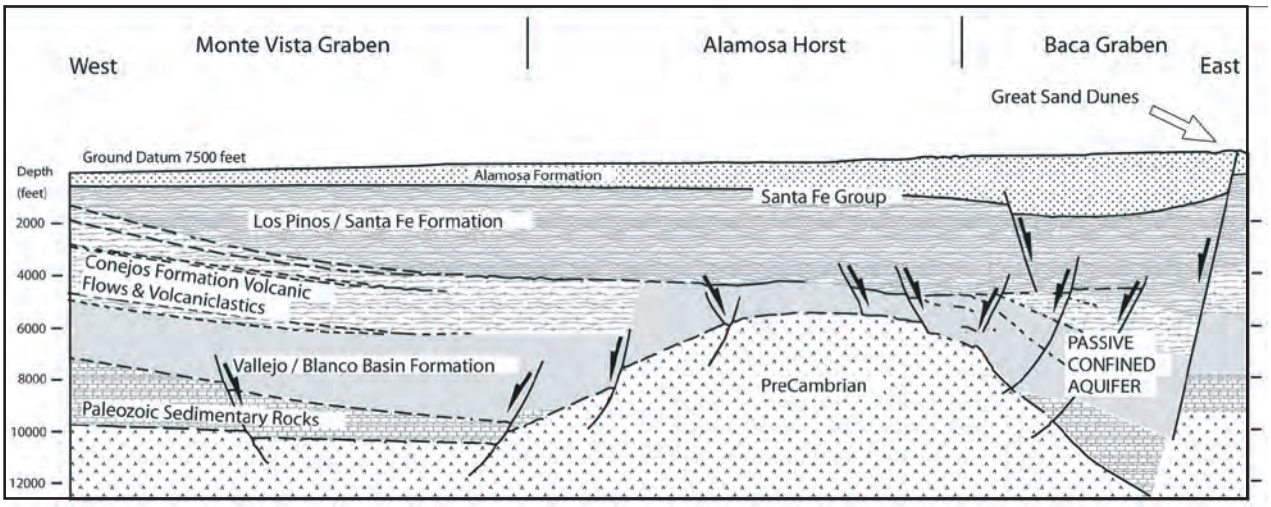

Figure A7–1. Geologic cross section of the San Luis Basin at the latitude of the Great Sand Dunes (37° 39' N.). Modified from Brister and Gries, 1994.

diagenesis of the sand (Krystinik, 1990). The most common evaporite is sodium bicarbonate (Fryberger, 1990b), likely in the mineral form of trona (H.N. Dixon, oral commun., 2006). U.S. Geological Survey research in the late 1970s and early 1980s subdivided the Great Sand Dunes eolian system into different depositional provinces. The playa area was termed "Province I, Dry Lakes" (Andrews, 1981). Later, USGS researchers identified the evaporite environment as a sabkha (Krystinik, 1990).

The majority of Great Sand Dunes' surficial eolian deposits can be traced upwind to the playa lake area, indicating that the processes that form the playa provide the fluvial source for eolian deflation (Madole and Romig, 2002). Without the development of playas, it is unlikely that eolian deposits would develop on the scale we see today. The process leading to the accumulation of eolian deposits requires that streams periodically fill playas; wave action concentrates sand on the beaches; and when the playa dries, beach sand is exposed to the wind and results in deposition of eolian sand downwind from the playa. The eolian sand forms lunettes (crescent- or tongue-shaped dunes) around playas, which tend to be round. In this area, they form on the northeast side of the playas because the dominate wind direction is from the southwest (Fig. A7–2).

The eolian system has resulted in formation of Great Sand Dunes downwind from the San Luis lakes, which are in the lowest and wettest part of the closed basin. Sand is plentiful enough in this system to promote dune development as indicated by active dune or vegetated dune forms. Eolian deposits exist north and south of the lakes, but the deposits generally consist of a thin veneer of sand and dunes are uncommon.

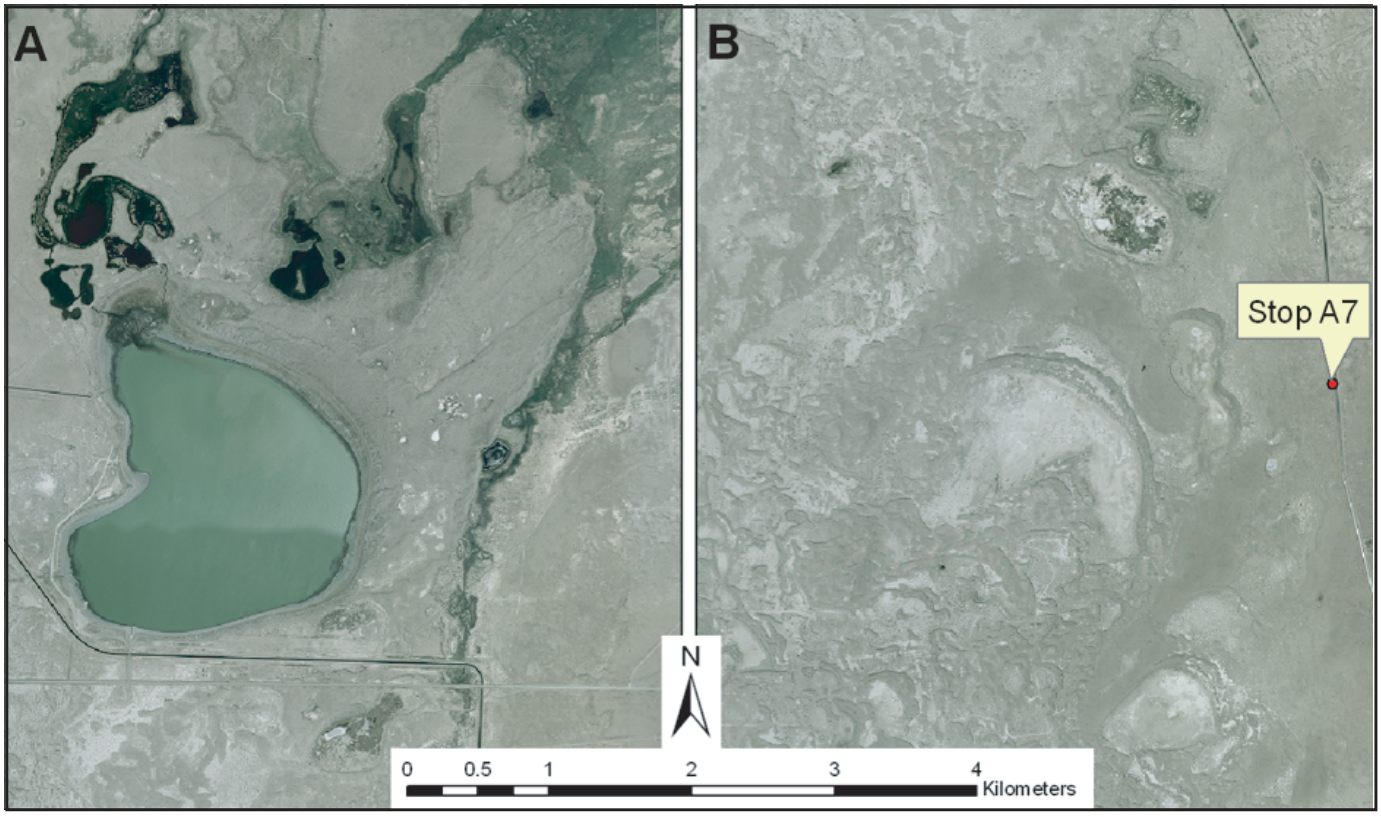

Figure A7–2. San Luis Lake and sabhka south of San Luis Lakes. *A*, San Luis Lake. *B*, Sahbka and dunes west of stop A7, about 3 km (2 mi) south of Lane 6 and San Luis Lake.

Stop A8 (Optional) — Closed Basin Overflow and Origin of Hansen Bluff

Author: Andrew Valdez
Location: Closed Basin Canal, Zapata Ranch
Medano Ranch 7.5' quadrangle
GPS: NAD27, Zone 13, 436490 m E., 4152416 m N.
Elevation: 7,522 ft

Synopsis

As this stop we will see the overflow point between the closed basin (stop A7) and the Rio Grande. Hansen Bluff, which is as much as 20 m high to the south (stop B7), extends north to this area, where it can be traced as a subtle fluvial scarp cut into the broad piedmont of the Sangre de Cristo Mountains. Historic accounts note that the closed basin did overflow during the 1920s, but now most of this stream water is diverted for agricultural use, so the opportunity for the basin to fill is reduced in all but extremely large-discharge years.

Discussion

Hansen Bluff is a north-south trending, 24-km-long topographic break in the otherwise planar surface of the Alamosa subbasin (fig. A8–1). The bluff extends from the southern end of the depression known as the "closed basin" to near the confluence of the Rio Grande and Trinchera Creek. The southern half is parallel to the trend of the Rio Grande and is positioned on the eastern edge of its topographic floodplain, adjacent to the Hansen Ranch (its namesake, stop B7). The Rio Grande and Hansen Bluff diverge from each other north of the bluff's midpoint where the trend of the river flow changes from south to southwest. The bluff's expression is subtle where it begins in the north, with a height of 1 m. The bluff's height increases with distance southward. Along the Rio Grande floodplain it reaches a height of 20 m (Siebenthal, 1910; McCalpin, 1996). At stop B7, the type section of the Alamosa Formation, Machette discusses the sediments exposed in Hansen Bluff (chapter B, this volume).

The origin of the bluff has long been a curiosity. Along the Rio Grande floodplain to the south, the scarp appears to be the result of lateral river erosion, but if so, why do the bluff and river diverge? Explanations include speculation about the Rio Grande approaching from a more northern position as well as the bluff being controlled by an underlying fault.

Interpretation of aerial photography suggests that the northern part of the bluff is a stream-cut escarpment, albeit low (fig. A8–2). The feature is sinuous, suggesting river loops and oxbow meanders. The northernmost extent begins near the point where a water-filled closed basin would overflow. The overflow point was determined by examining ponding in the small playas of the area. Adjacent to the bluff are dry stream channels, and the crescentic shape of the bluff mimics the oxbow pattern of the streambed, indicating lateral stream erosion. This pattern can be seen along the entire length of the bluff but is pronounced north of Highway 160. The extent of lateral stream erosion determines where valley margins are but, in this case, the area to the west of the overflow is essentially flat. Therefore, it lacks the sloping piedmont that would lead to formation of stream-cut escarpments. East of the overflow, the land gently slopes upward in a broad piedmont to the Sangre de Cristo Mountains and scarps can form in response to lateral erosion. Hansen Bluff appears, therefore, to be the eastern margin of an asymmetrical stream valley. The northern portion would have been cut by overflow from the closed basin and the southern portion by the Rio Grande. The height of the bluff increases southward as the overflow stream adjusts to the lower base level of the Rio Grande.

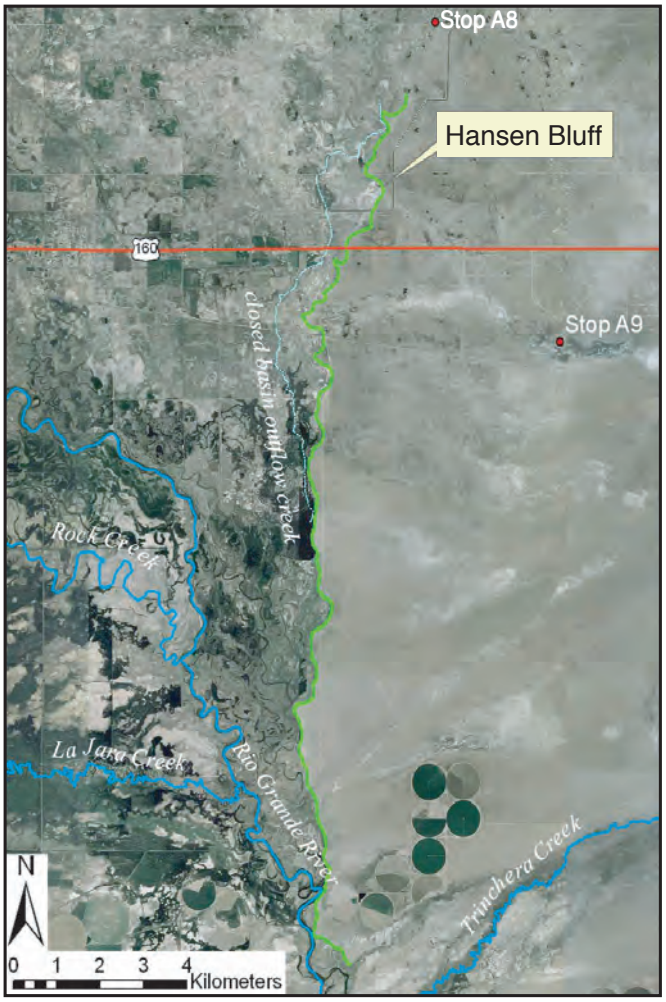

Figure A8–1. Hansen Bluff, the Rio Grande, and its tributary streams.

Historic accounts show that the closed basin did overflow during the 1920s. Water to fill the closed basin comes from the numerous streams that currently flow into it, including Saguache Creek, San Luis Creek, and Sand Creek. Most of this stream water is now diverted for agricultural use, so the closed basin can fill only during extremely large-discharge years (when supply exceeds agricultural use). Precipitation values reconstructed from tree-ring data (fig. A8–3) indicate that the 10-year (decadal) precipitation average has been cyclic during the last millennium. During wet periods, such as the first half of the 13th Century, the closed basin may have been filled frequently. Interpretation of aerial photography also suggests during extreme precipitation years, water from the Rio Grande fan system can enter the closed basin (R.F. Madole, oral commun., 2006).

Aeromagnetic data suggests possible subsurface faulting beneath the south end of Hansen Bluff, perhaps related to the Alamosa horst (V.J.S Grauch, written commun., 2007) or northern extension of Lasauses fault (Burroughs, 1972; Rogers, 1984), so the possibility exists for some structural influence on the bluff as well. However, the bluff has the sinuous shape associated with fluvial systems rather than that of a scarp formed by a normal fault (see also stop B7, chapter B, this volume).

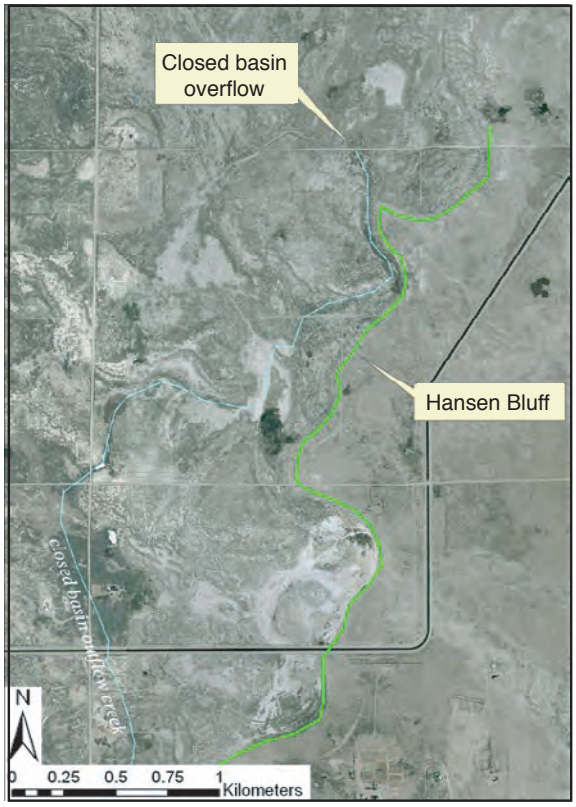

Figure A8–2. Hansen Bluff and the closed-basin overflow channel.

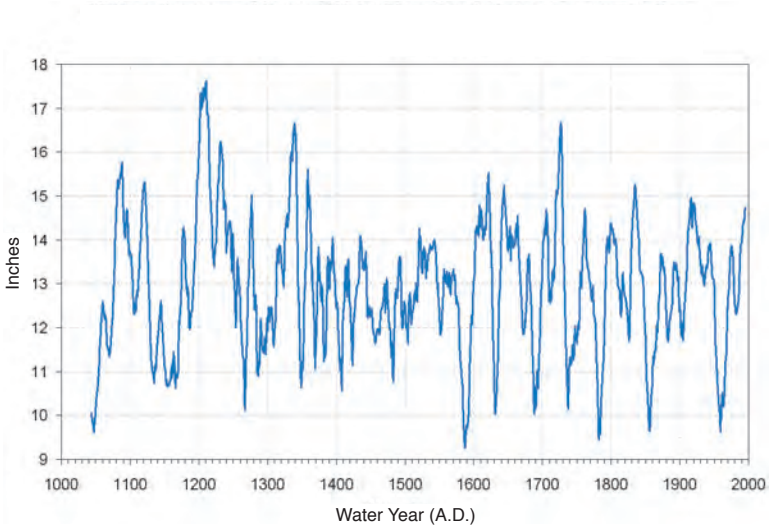

Figure A8–3. Decadal precipitation records for the Great Sand Dunes as interpreted from tree-ring data (modified from Grissino-Mayer and others, 1997).

Stop A9 (Optional) — Middle and Late Holocene Eolian Sand Dunes

Author: Michael Machette

Location: Baca Lane pit (informal name, private property)
Southeast corner of County Road 6S and Road S116 (Baca Lane), about 6 mi east of Alamosa, Colo.
Baldy 7.5' quadrangle (Sta. BA–MM04–25)
GPS: NAD27, Zone 13, 433910 m E., 4148955 m N.
Elevation: 7,525 ft (at gated entrance to pit)

Synopsis

This optional stop is at a restricted site (private property, trespassing not allowed) where a borrow pit was excavated into a stratified eolian sand dune. As part of his reconnaissance mapping of the Alamosa area in the summer of 2005, Machette made a quick description of the sand sequence, sampled organic materials and charcoal from buried soils that mark depositional hiatuses in the sequence of sands, and noted artifacts associated with a hearth site. Three samples of charcoal separated from the buried soils date from about 2800 to 5560 cal yr. This interval is a longer time sequence than normally exposed or seen in the basin or at Great Sand Dunes to the north (see stops A2 and A4, this chapter). The dating and stratigraphy of middle to late Holocene eolian sands exposed in the Baca pit are discussed more completely in chapter E of this volume.

Discussion

This stop is one of the few places in the Alamosa area where we can see a sequence of stratified Holocene eolian sand deposits separated by well-formed, organic-rich soils (buried A horizons). Unfortunately, this site is on private property that is posted as NO TRESPASSING, so please respect the landowner's rights. This area, and in particular the southeast corner of County Road 6S and Road S116 (Baca Lane), is characterized by largely stabilized sand dunes and interspersed blowouts that expose playa-like, organic-rich sediment. The site was discovered during the course of geologic mapping of the north-central part of the Alamosa sheet (M.N. Machette and Ren Thompson, unpub. mapping, 2007). Figure A9–1, which shows the surficial geology around field trip stop A9, has been modified from Machette and Thompson's (2005) 1:50,000-scale map.

In the summer of 2005 Machette made a quick description of the sand sequence, photographed the site (fig. A9–2),

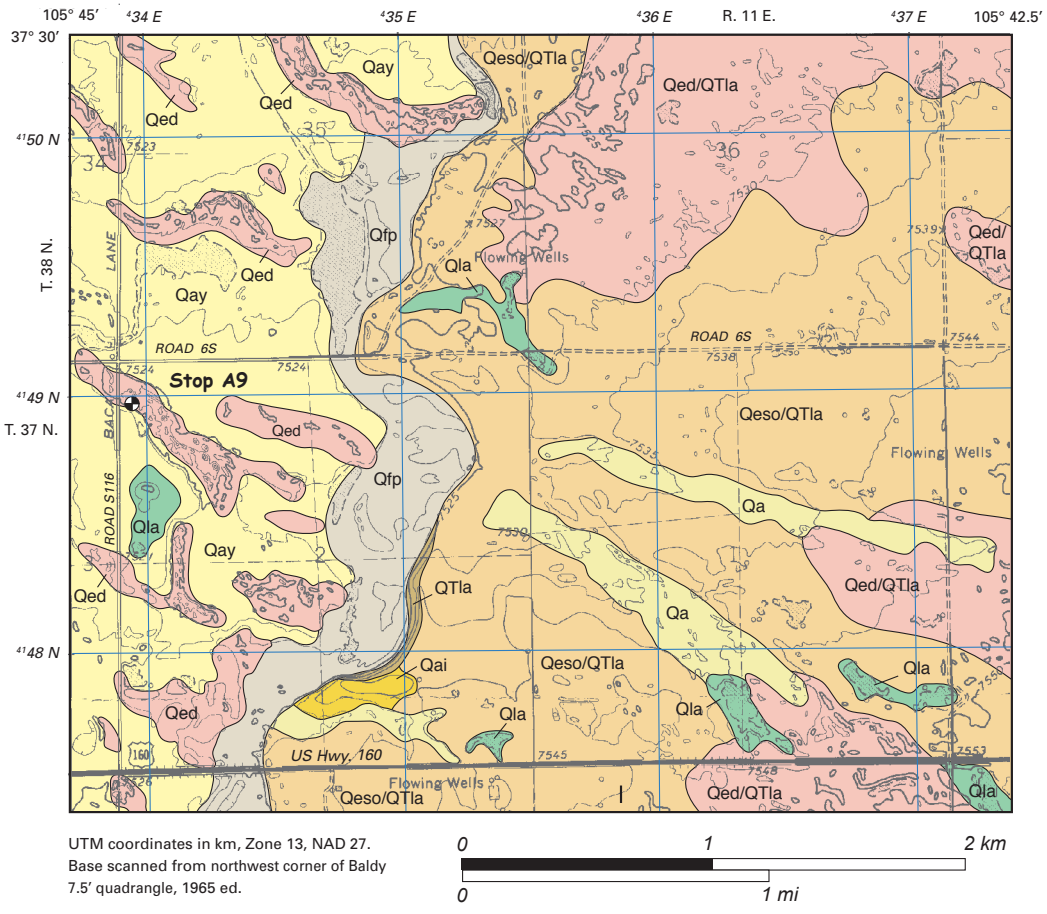

Figure A9–1. Eolian, alluvial, and lacustrine deposits at and east of stop A9. Map units: Qed, eolian dune sand; Qeso, older eolian sand; Qfp, floodplain alluvium; Qa, Holocene alluvium; Qla, Holocene lake and playa deposits; Qay, young (latest Pleistocene) alluvium; Qai, intermediate (middle Pleistocene) alluvium; QTla, Alamosa Formation. Geology simplified from M.N. Machette and Ren Thompson, unpub. mapping, 2007.

sampled organic materials and charcoal from buried soils, and noted artifacts associated with a hearth site. Flotation of bulk samples from the Baca Lane pit (site BA–MM04–25) resulted in recovery of charcoal and other charred plant remains for radiocarbon dating. Rabbitbrush charcoal in samples R2 and R4, saltbush charcoal in sample R2, greasewood charcoal in samples R2 and R4, and Chenopodiaceae charcoal in samples R1, R2, and R4 all were present in sufficient quantities for accelerator mass spectrometry radiocarbon analysis. Only sample R3 yielded insufficient charcoal or other charred organics for dating. A more complete discussion of this site is included in chapter E of this volume.

Three samples of charcoal separated from the buried soils that mark depositional hiatuses in the sequence of sands gave radiocarbon ages at about 2800 cal yr, 3900 cal yr, and 5560 cal yr (table A9–1), which is a much longer sequence than is normally exposed or seen in the basin. Animal and plant remains in these samples reveal paleovegetation that is similar to that of the present, as well as evidence of human occupation in the period between about 2.8 ka and 3.9 ka.

Paleoenvironments During the Late and Middle Holocene

Climatic and environmental conditions at the Baca Lane site appear to have fluctuated from moist to dry at least four times (that is, four eolian sand units with intercalated soils) during the past 6,000 years. During moister conditions, the sand was stable and soil organic matter accumulated at or near the surface of the dunes. Without OSL dating of the eolian sand, we cannot estimate how long it took each sand unit to accumulate (intervals of instability and sand transport) or the duration of soil formation (intervals of stability and no, or minimal, sand transport). Nevertheless, it appears that, on average, these sand dunes undergo periodic stabilization every 1–2 k.y.

The recovered charcoal types represent local shrubs that were processes as food sources by the prehistoric occupants of the site. Charred seeds of *Chenopodium* (goosefoot), *Portulaca* (purslane), *Sporobolus* (dropseed), and *Oxalis* (wood sorrel) were found in the samples that were processed. Samples R1 through R4 span 2.8 ka to about 5.56 ka, which equates to late and middle Holocene time. During these times, early man appears to have been occupying this area during the late summer or fall seasons when these seed resources are available for harvesting. Charred bone fragments recovered from all four samples most likely reflect processing of meat and fish (sample R1).

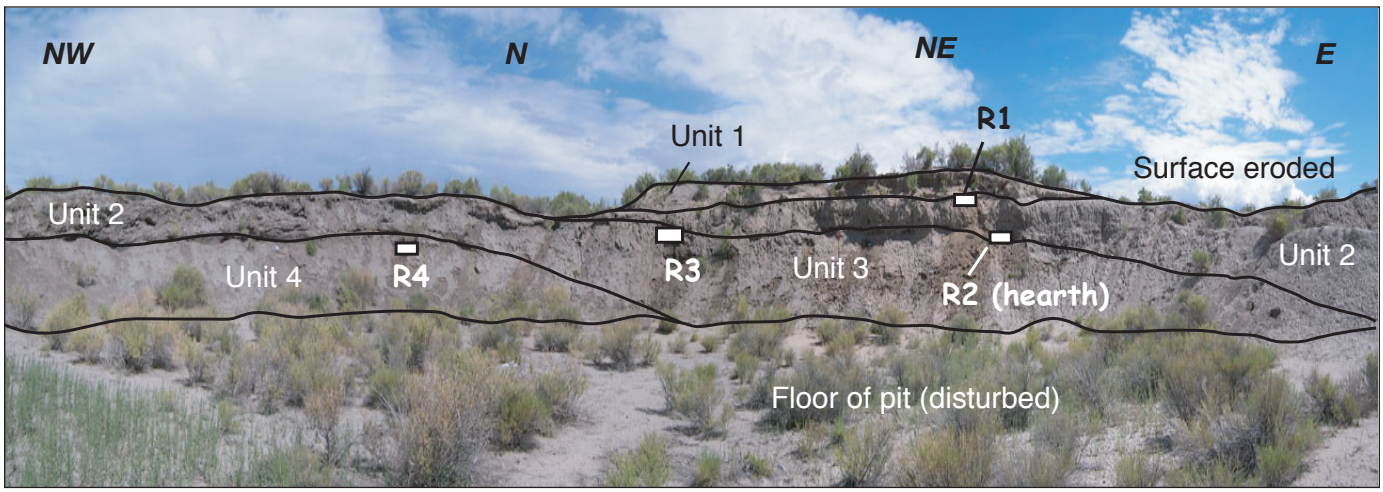

Figure A9–2. Stratigraphic units and soils exposed in the Baca Lane pit (sand borrow pit). Sampled soils are shown as R1 to R4 from eolian sand units 2, 3, and 4. View is to the northwest (on left) sweeping to the east (on right). The total vertical exposure in the pit is about 4 m. Image has 1.5x vertical exaggeration.

Table A9–1. Radiocarbon age determinations from charcoal samples at stop A9.

[Reported radiocarbon ages have 1-sigma errors; calendar-corrected ages have two 2-sigma errors. The radiocarbon ages were calendar corrected using the radiocarbon calibration program (CALIB REV. 5.0.1 of Stuiver and others, 2005; see also Stuvier and Reimer, 1993)]

USGS sample number (position)	Type and weight of charcoal	NOSAMS accession number	$\delta^{13}C$	Radiocarbon ages and errors (^{14}C yr B.P.)	Calendar ages and errors (years)
BA–MM04–25R1 (Soil on unit 2)	Artiplex (Saltbush), 0.025 g	OS–52749	–23.38	2700±35	2804±54
BA–MM04–25R2 (Hearth at base of unit 2, on unit 3)	Artiplex (Saltbush), 0.038 g	OS–52750	–11.21	3590±55	3905±98
BA–MM04–25R4 (Soil on unit 4)	Unidentified hardwood, 0.015g	OS–52751	–25.62	4820±45	5560±90

Stop A10 — Late Pleistocene to early Holocene wetland deposits in the Mr. Peat pit

Speakers: Michael Machette and Randy Schumann
Location: North edge of Mr. Peat pit, which extends about 2 mi east-west along an unnamed drainage.
Location is about 2 mi south of U.S. Highway 160 and about 10 mi east of Alamosa, Colo.
Baldy 7.5' quadrangle (Stations BA–MM05–73 and –74, BA–MM06–76)
GPS: NAD27, Zone 13, 440123 m E., 4145465 m N.
Elevation: 7,590 ft (at north edge of pit on section–line fence)

Synopsis

This stop provides an opportunity to see peat-rich wetland deposits related to paleospring waters that flowed down a now-abandoned late Pleistocene glacial-meltwater stream channel. The peat deposits have been commercially mined from what is known as the "Mr. Peat" pit by RMMP (Alamosa, Colo.) since about 1950. In the summer of 2006, we excavated four pits in these deposits to understand better the timing and duration of peat accumulation, facies of the peats, the age of underlying fossil-bearing alluvial deposits, and the age and origin of overlying tufa deposits. Radiocarbon dating of the peats show that most of the wetland deposits accumulated from 13.5 ka to about 11.6 ka and that deposition continued until middle Holocene time (4.3–6.7 ka), whereas locally overlying tufaceous spring deposits started to accumulate about 6.7 ka and that accumulation continued until about 3.9 ka. The peats lie in a late-glacial-age paleovalley that is underlain by well-bedded sand and sandy fluvial gravel. An organic seam in the alluvium about 1.4 m below the peat yielded an age of 14.4 ka, whereas OSL dating of the alluvium yielded a variety of stratigraphically consistent and inconsistent ages (6.5–34.3 ka) for sands below the peats. The dating, stratigraphy, and paleoecology of the Mr. Peat pit are discussed more completely in chapter F of this volume.

Discussion

This stop focuses on a spectacular, abandoned stream valley where we can see a sequence of stratified peats and overlying tufaceous spring deposits. A second smaller valley is located about 1 km to the northeast, and shallow peat deposits can be seen where the valley crosses U.S. Highway 160 (see fig. A10–1). In the fall of 2005, Machette found these peat-filled valleys during mapping of the surficial geology of the north-central part of the Alamosa sheet (M.N. Machette and Ren Thompson, unpub. mapping, 2007). Figure A10–1, which shows the surficial geology around field trip stop A10, has been modified from the previously cited 1:50,000-scale map.

Local Geology

The Mr. Peat pit is located south of U.S. Highway 160, which is the main highway across the San Luis valley. It connects Fort Garland on the east to Alamosa at the Rio Grande, and Monte Vista and Del Norte on the west. The pit is about 1.3 mi (2 km) south of the highway, in a west-trending, slightly entrenched stream valley (unnamed). The peats, which have been extensively mined, extend about a 1.5 km to the east and west of this stop (figs. A10–2 and A10–3). The stream valley is incised into gently west-sloping piedmont covered by eolian dune and cover sands (Holocene to upper Pleistocene). The piedmont is largely a relict basin floor of ancient Lake Alamosa (chapter G, this volume) of middle Pleistocene age.

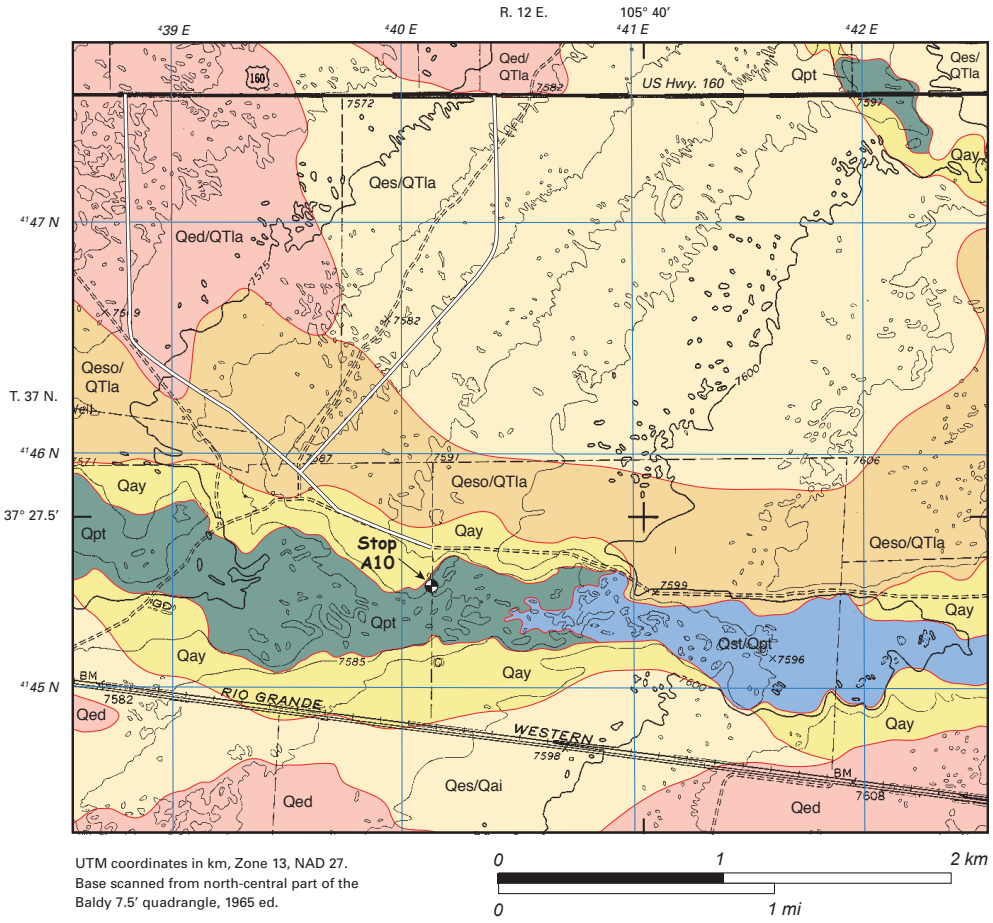

Figure A10–1. Paleospring deposits in unnamed valley east of Alamosa, Colo. Map units: Qed, eolian dune sand; Qes, eolian sand; Qeso, older eolian sand; Qpt, peat deposits; Qts, tufa from springs; Qay, young (latest Pleistocene) alluvium; Qai, intermediate (middle Pleistocene) alluvium; QTla, Alamosa Formation. Geology simplified from Machette and Thompson, unpub. mapping, 2007. Extensive subdivision roads (only two are shown) north of stop A10 were built after topographic base map was constructed.

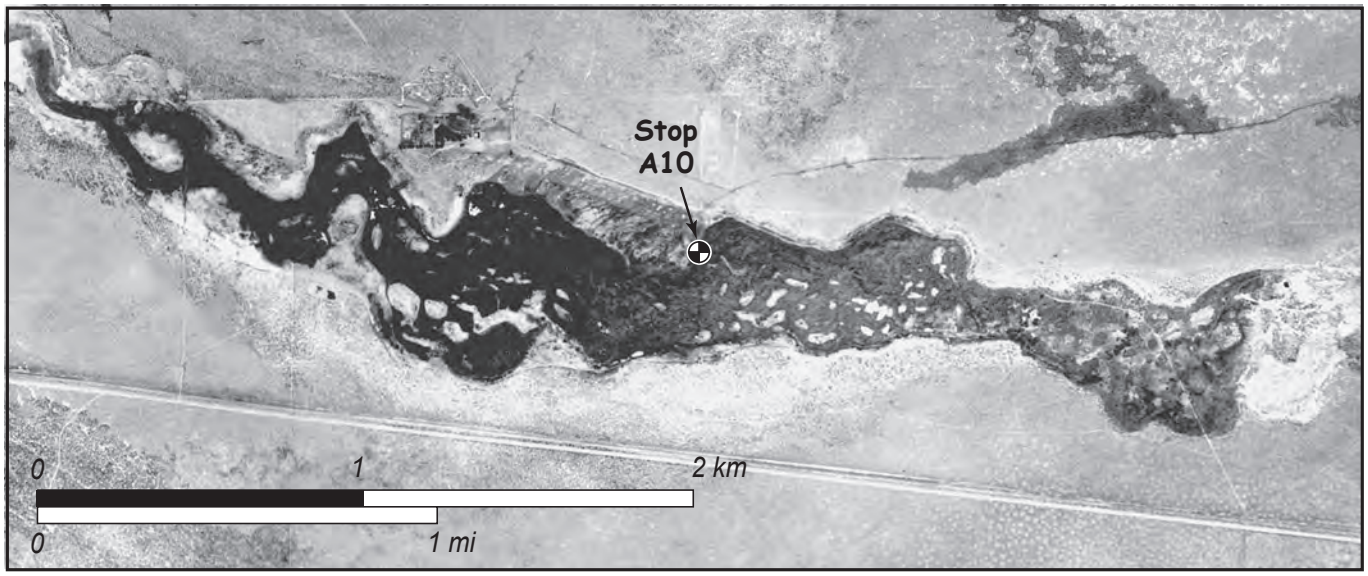

Figure A10–2. Area around the Mr. Peat pit, stop A10. This vintage aerial photograph taken in 1938 by the Soil Conservation Service, well before the peat was mined.

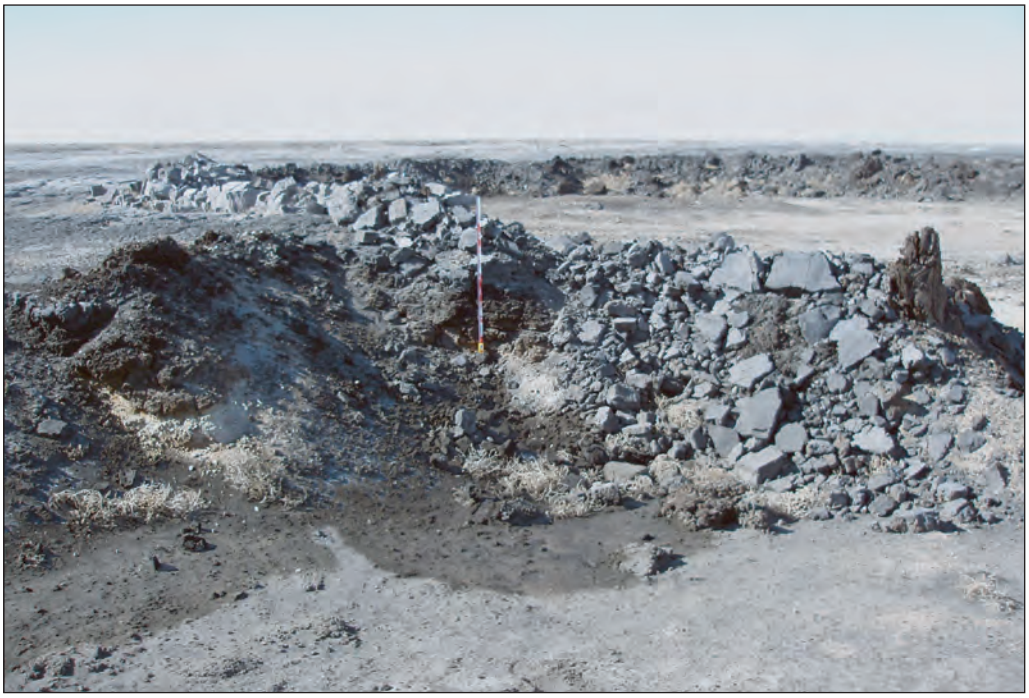

Figure A10–3. Actively mined peat in the Mr. Peat pit, stop A10. Photograph taken in October, 2006. Stadia rod (1.8 m long) for scale.

Shallow lacustrine and interbedded fluvial sediment under the piedmont are part of the uppermost part of the Alamosa Formation (middle Pleistocene to Pliocene). The Alamosa Formation is considered to be time equivalent to the upper part of the Santa Fe Group (middle Pleistocene to Pliocene, Machette and Thompson, unpub. mapping, 2007).

Mr. Peat Pit

In the summer of 2006, we excavated four pits in these deposits to understand better the timing and duration of peat accumulation, facies of the peats, the age of underlying fossil-bearing alluvial deposits and the age and origin of overlying tufa deposits. Fifteen radiocarbon samples were collected from the Mr. Peat pit: two from natural exposures and the remainder from the four trenches we excavated. The woody peats contained whole, fresh fragments of plant material, which were hand picked after ultrasonic cleaning in distilled water. The remaining samples were separated by Kathy Puseman of Paleo Research, Inc. (see also chapter F, this volume). Snails were found in the tufa samples, whereas organic matter or charcoal was concentrated from the remaining samples of organic silt and mucky peat (see table A10–1). All of the concentrated materials (either organic or inorganic) were sent to the radiocarbon laboratory at Woods Hole Oceanographic Institute (WHOI) for accelerator mass spectrometry radiocarbon dating. In addition, four samples of sand that did not contain datable organic matter were collected for OSL dating.

Stratigraphy

From our 2005 reconnaissance, it appeared that the stratigraphy of the Mr. Peat pit consisted of basal fluvial deposits, peats, and tufa mounds (upward in section). This basic stratigraphy was confirmed in four trenches and scattered fresh exposures in and adjacent to the pit, as shown in figure A10–4. The lower fluvial section is based on trench 3, which is shown in more detail in the accompanying paper (chapter F) in this volume, whereas the peat section is based on a composite of trenches 1 and 2.

The peat has three main facies: (1) a mucky (nondescript) black peat with scattered plant fragments, (2) a brown, woody peat that is composed almost entirely of fresh-appearing wood and plant fragments, and (3) a light to medium gray, porous (low density) organic silt. The mucky peat is commonly the basal facies and the dry peat is commonly the uppermost facies, although not all three facies are always present or preserved in the pit.

In the eastern part of the valley, the peats are locally overlain by tufa deposits. At the site of our first trench, the tufas are concentrated in round, domed mounds that are >25 cm to as much as 1 m thick (figs. F–7 and F–8, chapter F, this volume). Downstream, the tufas become less continuous and thinner, pinching out by the location of this field trip stop. Capping the entire section is a mantle of locally derived eolian sand that is composed of quartz and feldspar sands and of reworked fragments (typically granule size) of tufa and peat. A sample of these sands (MRP–DL1) was dated at about 1.6 ka by OSL techniques (see fig. F–4, chapter F in this volume).

Table A10–1. Radiocarbon ages from samples collected at Mr. Peat pit.

[Samples arranged in descending stratigraphic order (see fig. A10-3). Reported radiocarbon ages have one 1-sigma errors; calendar-corrected ages have two 2-sigma errors. The radiocarbon ages were calendar corrected using the radiocarbon calibration program (CALIB REV. 5.0.1 of Stuiver and others, 2005; see also Stuvier and Reimer, 1993). A more complete listing of laboratory parameters is included in table F–1 of chapter F, this volume]

USGS sample number	Material dated	Depth in section (cm)	NOSAMS accession number	Radiocarbon ages and errors (^{14}C yr B.P.)	Calendar ages used for discussion (ka)
BA–MM05–74	Snail shell in tufa	Grab sample	OS–53176	3580±30	3.9
MRP–A6	Snail shell in tufa	53–60	OS–57406	5880±45	6.7
MRP–B4	Dry peat	80–85	OS–57942	3850±85	4.3
BA–MM05–73	Dry peat	85–90	OS–53707	5880±50	6.7
MRP–A4	Woody peat	100–105	OS–56477	9960±40	11.3
MRP–B2	Woody peat	100–105	OS–56641	10150±55	11.8
MRP–A3	Woody peat	115–120	OS–56395	10250±55	12.0
MRP–A2(2)	Moss in organic silt	20–25	OS–57712	9930±60	11.3
MRP–A2(1)	Stems and roots in organic silt	80–85	OS–57672	10550±40	12.5
MRP–B1	Mucky peat	125–130	OS–57499	11350±45	13.2
MRP–A1	Mucky peat	155–160	OS–57714	11600±65	13.4
MRP–C1	Stems and roots in alluvium	Grab sample	OS–57740	12350±60	14.3

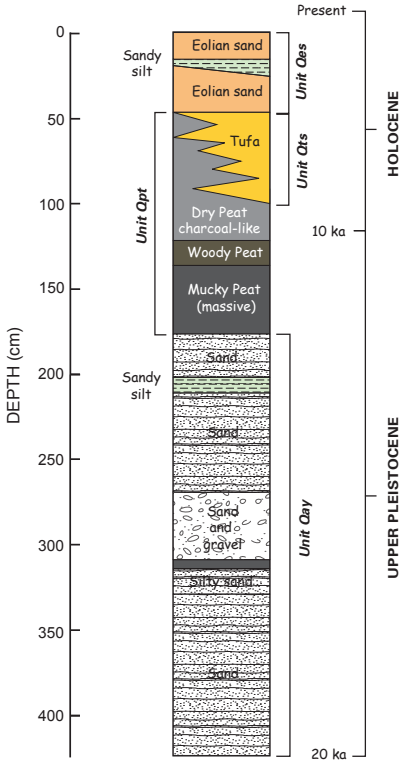

Figure A10–4. Composite stratigraphic section at the Mr. Peat pit, field-trip stop A10. Section described and sampled by Michael Machette, Randall Schumann, and Shannon Mahan, July 5–7, 2006.

Radiocarbon and OSL dating

Twelve radiocarbon samples and four OSL samples were processed for dating. The radiocarbon ages (see Table A10–1) were run at Woods Hole Oceanographic Institute National Ocean Sciences Accelerator Mass Spectrometry Facility (WHOI-NOSAMS) (http://nosams.whoi.edu/index.html), whereas the OSL ages were determined by Shannon A. Mahan (USGS). (See chapter F of this volume for a more complete discussion of sample preparation and dating results.)

In general, the radiocarbon ages are in proper stratigraphic order; the oldest ages come from the basal mucky peat and the youngest ages come from the organic silt and coeval tufa deposits. Most of the peat deposits accumulated from 13.5 ka to about 11.6 ka although deposition continued until middle Holocene time (4.3–6.7 ka), whereas locally overlying tufaceous spring deposits started to accumulate at about 6.7 ka and deposition continued until about 3.9 ka. The underlying sand and sandy fluvial gravel contained an organic seam located about 1.4 m below the peat that yielded an age of 14.3 ka, whereas IRSL and OSL dating of the alluvium yielded ages as young as 6.45 ka as old as 34.3 ka (see chapter F (this volume) for a more complete discussion of the luminescence dating).

Paleoenvironments During the Late Pleistocene to Middle Holocene

On the basis of these dating studies, we suggest that during the late Pleistocene, glacial-fed streams flowing west into the Rio Grande entrenched and backfilled valleys. By 15–20 ka, these stream channels had aggraded to within 5–10 m of the piedmont slope that they flowed across. High water tables on the piedmont intersected the paleostream valley and probably caused persistent spring discharge that might have been localized by faults in the underlying Alamosa Formation (see discussion in chapter F, this volume). Marsh-like or cienega wetland conditions in the valley caused slow accumulation of peats, but as ground-water levels fell, deposition shifted to charcoal-like dry peats and tufa.

References Cited

Aitken, M.J., 1998, An introduction to optical dating—The dating of Quaternary sediments by the use of photon-stimulated luminescence: New York, Oxford University Press, 280 p.

Alexander, B., 1979, Geology of Great Sand Dunes—A preliminary review of the literature: Unpublished National Park Service report, Great Sand Dunes National Park and Preserve library, 58 p.

Andrews, S., 1981, Sedimentology of Great Sand Dunes, Colorado, *in* Ethridge, F.G., and Flores, R.M., eds., Recent and ancient nonmarine depositional environments—Models for exploration: Tulsa, Oklahoma, Society of Economic Paleontologists and Mineralogists Special Publication 31, p. 279–291.

Bailey, S.D., Wintle, A.G., Duller, G.A.T., and Bristow, C.S., 2001, Sand deposition during the last millennium at Aberffraw, Anglesey, North Wales as determined by OSL dating of quartz: Quaternary Science Reviews, v. 20**,** p. 701–704.

Ballarini, M., Wallinga, J., Murray, A., van Heteren, S., Oost, A.P., Bos, A. J.J., and van Eijk, C. W.E., 2003, Optical dating of young coastal dunes on a decadal time scale: Quaternary Science Reviews, v. 22**,** p. 1011–1017.

Bøtter-Jensen, L., Bulur, E., Duller, G.A.T., and Murray, A.S., 2000, Advances in luminescence instrument systems: Radiation Measurements, v. 32, p. 523–528.

Brady, N.C., 1974, The nature and properties of soils, 8th ed.: New York, Macmillan Publishing, 639 p.

Brister, B.S., and Gries, R.R., 1994, Tertiary Stratigraphy and tectonic development of the Alamosa Basin (northern San Luis Basin), Rio Grande rift, south-central Colorado, *in* Keller, G.R., and Cather, S.M., eds., Basins of the Rio Grande rift—Structure, stratigraphy, and tectonic setting: Geological Society of America Special Paper 291, p. 39–58.

Bruce, R.M., and Johnson, B.R., 1991, Reconnaissance geologic map of parts of the Zapata Ranch and Mosca Pass quadrangles, Alamosa and Huerfano Counties, Colorado: U.S. Geological Survey Miscellaneous Field Studies Map MF–2168, scale 1:24,000.

Burroughs, R.L., 1972, Geology of the San Luis Hills, south-central Colorado: Albuquerque, University of New Mexico, Ph.D. dissertation, 139 p.

Carson, M.A., and MacLean, P.A., 1986, Development of hybrid dunes—The William River dunefield, northwest Saskatchewan, Canada: Canadian Journal of Earth Sciences, v. 23, p. 1974–1990.

Chen, J.S., Li, L., Wang, J.Y., Barry, D.A., Sheng, X.F., Gu, W.Z., Zhao, X., and Chen, L., 2004, Groundwater maintains dune landscape: Nature, v. 432, p. 459–460.

Cook, E.R., Krusic, P.J., and Woodhouse, C.A., 2003, North American drought atlas: Intergovernmental Panel on Climate Change Workshop on Droughts, Nov. 2003, v. 1–3 (http://www.ngdc.noaa.gov/paleo/newpsdi.html).

Fain, J., Soumana, S., Montret, M., Miallier, D., Pilleyre, T., and Sanzelle, S., 1999, Luminescence and ESR dating—Beta-dose attenuation for various grain shapes calculated by a Monte-Carlo method: Quaternary Science Reviews, v. 18, p. 231-234.

Fish, S.K., and Fish, P.R., 1994, Prehistoric desert farmers of the Southwest: Annual Review of Anthropology, v. 23, p. 83–108.

Forman, S.L., Goetz, A.F.H., and Yuhas, R.H., 1992, Large scale stabilized dunes on the High Plains of Colorado—Understanding the landscape response to Holocene climates with the aid of images from space: Geology, v. 20, p. 145–148.

Forman, S.L., Marín, L., Pierson, J., Gómez, J., Miller, G.H., and Webb, R.S., 2005, Aeolian sand depositional records from western Nebraska—Landscape response to droughts in the past 1500 years: The Holocene, v. 15, no. 7, p. 973–981.

Forman, S.L., Oglesby, R., Markgraf, V., and Stafford, T., 1995, Paleoclimatic significance of late Quaternary eolian deposition on the Piedmont and High Plains, central United States: Global and Planetary Change, v. 11, p. 35–55.

Forman, S.L., Oglesby, R., and Webb, R.S., 2001, Temporal and spatial patterns of Holocene dune activity on the Great Plains of North America—Megadroughts and climate links: Global and Planetary Change, v. 29, p. 1–29.

Forman, S.L., and Pierson, J., 2003, Formation of linear and parabolic dunes on the eastern Snake River Plain, Idaho, in the nineteenth century: Geomorphology, v. 56, p. 189–200.

Forman, S.L., Spaeth, M., Marín, L., Pierson, J., and Gómez, J., 2006, Episodic late Holocene dune movements on the sand sheet area, Great Sand Dunes National Park and Preserve, San Luis Valley, Colorado: Quaternary Research, v. 66, p. 97–108.

Fryberger, S.G., 1990a, Depositional Models for Modern Eolian Sand Seas (Chap. 6) *in* Fryberger, S.G., Krystinik, L.F., and Schenk, C.J., eds., Modern and ancient eolian deposits—Petroleum exploration and production: Denver, Rocky Mountain Section Society of Economic Paleontologists and Mineralogists, p. 6–5

Fryberger, S.G., 1990b, Great Sand Dunes depositional system—An overview (Chap. 1), *in* Modern and ancient eolian deposits—Petroleum exploration and production: Denver, Rocky Mountain Section Society of Economic Paleontologists and Mineralogists, p. 1–3.

Fryberger, S.G., 1999, Overview of the eolian depositional system, Great Sand Dunes National Monument and vicinity, *in* Schenk, C.J., ed., Hydrologic, geologic and biologic research at Great Sand Dunes National Monument, Colorado: National Park Service Research Symposium 1, Denver, Colorado, Proceedings, p. 195–214.

Fryberger, S.G., and Dean, G., 1979, Dune forms and wind regime, *in* McKee, E.D., ed., A study of global sand seas: U.S. Geological Survey Professional Paper 1052, p. 137–169.

Fye, F.K., Stahle, D.W., and Cook, E.R., 2003, Paleoclimatic analogs to twentieth-century moisture regimes across the United States: Bulletin of the American Meteorological Society, v. 84, p. 901–915.

Gaylord, D.R., 1989, Holocene paleoclimatic fluctuations revealed from dune and interdune strata in Wyoming: Journal of Arid Environments, v. 18, p. 123–138.

Goble, R.J., Mason, J.A., Loope, D.B., Swinehart, J.B., and Loope, D.B., 2004, Optical and radiocarbon ages of stacked paleosols and dune sands in the Nebraska Sand Hills, USA: Quaternary Science Reviews, v. 23, p. 1173–1182.

Greeley, R., and Iversen, J.D., 1987, Wind as a geological process on Earth, Mars, Venus and Titan: New York, Cambridge University Press, 333 p.

Grissino-Mayer, H.D., Baisan, C.H., Swetnam, C.W., 1998, A multicentury reconstruction of precipitation for Great Sand Dunes National Monument, southwestern Colorado: Final report submitted to Mid-continent Ecological Science Center for the National Park Service.

Hammond, D.J., 1998, Measuring changes in areal extent of historic wetlands at Great Sand Dunes National Monument, Colorado 1936–1995: Fort Collins, Colorado State University, M.S. thesis, 56 p.

Huenneke, L.F., Anderson, J.P., Remmenga, M., and Schlesinger, W.H., 2002, Desertification alters patterns of above ground net primary production in Chihuahuan ecosystems: Global Change Biology, v. 8, p. 247–264.

Jodry, M.A., 1987, Stewart's Cattle Guard site—A Folsom site in southern Colorado—A report on the 1981 and 1983 field seasons: Austin, University of Texas Department of Anthropology, unpublished M.A. thesis.

Jodry, M.A., and Stanford, D.J., 1992 Stewart's Cattle Guard site—An analysis of Bison remains in a Folsom kill–butchery campsite, *in* Stanford, D.J., and Day, J.S., eds., Ice age hunters of the Rockies: Niwot, University Press of Colorado, p. 101–168.

Jodry, M.A., Shafer, D.S., Stanford, D.J., and Davis, O.K., 1989, Late Quaternary environments and human adaptation in the San Luis valley, south-central Colorado, *in* Harmon, E. J., ed., Water in the valley—A 1989 perspective on water supplies, issues, and solutions in the San Luis Valley, Colorado: Colorado Ground-Water Association Guidebook, 8th annual field trip, p. 189–208.

Johnson, B.R., Bruce, R.M., and Lindsey, D.A., 1989, Reconnaissance geologic map of the Medano Pass quadrangle and part of the Liberty quadrangle, Alamosa, Huerfano, and Saguache Counties, Colorado: U.S. Geological Survey Miscellaneous Field Studies Map MF–2089, scale 1:24,000.

Johnson, R.B., 1967, The Great Sand Dunes of southern Colorado: U. S. Geological Survey Professional Paper 575–C, p. C177–C183.

Krystinik, L.F., 1990, Early diagenesis in continental eolian deposits (Chap. 8), *in* Fryberger, S.G., Krystinik, L.F., and Schenk, C.J., eds., Modern and ancient eolian deposits—Petroleum exploration and production: Denver, Colorado, Rocky Mountain Section Society of Economic Paleontologists and Mineralogists, p. 8–1.

Lancaster, N., 1997, Response of eolian geomorphic systems to minor climate change—Examples from the southern Californian deserts: Geomorphology, v. 19, no. 3–4, p. 333–347.

Lancaster, N., and Tchakerian, V.P., 2003, Late Quaternary eolian dynamics, Mojave Desert, California, *in* Enzel, Y., Wells, S.G., and Lancaster, N., eds., Paleoenvironments and paleohydrology of the Mojave and southern Great Basin deserts: Geological Society of America Special Paper 368, p. 231–249.

Larson, D.O., Neff, H., Graybill, D.A., Michaelsen, J., and Ambos, E., 1996, Risk, climatic variability, and the study of southwestern prehistory—An evolutionary perspective: American Antiquity, v. 61, p. 217–241.

Lekson, S.H., 2001, Casas Grandes and its hinterland—Prehistoric regional organization in northwest Mexico: Journal of Field Archaeology, v. 28, p. 216–222.

Lekson, S.H., 2002, Anasazi America—Seventeen centuries on the road from center place: American Antiquity, v. 67, p. 172–173.

Machette, M.N., and Thompson, R.A., 2005, Preliminary geologic map of the northwestern part of the Alamosa ½° x 1° quadrangle, Alamosa and Conejos Counties, Colorado: U.S. Geological Survey Open-File Report 2005–1392, 1 sheet, 1:50,000 scale.

Madole, R.F., 1994, Stratigraphic evidence of desertification in the west-central Great Plains within the past 1000 yr: Geology, v. 22, p. 483–486.

Madole, R.F., 1995, Spatial and temporal patterns of Late Quaternary eolian deposition, eastern Colorado, U. S. A.: Quaternary Science Reviews, v. 14, p. 155–178.

Madole, R.F., and Romig, J.H., 2002, The Great Sand Dunes (GSD) of south-central Colorado—Origin and implications [abs.]: Geological Society of America Abstracts with Programs, v. 34, no. 6, p. 275.

Mapmart, 2004: http://*www.mapmart.com* (last accessed in 2005)

Marín, L., Forman, S. L., Valdez, A., and Bunch, F., 2005, 20th Century dune migration at the Great Sand Dunes National Park and Preserve, Colorado and relation to drought variability: Geomorphology, v. 70, p. 163–183.

Mason, J.A., Swinehart, J.B., Globe, R.J. and Loope, D.B., 2004, Late Holocene dune activity linked to hydrological drought, Nebraska Sand Hills, USA: The Holocene, v. 14, p. 209–217.

McCalpin, J.P., 1982, Quaternary geology and neotectonics of the west flank of the northern Sangre de Cristo Mountains, south-central Colorado: Colorado School of Mines Quarterly, v. 77, no. 3, 97 p.

McCalpin, J.P., 1996, General geology of the northern San Luis Valley, Colorado (in section II, Geology and geohydrology), *in* Thompson, R.A., Hudson, M.R., and Pillmore, C.L., eds., Geologic excursions to the Rocky Mountains and beyond—Field trip guidebook for 1996 Annual Meeting of the Geological Society of America, Denver, Colorado, October 28–31: Colorado Geological Survey Special Publication 44, 11 p. (CD-ROM).

McCalpin, J.P., 2006, Active faults and seismic hazards to infrastructure at Great Sand Dunes National Monument and Preserve: Crestone, Colorado, GEO-HAZ Consulting, Inc., 49 p., 1 oversize plate.

McKee, E.D., 1979, A study of global sand seas: U.S. Geological Survey Professional Paper 1052, 429 p.

Mejdahl, V., and Christiansen, H.H., 1994, Procedures used for luminescence dating of sediments: Boreas, v. 13, p. 403–406.

Morrison, R.B., ed., 1991, Quaternary nonglacial geology—Conterminous U.S.: Boulder, Colorado, Geological Society of America, The Geology of North America, v. K–2, 672 p.

Muhs, D.R., Stafford, T.W., Beann, J., Mahan, S.A., Burdett, J., Skipp, G., and Rowland, Z.M., 1997, Holocene eolian activity in the Minot dune field, North Dakota: Canadian Journal of Earth Sciences, v. 34, p. 1442–1459.

Muhs, D.R., Stafford, T.W., Cowherd, S.D., Mahan, S.A., Kihl, R., Maat, P.B., Bush, C.A., and Nehring, J., 1996, Origin of the late Quaternary dune fields of northeastern Colorado: Geomorphology, v. 17, p. 129–149.

Muhs, D.R., Stafford, T.W., Swinehart, J.B., Cowherd, S.D., Mahan, S.A., Bush, C.A. Madole, R.F. and Maat, P.B., 1997, Late Holocene eolian activity in the mineralogically mature Nebraska Sand Hills: Quaternary Research, v. 48, no. 2, p. 162–176.

Murray, A.S., and Wintle, A.G., 2000, Quartz OSL—Effects of thermal treatment and their relevance to laboratory dating procedures: Radiation Measurements, v. 32, p. 387–400.

Murray, A.S., and Wintle, A.G., 2003, The single aliquot regenerative dose protocol—Potential for improvements in reliability: Radiation Measurements, v. 37, p. 377–381.

National Climatic Data Center, 1950–2002: U.S. Department of Commerce, NOAA Satellite and Information Service. http;//www.ncdc.noaa.gov/oa/ncdc.html.

Nelson, M.C., and Schachner, G., 2002, Understanding abandonments in the North American Southwest: Journal of Archaeological Research, v. 10, p. 167–206.

Overpeck, J.T., 1996, Warm climate surprises: Science, v. 271, p. 1820–1821.

Prescott, J.R., and Hutton, J.T., 1994, Cosmic-ray contributions to dose rates for luminescence and ESR dating—Large depths and long-term time variations: Radiation Measurements, v. 23, p. 497–500.

Rogers, K.L., 1984, A paleontologic analysis of the Alamosa Formation (south-central Colorado; Pleistocene, Irvingtonian), *in* Baldridge, W.S., Dickerson, P.W., Riecher, E., and Zidek, J., eds., Rio Grande rift—Northern New Mexico: New Mexico Geological Society 35th Annual Field Conference, Guidebook, v. 35, p. 151–155.

Sadler, P.M., 2004, Quantitative biostratigraphy—Achieving finer resolution in global correlation: Annual Review of Earth and Planetary Sciences, v. 32, p. 187–213.

Sadler, P.M., and Strauss, D.J., 1990, Estimation of completeness of stratigraphical sections using empirical data and theoretical models: Journal of the Geological Society, v. 147, p. 471–485.

Schlesinger, W.H., Reynolds, J.F., Cunningham, G.L., Huenneke, L.F., Jarrel, W.M., Virginia, R.A., and Whitford, W.G., 1990, Biological feedbacks in global desertification: Science, v. 247, p. 1043–1048.

Shulka, J. and Mintz, Y., 1982, Influence of land-surface evapotranspiration on the Earth's climate: Science, v. 215, p. 1498–1501.

Siebenthal, C.E., 1910, Geology and water resources of the San Luis Valley, Colorado: U.S. Geological Survey Water-Supply Report 240, 128 p.

Stahle, D.W., Cook, E.R., Cleaveland, M.K., Therrell, M.D., Meko, D.M., Grissino-Mayer, H.D., Watson, E., and Luckman, B.H., 2000, Tree-ring data document 16th Century megadrought over North America: EOS, Transactions of the American Geophysical Union, v. 81, p. 121–125.

Stokes, S., Bailey, R.M., Fedoroff, N., and O'Marah, K.E., 2004, Optical dating of aeolian dynamism on the West African Sahelian margin: Geomorphology, v. 59, p. 281–291.

Stokes, S., and Gaylord, D.R., 1993, Optical dating of Holocene dune sands in the Ferris dune field, Wyoming: Quaternary Research, v. 39, p. 274–281.

Stokes, S., and Swinehart, J.B., 1997, Middle- and late-Holocene dune reactivation in the Nebraska Sand Hills, USA: The Holocene, v. 7, p. 263–272.

Stuiver, Minze, and Reimer, P.J., 1993, Extended ^{14}C database and revised CALIB 3.0 ^{14}C age calibration program: Radiocarbon, v. 35, no. 1, p. 215–230.

Stuvier, Minze, Reimer, P.J., and Reimer, Ron, 2005, CALIB Radiocarbon Calibration, v. 5.0.1 [online program], http://radiocarbon.pa.qub.ac.uk/calib/ (last accessed in 2006; to be used in conjunction with Stuiver and Reimer, 1993).

Terraserver, 2004: *http://terraserver.microsoft.com* (last accessed in 2005)

Wells, D.L., and Coppersmith, K.J., 1994, Empirical relationships among magnitude, rupture length, rupture area, and surface displacement: Bulletin of the Seismological Society of America, v. 84, p. 974–1002.

Wells, S.G., McFadden, L.D., and Schulz, J.D., 1990, Eolian landscape evolution and soil formation in the Chaco dune field, southern Colorado Plateau, New Mexico: Geomorphology, v. 3, p. 517–546.

Widmann, B.L., Kirkham, R.M., and Rogers, W.P., 1998, Preliminary Quaternary fault and fold map and database of Colorado: Colorado Geological Survey Open-File Report 98–8, 331 p.

Wiegland, J.P., 1977, Dune morphology and sedimentology at Great Sand Dunes National Monument: Fort Collins, Colorado State University, unpublished M.S. thesis.

Wolfe, S.A., Huntley, D.J., David, P.P., Ollerhead, J., Sauchyn, D.J., and MacDonald, G.M., 2001, Late 18th century drought-induced sand dune activity, Great Sand Hills, Saskatchewan: Canadian Journal of Earth Sciences, v. 38, 105–117.

Wolfe, S.A., Ollerhead, J., and Lian, O.B., 2002, Holocene eolian activity in south-central Saskatchewan and the southern Canadian Prairies: Geographie Physique et Quaternaire, v. 56, p. 215–227.

Woodhouse, C.A., Lukas, J.J., and Brown, P.M., 2002, Drought in the western Great Plains, 1845–56—Impacts and implications: Bulletin of the American Meteorological Society, v. 83, p. 1485–1493.

Woodhouse, C.A. and Overpeck, J.T., 1998, 2000 years of drought variability in the central United States: Bulletin of the American Meteorological Society, v. 79, p. 2693–271.